Final Report Submitted to the National Aeronautics and Space Administration

Contract NAS1-18239

Scientific Studies in Association with the Halogen Occultation Experiment

Loretta J. Mickley and John E. Frederick

Department of the Geophysical Sciences

The University of Chicago

5734 South Ellis Avenue

Chicago, IL 60637

July 1996

Executive Summary

This report summarizes research completed under Contract NAS1-18239 to the University of Chicago. The effort has involved application of photochemical models to interpret measurements made by the Halogen Occultation Experiment (HALOE) and the use of HALOE data to examine stratospheric chemical processes which influence the Earth's ozone layer. This work constitutes the Ph.D. research of Loretta J. Mickley at the University of Chicago.

This research has emphasized the partitioning of members of the odd nitrogen (NO_y) and odd chlorine (Cl_y) families in the stratosphere. Use of two tracer molecules measured by HALOE, CH_4 and HF, enabled us to follow the partitioning of the families over time scales ranging from weeks to years. In one study (Project 1) we determined the effect of aerosol from the Mount Pinatubo volcano on NO_x (NO and NO_2) and ozone at altitudes which are not assessable by research aircraft. In a second study (Project 2), we investigated the effect of the NO and NO_2 on Cl_y partitioning during Antarctic spring, after significant ozone depletion had taken place. In addition to these projects, we also worked with scientists at NASA/Langley to validate HALOE measurements of NO and NO_2. For this work, we compared the instrument's measurements with observations from other sensors and with model-based predictions. A summary of the two major projects appears below.

Project 1: Response of Stratospheric Odd Nitrogen and Ozone at 17 mb to Mount Pinatubo Aerosol in the Southern Mid-Latitudes

Observations of stratospheric NO, NO_2, and O_3 from HALOE were examined over the Southern mid-latitudes (35-45 degrees South) in the years following the eruption of Mount Pinatubo, from early 1992 through mid-1995. The tracers HF and CH_4, also observed by HALOE, were used to distinguish between the effects of transport on the distribution of ozone and total reactive nitrogen (NO_y) and the chemical effects of aerosol on NO_y

partitioning and ozone loss processes. Mixing ratios of HF were adjusted to take into account its increasing burden due to emission of chlorofluorocarbons at the Earth's surface.

Results show that at 17 mb (about 28 km), in parcels containing similar values of HF, the abundance of $NO+NO_2$ (NO_x) almost doubled during the first two years of the observation period. Since model results show that HF correlates with NO_y in this part of the stratosphere, the increase must be due to changes in the partitioning of NO_y. Data on aerosol surface area from SAGE II show a sharp decline during 1992 at this altitude, followed by a leveling off. Thus the increase in NO_x may be linked to a decline in the rate of hydrolysis of N_2O_5 on sulfate aerosol as the Pinatubo aerosol gradually settled out of the stratosphere. Similar results were obtained when CH_4 was used as a tracer.

Again using HF and CH_4 as tracers, results show that ozone abundances at 17 mb declined by about 10 percent during the first year of the observation period. The trend in ozone is opposite in sign to that observed by instruments at lower altitudes (18-22 km) following the Mount Pinatubo eruption. At the lower altitudes, NO_x acts as a brake on the active chlorine and hydrogen cycles that destroy odd oxygen, and a return to pre-Pinatubo values of NO_x resulted in an increase in ozone amounts. The ozone trend observed at higher altitudes is consistent with model calculations which show that above about 26 km, where NO_x mixing ratios begin increasing rapidly with height, the NO_x catalytic cycle dominates all other ozone loss processes. Thus the data suggest that in 1991 and 1992 at 17 mb, the loss in NO_x due to heterogeneous chemistry on Pinatubo aerosols may have temporarily elevated levels of ozone.

Project 2: Evolution of Chlorine and Nitrogen Species in the Lower Stratosphere during Antarctic Spring

Observations of O_3, HCl, NO, and NO_2 from HALOE provided a means to investigate chemical change in the lower stratosphere over Antarctica during 23 days in October of 1992. Two long-lived species also observed by HALOE, HF and CH_4, were used as

tracers to identify a series of air parcels having similar Cl_y and NO_y abundances and similar temperature histories. Most of the parcels chosen using tracer analysis show low ozone mixing ratios, less than 1 ppm on the 480 Kelvin surface (about 20 km). The low O_3 content of these parcels suggests that ozone depletion had already taken place, during the month of September. HCl mixing ratios in these parcels more than doubled from early to late October, and the NO and NO_2 abundances rose sharply, by a factor of five for NO and a factor of three to four for NO_2.

The trends observed in NO, NO_2, and HCl agree with model calculations which show that the formation of HCl proceeds quickly when ozone levels fall so low that (1) the rate of the reaction $Cl + O_3 \rightarrow ClO + O_2$ slows and (2) the rate of the reaction $NO + ClO \rightarrow NO_2 + Cl$ becomes faster than the rate of the competing reaction $NO + O_3 \rightarrow NO_2 + O_2$. Under these conditions, Cl increases at the expense of ClO, and HCl is formed via the reaction $Cl + CH_4 \rightarrow HCl + CH_3$. Stratospheric chlorine is thus shifted from reactive species to the long-lived reservoir molecule, HCl. The repartitioning of the active chlorine family in favor of HCl may limit the extent of ozone depletion during spring, and may have importance as the polar vortex breaks up and parcels are transported toward mid-latitudes.

Table of Contents

CHAPTER 1

INTRODUCTION

Ozone in the stratosphere is of major importance to life on earth. The gas absorbs strongly in the ultraviolet region of the spectrum (200 to 320 nm), light that in large enough doses can severely damage plant and animal life by breaking chemical bonds. By filtering out these wavelengths of sunlight, the stratospheric ozone layer protects the biosphere. The ozone layer also plays a role in the radiative balance of the atmosphere. Absorption of incoming sunlight by ozone prevents a fraction of that light from reaching the earth's surface. The absorption also warms the stratosphere, influencing temperatures at the tropopause.

In recent years, disturbing trends in stratospheric ozone have been observed over the mid-latitudes and polar regions. The first sign of a perturbation to the ozone layer was detected during spring over Antarctica (Farman et al., 1985). There ground-based instruments measuring total column amounts showed large losses of total ozone each October beginning in the mid-1970s. The Antarctic ozone hole, monitored now by satellites, balloons and aircraft as well as ground-based instruments, has occurred each spring since then, with especially severe depletions taking place in spring 1992 and 1993 (Hofmann et al., 1989a; Waters et al., 1993; WMO, 1995). The data show losses in total ozone of 50-60 per cent over a region of 20 million square kilometers in area, or from the pole to about 65 S. Nearly complete loss of ozone has been observed in the 14-17 km layer of the stratosphere (Hofmann

et al., 1994a). Similar, though not as severe, losses of ozone have been observed over the Artic in spring (Profitt et al., 1990; Browell et al., 1990; Waters et al., 1993).

Beginning in the mid-1980s, long-term trends in ozone loss over the mid-latitudes have also been reported. Data from satellites, ozonesondes, and ground-based instruments all show trends in ozone loss of a few per cent per decade, with greater loss occurring in the Northern Hemisphere (Reinsel et al., 1984; Stolarski et al., 1992; Reinsel et al., 1994; WMO, 1995). These trends in ozone appear to have begun in the early to mid-1970s. Since total column ozone has been measured by ground-based spectrometers since the 1920s, the loss trends can be determined with some confidence. Briefly, the data show recent losses of about 4 to 5 per cent per decade over the northern mid-latitudes, and 3 to 4 per cent per decade over the southern mid-latitudes. In the Northern Hemisphere, losses are greatest in late winter through early spring. Data from the Stratospheric Aerosol and Gas Experiment (SAGE) and from a network of ozonesondes show that most of the loss over mid-latitudes occurs in the 15-20 km region (McCormick et al., 1992; Logan, 1994). Over the tropics, ozone appears to have declined only a fraction of a per cent per decade (WMO, 1995).

Recent work has been done to try to detect trends in ultraviolet flux at the earth's surface that are consistent with these trends in ozone. Over mid-latitudes, problems in instrument calibration together with the challenge of removing the effects of clouds, aerosol, and pollution have made it difficult to determine trends in ultraviolet flux due solely to trends in stratospheric ozone. (See, for example, Frederick et al., 1992.) Lubin and Jensen (1995) show that up till now the large natural variability in ultraviolet flux due to variable cloudiness probably swamps

any change in the irradiance due to loss of stratospheric ozone. Frederick and Erlick (1995) have reached a similar conclusion. However, changes in summertime ultraviolet radiation due to changes in the ozone layer may in fact become significant by the end of this century (Lubin and Jensen, 1995). Over the southern high latitudes in spring, enhanced flux of ultraviolet sunlight has already been reported (Frederick and Alberts, 1991).

In the next two sections I present a brief background to ozone chemistry and describe current issues in stratospheric ozone. The last section of this Chapter outlines the contribution of this work to research ongoing in the scientific community.

1.1. Background on Ozone Chemistry

Ozone in the stratosphere is produced via photolysis of molecular oxygen:

$$O_2 + h\nu\,(\lambda < 242\,nm) \rightarrow O + O \tag{1.1}$$

$$O + O_2 + M \rightarrow O_3 + M \tag{1.2}$$

where M is any molecule. Production is greatest over the tropics and low latitudes where the flux of ultraviolet radiation is greatest. Reaction 1.2 proceeds rapidly, as does the photolysis of ozone, which regenerates the oxygen atom:

$$O_3 + h\nu \rightarrow O + O_2. \tag{1.3}$$

Throughout the daylit stratosphere, ozone is in fast photochemical equilibrium with atomic oxygen. The sum of ozone and atomic oxgen is called odd oxygen. A fourth reaction acts as a sink of odd oxygen:

$$O_3 + O \rightarrow 2\,O_2. \tag{1.4}$$

Reactions 1.1 through 1.4 are known as the Chapman reactions and represent a first attempt to describe the ozone budget (Chapman, 1930).

The average motion of the stratosphere can be described as a kind of fountain, with warm air upwelling through the tropical tropopause, spreading out over the mid-latitudes, and then cooling and subsiding at high latitudes. This motion is known as the Brewer-Dobson circulation. The air above the tropical tropopause is photochemically "young" air — that is, air that has not been exposed long to the ultraviolet radiation levels typical of the stratosphere. Such air contains high levels of tropospheric gases — e.g., CH_4, N_2O, and the chlorofluorocarbons (CFCs) — and low levels of some of the radicals derived from these source gases — e.g., NO or ClO. As the air is pushed to higher altitudes and out over the mid-latitudes, the period of exposure to ultraviolet light lengthens, the source gases break down, and the abundances of radicals builds up. These radicals play important roles in catalytic ozone loss processes.

One such cycle, involving odd hydrogen ($OH+HO_2$), proceeds as follows:

$$OH + O_3 \rightarrow HO_2 + O_2 \tag{1.5}$$

$$HO_2 + O_3 \rightarrow OH + 2O_2 \tag{1.6}$$

$$net: 2\,O_3 \rightarrow 3\,O_2.$$

An important cycle involving chlorine and bromine radicals is:

$$HO_2 + ZO \rightarrow HOZ + O_2 \tag{1.7}$$

$$HOZ + h\nu \rightarrow OH + Z \tag{1.8}$$

$$Z + O_3 \rightarrow ZO + O_2 \tag{1.9}$$

$$OH + O_3 \rightarrow HO_2 + O_2 \tag{1.10}$$

$$net: 2\,O_3 \rightarrow 3\,O_2$$

where Z represents either Cl or Br. Other halogen cycles include:

$$BrO + ClO \rightarrow Br + Cl + O_2 \tag{1.11}$$

$$Br + O_3 \rightarrow BrO + O_2 \tag{1.12}$$

$$Cl + O_3 \rightarrow ClO + O_2 \tag{1.13}$$

$$net: 2\,O_3 \rightarrow 3\,O_2$$

and

$$ClO + O \rightarrow Cl + O_2 \tag{1.14}$$

$$Cl + O_3 \rightarrow ClO + O_2 \tag{1.15}$$

$$net: O + O_3 \rightarrow O_2.$$

Two cycles involving the nitrogen radicals NO and NO_2 are:

$$NO + O_3 \rightarrow NO_2 + O_2 \tag{1.16}$$

$$NO_2 + O \rightarrow NO + O_2 \tag{1.17}$$

$$net: O_3 + O \rightarrow 2\,O_2.$$

and

$$NO + O_3 \rightarrow NO_2 + O_2 \tag{1.18}$$

$$NO_2 + O_3 \rightarrow NO_3 + O_2 \tag{1.19}$$

$$NO_3 + h\nu \rightarrow NO + O_2 \tag{1.20}$$

$$net: 2\,O_3 \rightarrow 3\,O_2.$$

Together the two nitrogen radicals are known as NOx, or odd nitrogen.

The task of identifying these cycles and determining their relative importance has occupied atmospheric chemists since the 1960s, when calculations showed that the Chapman cycle led to an overestimate of ozone in the stratosphere. The nitrogen cycle, Reaction 1.16-1.17, was first described in the early 1970s (Crutzen, 1970; Crutzen, 1971); the role of chlorine in the ozone budget was suggested shortly thereafter (Stolarski and Cicerone, 1974). More recently, measurements of radicals made from instruments onboard ER-2 aircraft have permitted careful analysis of the loss cycles in the lower stratosphere (e.g., Wennberg et al., 1994). The ER-2 data show that in this region, the hydrogen cycle (Reactions 1.5-1.6) and the halogen cycles (Reactions 1.7-1.10 and Reactions 1.11-1.13) dominate all other cycles. In the middle stratosphere, satellite data together with model calculations demonstrate the importance of the NOx cycles (Garcia and Solomon, 1994). Analysis of satellite data from the upper stratosphere show that the odd hydrogen cycle regains importance here (Jackman et al., 1986; Crutzen et al., 1995).

Complicating the ozone budget are reactions that take place among the radicals themselves. For example, NO_2 can slow the chlorine catalytic cycles by tying up the chlorine radical ClO in the longer-lived, less reactive molecule $ClONO_2$:

$$ClO + NO_2 + M \rightarrow ClONO_2 + M. \qquad (1.21)$$

The radical NO, on the other hand, influences the odd hydrogen cycle via this reaction:

$$NO + HO_2 \rightarrow NO_2 + OH. \qquad (1.22)$$

This reaction competes with Reaction 1.6, the rate-limiting step in the odd hydrogen cycle. In other words, the two odd nitrogen species, NO and NO_2, can short-circuit the catalytic cycles involving chlorine and odd hydrogen, leading to slower ozone loss rates.

In the lower and middle stratosphere under most conditions, the production and loss rates of ozone are slow, on timescales of months. The long chemical lifetime of ozone means that its distribution is governed in large part by transport. Distinguishing between the effects of transport and chemistry on the ozone budget in these regions of the atmosphere is tricky, as is discussed in Chapter 5. In the upper stratosphere, above about 40 km, the flux of ultraviolet sunlight increases and production of ozone via the photolysis of molecular oxygen proceeds rapidly. Loss processes are also rapid due to the presence here of large abundances of the necessary radicals. In this region, ozone is considered to be in photochemical steady-state.

1.2. Issues in Stratospheric Ozone

Not long after it was first suggested that chlorine played an important role in the ozone budget (Stolarski and Cicerone, 1974), Molina and Rowland (1974) perceived the possible consequences that increasing emissions of CFCs could have on the stratospheric ozone layer. Molina and Rowland pointed out that the CFCs, though stable in the troposphere where the flux of ultraviolet sunlight is greatly attenuated, would photodissociate much more readily in the harsher radiation environment of the stratosphere. Breakdown of the CFCs would increase abundances

of atomic chlorine and ClO radicals, which could then participate in cycles such as Reactions 1.14-1.15, accelerating ozone loss rates.

In response to the ideas of Molina and Rowland, missions such as the Upper Atmosphere Research Satellite (UARS) were planned. These satellites were designed to monitor chemistry in the mid- to upper stratosphere over the tropics and mid-latitudes. Ironically, the first signs of ozone perturbation were reported by Farman (1985) over Antarctica. His discovery marked the beginning of intense research activity in polar regions as well as in laboratories worldwide. (See, for example, Solomon et al., 1986; McElroy et al., 1986; Toon et al., 1986; Crutzen and Arnold, 1986; Tolbert et al., 1987; and the special issues of the *Journal of Geophysical Research*, *94*, nos. D9 and D14.) By the early 1990s, an explanation of the annual loss of springtime ozone over Antarctica had been pieced together (Solomon, 1990). In brief, the theory states during the long, dark polar winter, reactions taking place on the surfaces of polar stratospheric clouds shift atmospheric chlorine from relatively unreactive forms to much less stable forms. At the same time, heterogeneous reactions on the cloud particles shift atmospheric nitrogen in the opposite direction, from reactive to reservoir species. The reservoir nitrogen, HNO_3, may remain dissolved in the cloud particle. Over the Antarctic, where winter temperatures drop to extremely low values and the cloud particles grow to large sizes, some reactive nitrogen may be carried permanently out of the stratosphere by particle sedimentation. In spring, when sunlight returns to the region, the less stable chlorine molecules quickly photolyze, leading to abundances of chlorine radicals many times that ususually encountered in the stratosphere. The low levels of reactive nitrogen mean that Reaction 1.21 proceeds slowly, and the abundances of reactive

chlorine may persist for periods of days to weeks. The reactive chlorine species include atomic chlorine and ClO, which together drive rapid catalytic cycles such as those described in the previous section, destroying ozone at the rate of about one per cent per day (Manney et al., 1993).

Work continues on many issues concerning the annual loss of ozone over Antarctica. For example, the tie between stratospheric chlorine abundances and Antarctic ozone loss rates was strengthened by recent data from aircraft and satellites, thus implicating chlorine in ozone hole chemistry (Waters et al., 1993). Ozone loss during Arctic spring has also been carefully monitored (Webster et al., 1993; Profitt et al., 1993; Manney et al., 1994a). The composition of the particles that make up polar stratospheric clouds is under investigation, as are the uptake coefficients for gases that react in or on the surfaces of these particles (e.g., Abbatt and Molina, 1992; Molina et al., 1993; Middlebrook et al., 1993). One important issue to be settled is how readily air flows through the Arctic polar vortex in late winter and early spring, when the winds that set up this vortex act as a barrier against large-scale mixing with mid-latitude air (Tuck et al., 1992; Plumb et al., 1994). A porous barrier could lead to the propagation of ozone-depleted air to lower latitudes. Over the Antarctic, the current consensus seems to be that mixing with mid-latitude air occurs only at the vortex edge, and that air deep within the vortex remains isolated until long into spring (Manney et al., 1994b; WMO 1995). Lastly, the chemical mechanisms that shut down the the ozone loss processes in spring are under review.

Work also continues on analysis of the chemistry of ozone over the tropics and mid-latitudes. As mentioned above, the main focus of this research has been on

identifying the various ozone loss cycles, and determining their relative importance at different times of the year and in different regions of the stratosphere. Much progress in understanding ozone chemistry was made in the late 1980s, when the importance of heterogeneous chemistry occurring on the surfaces of sulfate particles was understood (Hofmann and Solomon, 1989b). Like particles in polar stratospheric clouds, these particles provide a means to convert reactive nitrogen to the reservoir species HNO_3, thus affecting not only the NOx catalytic cycles, but also, indirectly, the chlorine and odd hydrogen cycles. Sulfate particles are ubiquitous in the lower stratosphere, but their abundances can grow by many orders of magnitude in the aftermath of a volcanic eruption forceful enough to inject clouds of SO_2 into the stratosphere. The indirect role these particles play in the ozone budget has been the subject of much research, especially in the years following the eruption of Mount Pinatubo in 1991 (Fahey et al., 1993; Kawa et al., 1993; Mills et al., 1993).

Much current research also focusses on assigning causes to the long-term decadal trends in ozone abundances observed over the mid-latitudes. As a first step, knowledge of the ozone budget has been tested in the middle and upper stratosphere, where ozone is thought to be in photochemical equilibrium. Since photochemistry, not transport, determines the the ozone distribution in this region, testing the budget here is straightforward. Early satellite observations from the late 1970s and mid-1980s showed larger abundances of ozone than predicted (Jackman et al., 1986; Natarajan and Callis, 1989). In the 1990s, new ozone observations made by UARS provided an opportunity to revisit the issue of the ozone budget. While the calculations of Crutzen et al. (1995) showed a good match with observations, those of Dessler et al. (1996) showed some discrepancies. Reasons for the different outcomes

of the two studies are not clear. It is not surprising then that much remains uncertain about the causes of the long-term ozone trends. Calculations constrained by plausible scenarios of anthropogenic chlorine emissions do not simulate the observed decline in mid-latitude ozone (Chandra et al., 1995; C. Jackman, personal communication). These calculations include simulations of heterogeneous chemistry taking place on sulfate aerosol. While chlorine is certainly implicated in the ozone loss, other possible causes are under investigation. For example, the role of bromine and the possible role of iodine in the stratospheric ozone budget are both being studied (Garcia and Solomon, 1994; Solomon et al., 1994; Avallone et al., 1995; Wennberg et al., 1996).

Still another major issue involving stratospheric ozone focusses on the possible impact that supersonic transports (also called high-speed civilian transports, or HSCTs) could have on stratospheric ozone abundances. The emissions of these aircraft include large quantities of reactive nitrogen oxides (NOy), water vapor, and SO_2 (which may be rapidly converted to sulfate aerosol). The HSCT issue, first investigated in the early 1970s (Johnston, 1971), is still the subject of much research. Over the years, atmospheric chemists have debated the magnitude and even the sign of the change in stratospheric ozone abundances that would follow the deployment of a fleet of such aircraft. One problem that chemists encounter in their attempts to resolve this issue is that transport processes in the stratosphere are not well understood, and so the ultimate fate of the HSCT emissions is not known. For example, if mid-latitude air, rich in HSCT NOy emissions, can mix with tropical air, then the upwelling motions typical of the tropics may carry the NOy-perturbed air up to the

middle stratosphere (Avallone and Prather, 1996). In this region, as noted above, the odd nitrogen catalytic cycles are thought to dominate ozone loss processes.

A last ozone issue concerns the temperature changes and radiative forcing effects that may accompany loss of stratospheric ozone or increases in greenhouse gases such as CO_2. While the net effect of stratospheric ozone loss on the earth's surface temperature is under debate, there is consensus that a thinner ozone layer would cool the stratosphere as would an increase of greenhouse gases (Ramaswamy et al., 1992; Hauglustaine et al., 1994). The chemical consequences of a colder stratosphere are currently being examined. For example, Pitari and Ricciardulli (1994) have speculated that colder temperatures over the Arctic in winter could lead to larger ozone losses there.

1.3. This Work

This work focusses on chemical processes important to ozone chemisty in the mid- and lower stratosphere. The research analyzes observations made by the Halogen Occultation Experiment (HALOE), an instrument onboard the UARS satellite. HALOE measures the abundances of a suite of gases important in ozone chemistry, including ozone itself. To solve the problem of distinguishing between chemical change and change due to transport, we make use of two tracers measured by HALOE. In brief, we use tracer analysis to "tag" each air parcel observed with an identity related to its photochemical age. To our knowledge, no previous work has followed the evolution of short-lived species over time with this system of tagging. We apply this technique of tracer analysis to two problems: first, we examine the

response of odd nitrogen and ozone to the 1991 Mount Pinatubo eruption, which injected huge quantities of sulfate aerosol into the stratosphere. This work confirms earlier predictions of the sensitivity of ozone to changes in NOx in the middle stratosphere. Second, we examine the recovery phase of the Antarctic ozone hole during spring. The second work shows how reactive chlorine may be quickly converted to the reservoir species HCl in the aftermath of severe ozone depletion, putting an end to further ozone loss.

CHAPTER 2

THE DATA SET

Planning for HALOE began in 1975, shortly after Rowland and Molina (1974) first suggested that increasing emissions of CFCs could harm the stratospheric ozone layer. In the early 1980's, HALOE was chosen as one of ten instruments to be included on UARS. The satellite was finally launched in September 1991, and the instrument began making measurements that October (Russell et al., 1993a). As of this writing, HALOE continues observations.

HALOE takes advantage of the geometry of occultation to look through the atmosphere toward the sun at local sunrise and sunset. (See Figure 1.) The instrument determines the abundances of seven gases — ozone, NO, NO_2, HCl, HF, CH_4, and H_2O — by measuring the absorption of infrared sunlight within specified wavelength intervals. These seven gases were carefully chosen. Measurements of ozone provide information on long- and short-term trends of this important molecule. Observations of NO and NO_2 are useful since these radicals play direct and indirect roles in the ozone budget. Observations of CH_4 together with those of H_2O can be used to derive abundances of OH, another radical important in the ozone budget. The molecule HCl was chosen as part of the observation set since it is a reservoir of atmospheric chlorine. Since all HF in the stratosphere derives from CFCs, HALOE measurements of HF can provide information on the influx of CFCs up through the tropopause. Tracking HCl and HF together can tell us how much the chlorine

content of the stratosphere has increased due to increasing emissions of the CFCs. In addition, HF and CH_4, both very long-lived molecules with lifetimes on the order of years through much of the range of HALOE, serve as useful tracers of atmospheric motion.

Concentrations of an eighth molecule, CO_2, are also measured. As is described below, the measurements of CO_2 provide a means to determine the altitude grid of the profiles, as well as atmospheric temperature and pressure.

In the following sections, I discuss in further detail the following topics: (1) observation geometry and geographic coverage, (2) measurement techniques, (3) determination of pressure and temperature, (4) sources of error, and (5) efforts to validate the measurements.

2.1. Observation Geometry and Geographic Coverage

UARS circles the globe 15 times every 24 hours in an orbit inclined 57 degrees to the equatorial plane. During occultation, when the atmosphere comes between the satellite and the sun, HALOE's telescope aims toward the sun and obtains a vertical scan of the atmosphere. The time of the measurement coincides with sunrise or sunset at the tangent point on the earth's surface. The instrument makes about 30 scans a day, corresponding to 15 sunrise and 15 sunset events. Figure 1 shows the geometry of the solar occultation experiment. HALOE observations range from the lower stratosphere up to about 150 km. For those species with insignificant concentrations in the mesosphere and thermosphere, HALOE profiles reach an upper limit of about 50 km. Below the tropopause, water vapor and clouds

cause considerable interference in the measurements. The vertical resolution of the instrument ranges from 2 to 4 km, depending on the channel, and the horizontal resolution is about 300 km along the limb.

Since the earth is turning slowly during the course of a day's measurements, the sunrise measurements for each day fall at different locations along a narrow latitude band, as do the sunsets. In addition, the orbit of the satellite precesses slowly along the earth-sun line, with one complete revolution around the earth-sun line taking about 8 weeks. This precession enables the instrument to sample sunrises and sunsets within a different latitude band each day. Precession of the satellite's orbit together with the earth's rotation and revolution about the sun result in a complicated measurement pattern that spirals up and down the earth. Figure 2 shows the measurement pattern for the first 30 days of operation, from October 10, 1991, to November 11 of that year. The circles represent sunrises and the crosses, sunsets. As can be seen from the plot, the sunrise and sunset measurements during this time period together covered most of the globe, from about 55 N to 80 S. It is also apparent in the plot that the measurement points tended to cluster at high latitudes.

To derive vertical profiles of the species measured at local sunrise and sunset, an "onion peel" method is employed. The method takes advantage of the curvature of the atmosphere to build a profile at the tangent point. To understand this method, it is helpful to imagine the atmosphere divided up into very thin shells or layers. The onion-peel method rests on the assumption that the concentration of each gas measured is uniform across each thin shell. At the top of a HALOE scan, the viewing limb crosses through shells containing little or no target gas. As

the instruments scans deeper into the atmosphere, the viewing limb finally reaches the uppermost shell of the gas — that is, the first shell that contains measurable quantities of that gas. At that time, nearly all of the viewing limb crosses shells in which where the species is not present, and the absorption signal is due entirely to the target gas located at the tangent point. A calculation to determine the concentration of the target gas at the tangent point may then be performed. A little lower in the atmosphere, the limb passes through the empty shells, part of the uppermost shell, and a small increment of a new shell at the tangent point. Since the target gas concentration of the uppermost shell is now known, the distribution of the gas along the limb can be determined together with the concentration of the new shell at the tangent point. In this way, working increment by increment from higher altitudes to lower ones and constructing distributions of gases along each viewing limb, vertical profiles of each gas can be obtained.

The solar occultation technique has several advantages over nadir-viewing instruments that may depend on, for example, radiative emission of molecules. First, the abundance of the absorbers along the limb path is 30 to 60 times that along the viewing path of a downward-looking instrument. The thick optical depth enables the instrument to measure with greater accuracy molecules in small abundance such as NO or NO_2. Second, the occultation geometry also allows for higher vertical resolution. Third, calibration of the instrument can easily be made by pointing the instrument toward the sun during that part of the satellite's orbit when no atmosphere intervenes between the instrument and the sun. Lastly, the solar occulation technique requires somewhat less precise knowledge of atmospheric temperature than do

techniques relying on radiative emission. Radiative equilibrium in the atmosphere is not a necessary condition for observation.

The technique also has several disadvantages. To begin with, the assumption that each thin shell of the amosphere has a uniform concentration can be flawed. In regions of high horizontal gradients, the concentrations of gases across the shells may vary considerably. For most molecules under most conditions, however, errors arising from this assumption are minimal since the decreasing density of the atmosphere with height means that the contribution to the signal is usually greatest at or close to the tangent point. The uniform-shell assumption leads to greatest error for those molecules that have a diurnal cycle — NO and NO_2 in this case. During sunset, NO converts rapidly to NO_2; at sunrise, the opposite takes place. While no part of the observing limb lies in darkness, the solar zenith angle varies along the limb, giving rise to distributions of NO and NO_2 that are not symmetric about the tangent point. To take this asymmetry into account, the measurements of NO and NO_2 are adjusted using known chemical theory (Boughner et al., 1980). Above about 30 mb, the adjustment is small, resulting in changes in NO or NO_2 mixing ratios of less than 5 per cent. Below 30 mb, the adjustment is much greater, resulting in changes up to 50 per cent. The larger adjustment at lower altitudes is necessary since in this region the viewing limb crosses through so many layers of atmosphere, including layers containing large abundances of NO and NO_2.

Another disadvantage of the solar occultation technique is that on any given day it provides information over only a limited part of the globe. Figure 3 shows the daily average latitude of sunrise and sunset measurements during late spring and early summer of 1992. Again the circles represent sunrise observations,

and the crosses, sunset. As is clear from the plot, a picture of the atmosphere as a whole must be pieced together from a succession of measurements. This piecemeal approach to observation presents less of a problem when tracking short-term trends at high latitudes during those intervals when the instrument repeatedly samples the same region several days in a row.

2.2. Measurement Techniques

HALOE measures the abundances of trace gases in the atmosphere via two methods — the gas filter correlation method and broadband radiometry. Both methods involve measuring the absorption of infrared sunlight taking place in the atmosphere within certain narrow wavelength intervals. The wavelength intervals chosen are spectral regions where the target molecules absorb strongly. The central wavelengths of these intervals range from 2.452 microns for HF to 9.852 microns for ozone; bandwidths range from 15 cm^{-1} for NO_2 to 100 cm^{-1} for ozone. With independent knowledge of the absorbtion spectra of these molecules, one can calculate the distribution of each species present along the limb. The gas filter correlation method is the more sensitive of the two methods, and is used to measure NO, HCl, HF, and CH_4. Broadband radiometry is used for ozone, NO_2, H_2O, and CO_2. Both methods are discussed in greater detail below.

HALOE measures the abundances of all eight traces gases simultaneously during sunrise and sunset events. Sunlight entering the instrument's telescope is split by a chopper that is gold-plated and polished (and thus highly reflective) on one side. Half the solar energy is reflected off the chopper toward the broadband

radiometers, and half is directed toward the gas filter correlation channels. Figure 4 shows the layout of the optical train. Beam splitters, marked BS in the diagram, route the sunlight to the different components. Broadband filters, labeled BF, cut out undesired wavelengths of light so that the energy reaching each of the detectors belongs to a narrow wavelength interval, between 44 and 110 cm^{-1} in width. The central wavelengths of the intervals measured by the eight channels are marked on the diagram. For example, the central wavelength for the NO channel is 5.263 microns.

2.2.1. Gas filter correlation technique

The absorption spectra of many molecules in the atmosphere overlap to some degree, and isolating the absorption bands of one species can be difficult. For example, CH_4 is a major interfering species in the absorption spectra of HCl. The problem is especially acute since CH_4 is 1000 times more abundant in the atmosphere than is HCl. Filtering out such interferences requires special techniques. It should be kept in mind that the detectors on HALOE "see" an entire wavelength interval at once; the instrument is not capable of scanning slowly through an interval, wavelength increment by increment.

To overcome the problem of interfering species, HALOE employs the gas correlation method. (See Figure 5a and b.) In this method, incoming sunlight in each channel is split into two beams. One beam passes through a reference cell containing the target gas and then on to a detector; the other beam passes through a vacuum and thence to the detector. Calibration takes place once each orbit, when

the satellite travels between the earth and the sun, and the instrument can look directly toward the sun, without any atmosphere intervening. At this time, the detector at the end of the gas-cell path records the transmission of sunlight through the cell:

$$T_{cell} = e^{-\tau_g} \tag{2.1}$$

where τ_g is the effective optical depth of the cell integrated over the wavelength interval. At the same time, transmission through the vacuum path, T_{vacuum}, is, of course, unity. A gain factor G is then applied to the signal arising from the gas-cell path so that transmission through the two paths balance:

$$G\,T_{cell} = T_{vacuum} = 1. \tag{2.2}$$

During occultation, when the instrument encounters the atmosphere in its view toward the sun, the transmission of sunlight along the two paths changes. The detector at the end of the vacuum path sees the attenuation of infrared sunlight due to the target gas within the atmosphere as well as that due to interfering gases:

$$T_{vacuum} = e^{-\tau_a}\, e^{-\tau_i}, \tag{2.3}$$

where τ_a is the optical depth of the species of interest and τ_i is the optical depth of the interfering species. The detector at the end of the gas-cell path, on the other hand, sees a different transmission. Since the sunlight that travels this path is already strongly attenuated by the gas enclosed inside the reference cell, the detector cannot, in fact, see any additional absorption taking place due to the target species within the atmosphere. (Absorption of sunlight is linear with absorber abundance

only in the limit of very small concentrations of absorbing material.) Within the cell, absorption processes become saturated — that is, the incoming sunlight excites the gas cell molecules to higher vibrational levels, but the relaxation processes taking place cannot keep up with the continued influx of energy. The detector in the gas-cell path can, however, monitor the attenuation of sunlight due to interfering species since absorption within these bands is *not* saturated. Transmission through the gas-cell path may therefore be written:

$$T_{cell} = G\, e^{-\tau_g}\, e^{-\tau_i}. \tag{2.4}$$

Abundance of the species of interest along the limb may be calculated by taking the ratio of the difference in transmission along the two paths to the transmission along the vacuum path:

$$\frac{T_{cell} - T_{vacuum}}{T_{vacuum}} = \frac{G\, e^{-\tau_g}\, e^{-\tau_i} - e^{-\tau_a}\, e^{-\tau_i}}{e^{-\tau_a}\, e^{-\tau_i}} \tag{2.5}$$

$$= 1 - e^{-\tau_a} \tag{2.6}$$

$$= 1 - e^{-\int \rho(l)\, \sigma(l)\, dl}. \tag{2.7}$$

Here ρ is the density of the absorbing species, σ is the cross section of the species, and dl is a horizontal increment along the limb. The gas cell in this way acts as filter to remove the effects of the interfering gases within the wavelength interval, even when absorption due to the interfering gas is many times greater than that due to the species of interest.

A slightly different set-up is used to measure HCl. Since CH_4 absorbs so strongly in the HCl wavelength region, an extra cell containing CH_4 intercepts the sunlight before it is split into the HCl gas-cell path and the vacuum path (Figure 5b).

In this way, a significant part of $e^{-\tau_i}$ is pulled out of the subtraction in the numerator on the righthand side of Equation 2.6, and the ratio on the lefthand side of the equation is calculated with greater accuracy.

2.2.2. Broadband radiometry

Measurement of relatively abundant species in the atmosphere can be made more simply than the above method. Both ozone and H_2O are present in large enough quantities and absorb so strongly within their specified wavelength intervals that under most conditions we can assume that the absorption taking place within the intervals is due entirely to ozone or to H_2O. In other words, the absorption due to interfering gases in these channels is minimal, and a simpler method of measurement, broadband radiometry, may be employed. (See Figure 5c.) A third gas measured by broadband radiometry, NO_2, is not in fact present in large quantities in the atmosphere, but under normal conditions this gas is the dominant absorber in the spectral region chosen. Only water as a minor but significant interferent.

In broadband radiometry, the detectors are first calibrated by measuring the intensity of sunlight during that time of the orbit when no atmosphere lies between the satellite and the sun. The ratio of that intensity, I_0, to the intensity of light attenuated by the atmosphere during occultation gives the abundance of the absorbing gas along the limb:

$$\frac{I_0\, e^{-\tau_a}}{I_0} = e^{-\tau_a} \tag{2.8}$$

$$= e^{-\int \rho(l)\, \sigma\, dl}. \tag{2.9}$$

Since H_2O and CH_4 absorb in the same wavelength region as NO_2, the abundance of these interfering gases along the limb are first calculated and the effect of these abundances on the NO_2 signal determined. In this way, the absorption due solely to NO_2 may be evaluated.

2.2.3. Measuring pressure and temperature

HALOE measurements of CO_2 provide a means to determine the pressure and temperature profiles for each sunrise and sunset event, and to assign an altitude to each data point. The algorithms developed to calculate these variables take advantage of the fact that CO_2 is extremely well-mixed througout much of the atmosphere, with a nearly constant mixing ratio of 350 ppm.

As a first step, the altitude of each data point in a profile is estimated from flight path information together with the apparent oblateness of the sun at the time of measurement. To determine the altitude with greater certainty, we next make use of measurements supplied by the National Meteorological Center (NMC). In the 29-39 km region, the measured absorbance of sunlight by CO_2 at 2.8 microns at each estimated altitude gridpoint is compared to the CO_2 absorbance calculated from NMC pressure and temperature profiles. The 29-39 km region was chosen as one in which both HALOE and NMC make measurements with reasonable accuracy. Differences between the observed and calculated absorption are minimized by adjusting the estimated altitude grid of the HALOE observations. Once the two CO_2 profiles match, the altitude grid of the HALOE data between 29 and 39 km is known, as well as the "sink rate" of HALOE observations — that is, the distance up

or down in the atmosphere the HALOE observations shifts per increment of time. Since the sink rate is nearly constant during an event, the altitude of every data point may be easily determined by extrapolation from the 29-39 km region.

Next, knowledge of the absorption due to CO_2 at 2.8 microns allows us to calculate the concentration of CO_2 along the tangent profile. Since the mixing ratio of CO_2 is nearly constant up to about 85 km, a profile of total air density is readily calculated up to that altitude. Some adjustment of the total air density is made to take into account the increasing abundance of CO_2 due to increasing emissions of hydrocarbons at the earth's surface. Lastly, profiles of pressure and temperature up to 85 km can be constructed using the hydrostatic approximation and the ideal gas law. Above 85 km, a model based on climatology is used to determine these quantities.

2.3. Sources of Error

Sources of random error in the HALOE observations of trace species include instrument noise, sun-tracker jitter, and atmospheric temperature uncertainties. Uncertainty in temperature leads to uncertainty in interpreting the absorption spectra. Random error may also propagate from one channel to another when calculating the effects of interfering gases. Sources of systematic error include uncertainty in absorption line strengths and the reference pressures calculated with CO_2. Other sources of systematic error include the error introduced when calculating the variation of the diurnally changing species NO and NO_2 along the viewing limb. In regions of steep horizontal gradients, systematic error may also be caused by as-

suming that the distributions of the longer lived species are symmetric along the viewing limb.

To evaluate these errors, workers at NASA Langley performed a Monte Carlo analysis which repeatedly simulated the retrieval of mixing ratios, introducing a new set of errors with each iteration. These calculations predict 10 to 15 per cent error in all species between about 30 and 1 mb. Above 1 mb, concentrations fall rapidly with height, increasing signal-to-noise ratios and thus error. Below 30 mb, retrieval of the mixing ratios is made difficult by the increasing opacity of the atmosphere along the limb and, for some species, small concentrations typical of the lower stratosphere. Under normal conditions, per cent error for most molecules above 1 mb and below 30 mb ranges from 20 to 100 per cent. During the early years of the mission, however, observations at the lower altitudes were made especially uncertain by the presence in this region of large abundances of sulfate aerosol leftover from the June 1991 eruption of Mount Pinatubo. Under heavy aerosol conditions, relative error could increase to several hundred per cent for NO_2, measured by the broadband radiometry method. Meausrements of the other broadband-radiometer species were also affected, though not to the same degree. Using information from the gas-correlation channels, transmission in the NO_2 channel was corrected to take aerosol absorption into account.

2.4. Validation Efforts

Efforts were made to validate the HALOE data set — that is, we attempted to judge the quality of the data by comparing HALOE data to measurements made

by other instruments and by performing consistency checks. Our group focussed on validating observations of HALOE NO and NO_2.

2.4.1. Comparison to other measurements

I present here a brief overview of the work done to compare HALOE NO and NO_2 to observations of these molecules made by other intstruments. The reader is referred to Gordley et al. (1996) for a more detailed description of this effort.

Because of the short chemical lifetimes of NO and NO_2 (on the order of seconds), stringent requirements were made on the time and space coincidence of pairs of observations. For example, Figure 6 compares a HALOE NO_2 profile to a profile measured by a balloon-borne interferometer (Toon, 1991). The HALOE measurements were made September 25, 1993, and the balloon measurements, the next day. The two profiles are located within 1 degree latitude and 0.5 degrees longitude of each other, at about 34 N. Observations made by the interferometer are represented by diamonds; HALOE measurements are denoted by stars. The two profiles show relatively good agreement, though HALOE observations fall short of the balloon observations at the maximum and below about 40 mb. A similar comparison for NO is shown in Figure 7. Again the two profiles match fairly well.

As a second example, Figure 8 compares sunrise HALOE NO_2 total column amount to measurements made by a ground-based spectrometer at Fritz Peak Observatory in Colorado for the years 1992 and 1993. Figure 9 shows a similar comparison for sunset data. In both plots, the circles and triangles represent HALOE data for 1992 and 1993, respectively. The stars and dashes represent the two years

of ground-based measurements. All of the HALOE data included in the two plots fall within 6 degrees latitude and 12 degrees longitude of Fritz Peak, located at 40 N and 106 W. The plots show the seasonal maximum for both years occurs in summer, when HNO_3 photolysis is fastest, and more NO_2 forms. For both sunset and sunrise measurements, HALOE tends to show low amounts of column NO_2 relative to the Fritz Peak measurements.

Analyzing several such comparisons for NO and NO_2, we came to the following conclusions. First, both HALOE observations of both NO and NO_2 show relatively good agreement with observations made by other instruments. HALOE NO_2 in the lower stratosphere, below about 40 mb, tends to be somewhat low, perhaps due in large part to an overcorrection for sulfate aerosol absorption. (See Section 2.3). Another possible source of error at low altitudes may be uncertainties in the CO_2 retrieval in a region where significant CO_2 line broadening occurs. Errors in interpreting the CO_2 signal would lead to errors in calculating total air density and pressure. For NO_2, whose mixing ratio changes rapidly with height in the lower stratosphere, accurate knowledge of air density and pressure is critical in the retrieval. It is conceivable that an underestimate of NO_2 in the lowest few kilometers of the stratosphere may have led to the low NO_2 column amounts noted in Figures 8 and 9.

2.4.2. Sunrise to sunset comparisons

An important internal consistency check on HALOE NO and NO_2 data may be done by comparing sunrise and sunset profiles at times in the mission when

the two narrow latitude bands of sunrise and sunset observations overlap. This coincidence of sunrise and sunset measurements occurs about 6 to 7 times a year, usually over low latitudes. Comparing measurements of NO and NO_2 at sunrise and sunset requires some care since the concentrations of both species are changing rapidly at these times. During the day, a set of fast chemical reactions establishes photochemical equilibrium between the two species. But at sunset, the reactions that during the day convert NO_2 back to NO — i.e., the photolysis of NO_2 and the reaction of NO_2 with atomic oxygen — slow down and finally cease. NO concentrations quickly fall by reaction with ozone, and NO_2 quickly rises. At sunrise, as NO_2 once again begins to photolyze and the concentrations of atomic oxygen increase, NO abundances rapidly recover and NO_2 declines. Because of the fast chemistry occuring between NO and NO_2 at sunrise and sunset, it is best for this task to look at the sum of the two species, $NO+NO_2$.

Still another factor to consider in making sunrise to sunset comparisons is that during the night NO_2 is slowly converted to N_2O_5 through the reactions:

$$NO_2 + O_3 \rightarrow NO_3 + O_2 \tag{2.10}$$

$$NO_2 + NO_3 + M \rightarrow N_2O_5 + M \tag{2.11}$$

where M is any molecule. The rate-limiting step in this pair of reactions is Reaction 2.10, and NO_3 is considered to be in steady state. The rate of decay NO_2 during the night may then be written:

$$d\,ln[NO_2]/dt = -2k[O_3] \tag{2.12}$$

where the reaction rate k is a function of temperature, T (DeMore et al. 1992),

$$k = 1.2 \times 10^{-13} exp(-2450/T) \ cm^3 s^{-1}. \tag{2.13}$$

Using HALOE O_3 data and temperatures, one may calculate the expected sunrise $NO+NO_2$ values from the measured $NO+NO_2$ at sunset. The predicted sunrise concentrations can then be compared to the sunrise sums of $NO+NO_2$ as measured by HALOE.

In carrying out these comparisons, pairs of sunrise and sunset events were chosen such that the sunrise event took place the morning following the sunset event in a location not more than 3 degrees latitude and 10 degrees longitude distant from the sunset. Ozone values were taken from the sunset events as were the temperature profiles. Figure 10 shows a sample comparison of HALOE sunrise to model sunrise. The data are from November 9, 1993, at about 17 N. It can be seen in Figure 10 that the match between predicted and measured $NO+NO_2$ at sunrise is quite good. This agreement shows the internal consistency of HALOE's NO and NO_2, as well as the instrument's ozone measurements.

The above calculation was performed for many pairs of sunrise and sunset profiles with similarly good results, especially over low latitudes. For the few pairs at mid-latitudes, agreement was not as good for reasons that are unclear. Above about 1 mb, HALOE measures little or no NO_2 at sunrise or sunset. In the mesosphere at night, NO converts to NO_2 but the NO_2 photolyzes extremely rapidly once daylight arrives. Insufficient ozone is available at these altitudes to convert significant amounts of nighttime NO_2 to N_2O_5. Therefore it comes as a surprise that HALOE tends to measure low NO at sunrise as compared to sunset. This mismatch

of sunrise to sunset at the higher altitudes may be due to some unknown, nighttime chemical process or perhaps simply to problems measuring NO abundances at these altitudes where concentrations are very small.

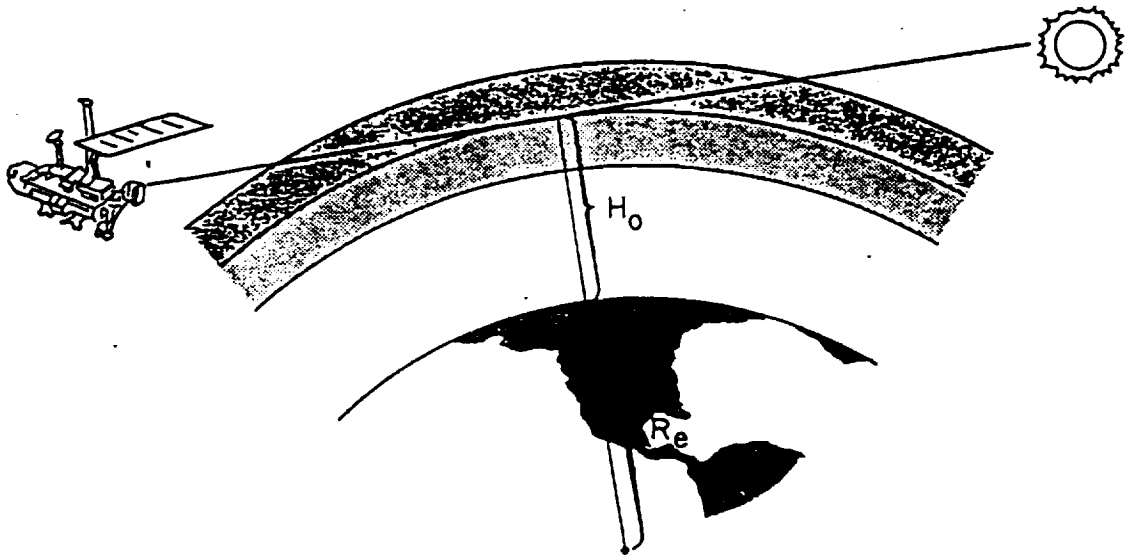

Figure 1. Solar occultation experiment geometry.

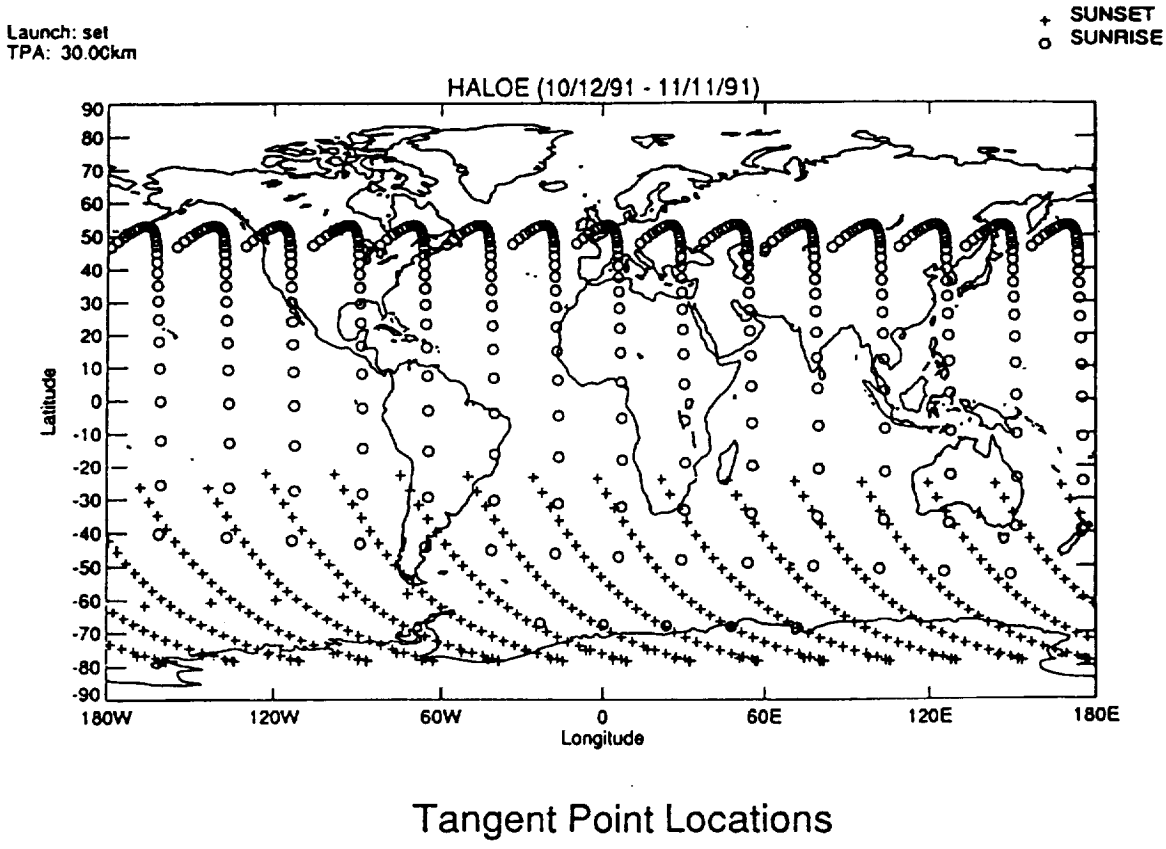

Figure 2. Latitude of HALOE observation for the first month of operation. The circles represent sunrise; the stars, sunset.

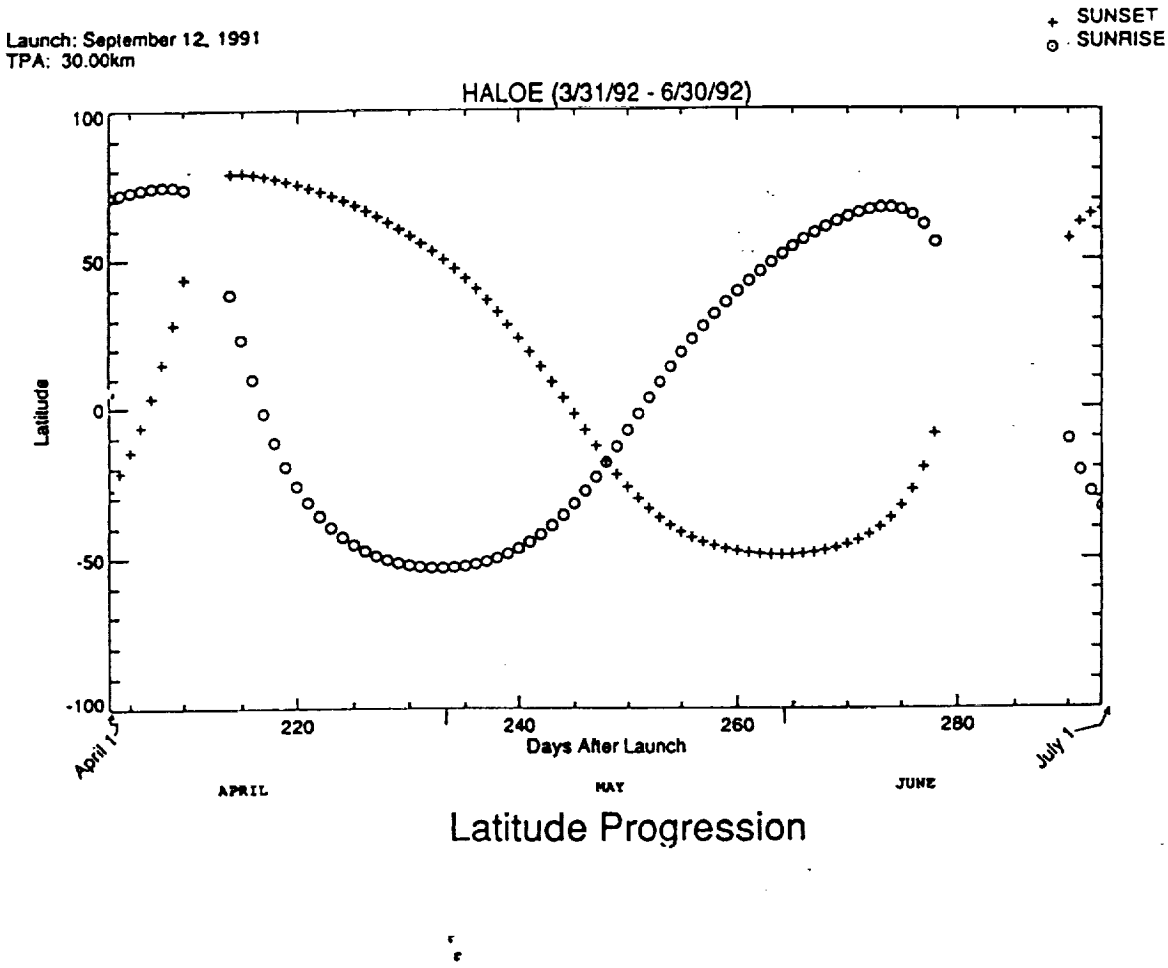

Figure 3. Average daily latitude for late spring and summer of 1992. The circles represent sunrise; the stars, sunset.

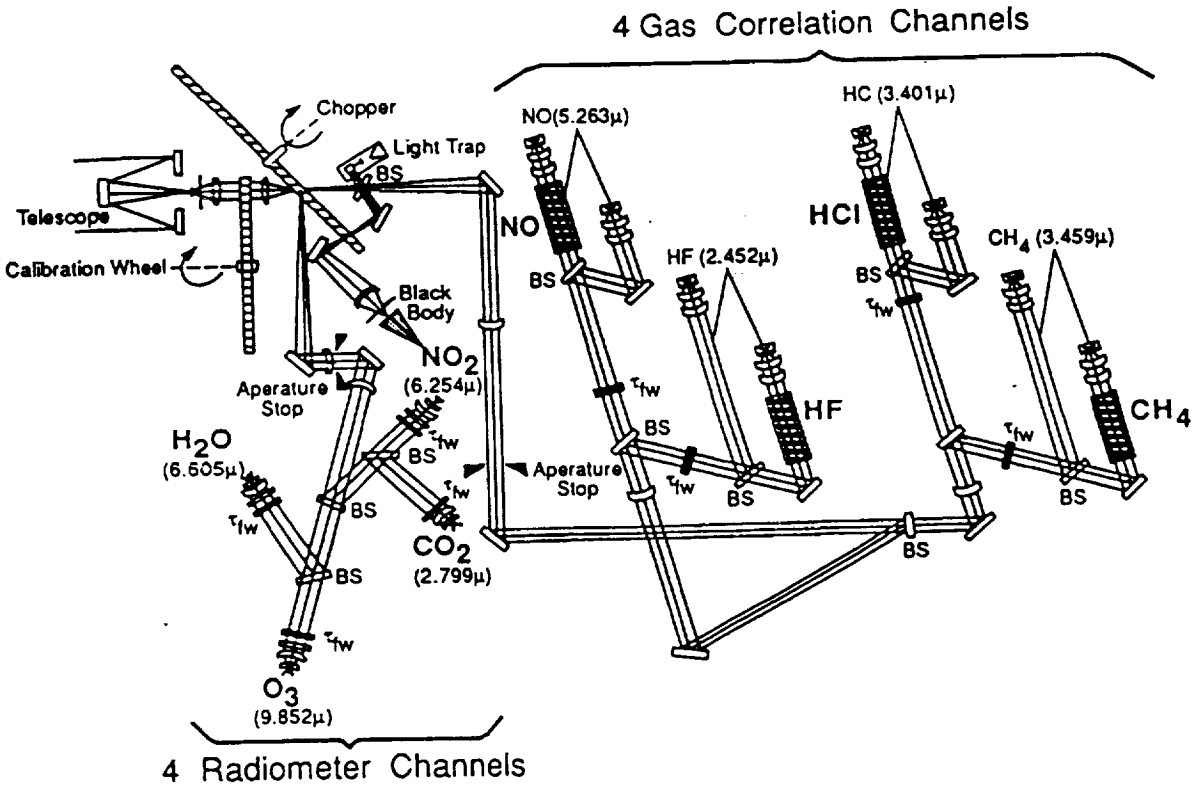

Figure 4. HALOE optical diagram (Russell et al., 1993a).

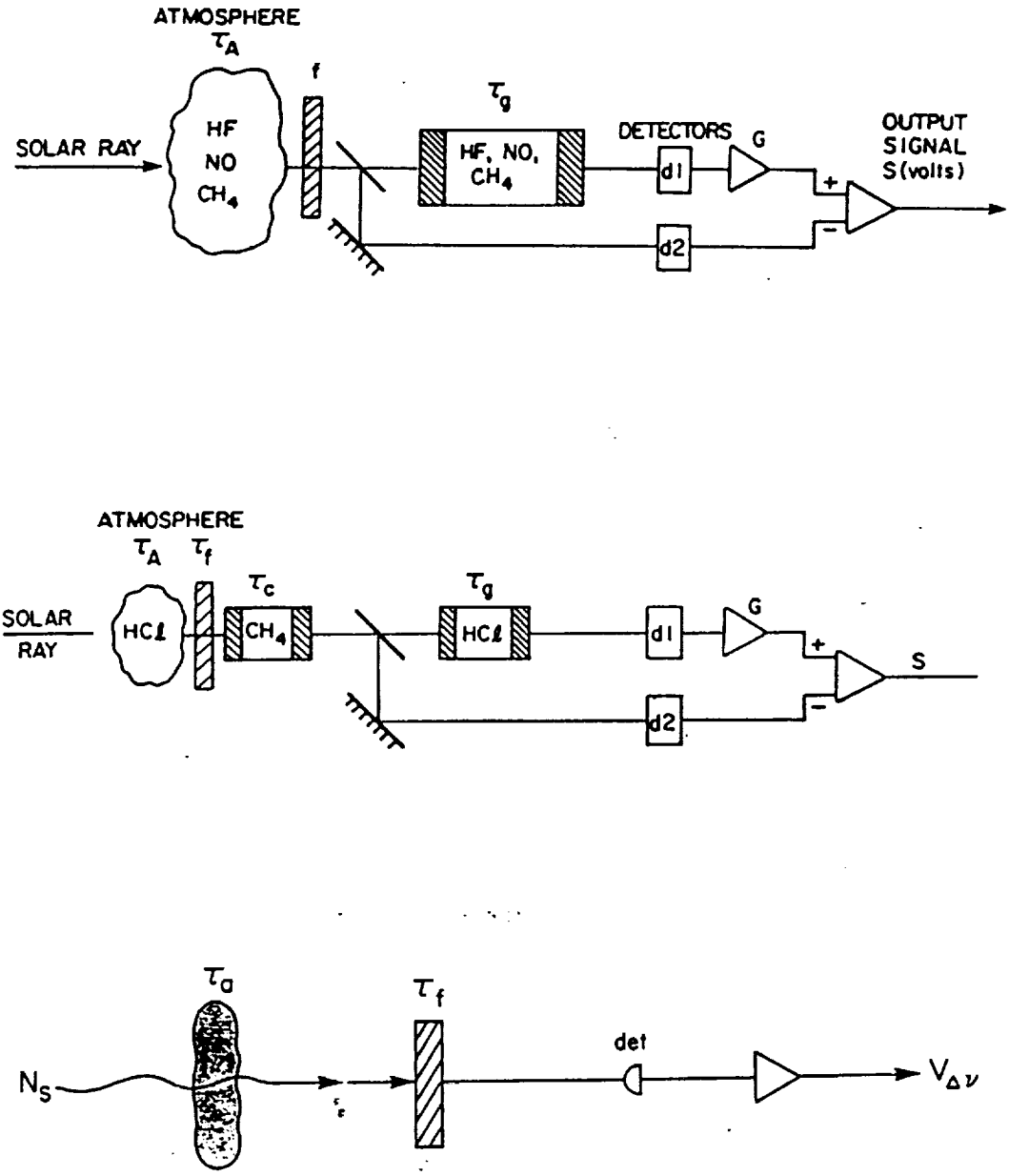

Figure 5. HALOE measurement techniques. (a) Gas filter correlation technique, (b) Special gas filter correlation technique for HCl, (c) Broadband Radiometry (Russell et al., 1993a).

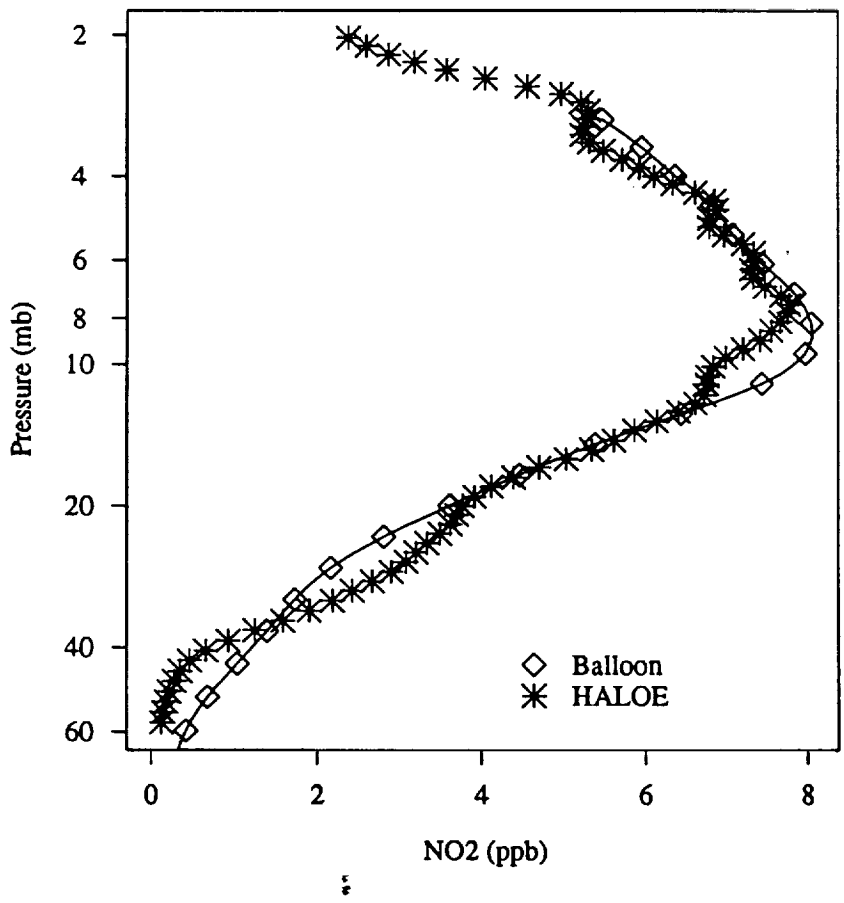

Figure 6. Comparison of balloon NO_2 measurements to HALOE NO_2. The stars represent HALOE data, and the diamonds, balloon data. HALOE data are from Sept. 25, 1993, at 33 N and 110 W. Balloon data are from Sept. 26, 1993, at 34 N and 110 W.

Comparison of Balloon Observations to HALOE

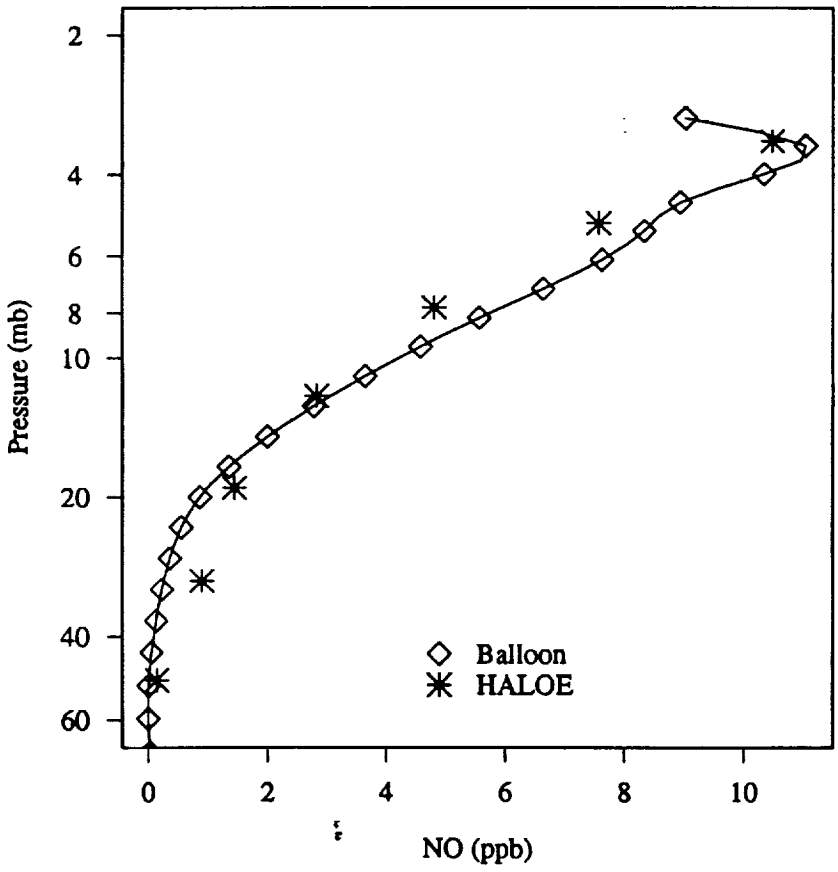

Figure 7. Same as preceding figure, but for NO.

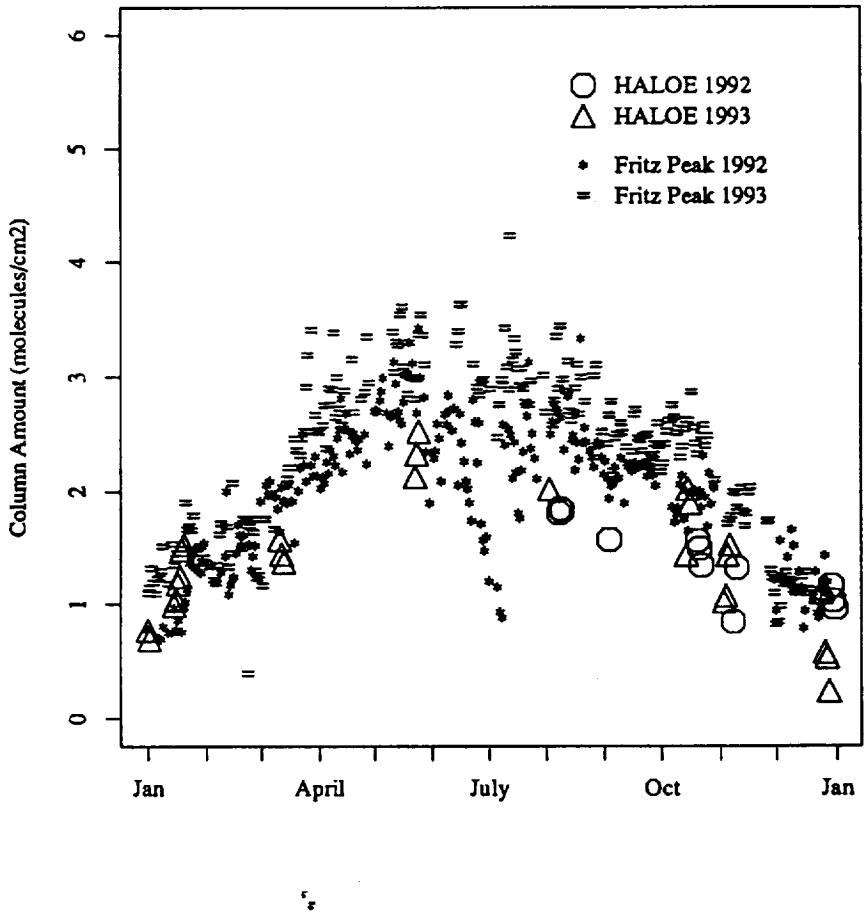

Figure 8. Ground-based observations of total column NO_2 at sunrise compared to HALOE total column NO_2. Column abundances are in mol/cm$^2 \times 10^{15}$. The circles and triangles represent HALOE data from 1992 and 1993, respectively. The stars and equal signs denote the ground-based data for the two years. For location, see text.

Sunrise Column NO2 in 1992-1993

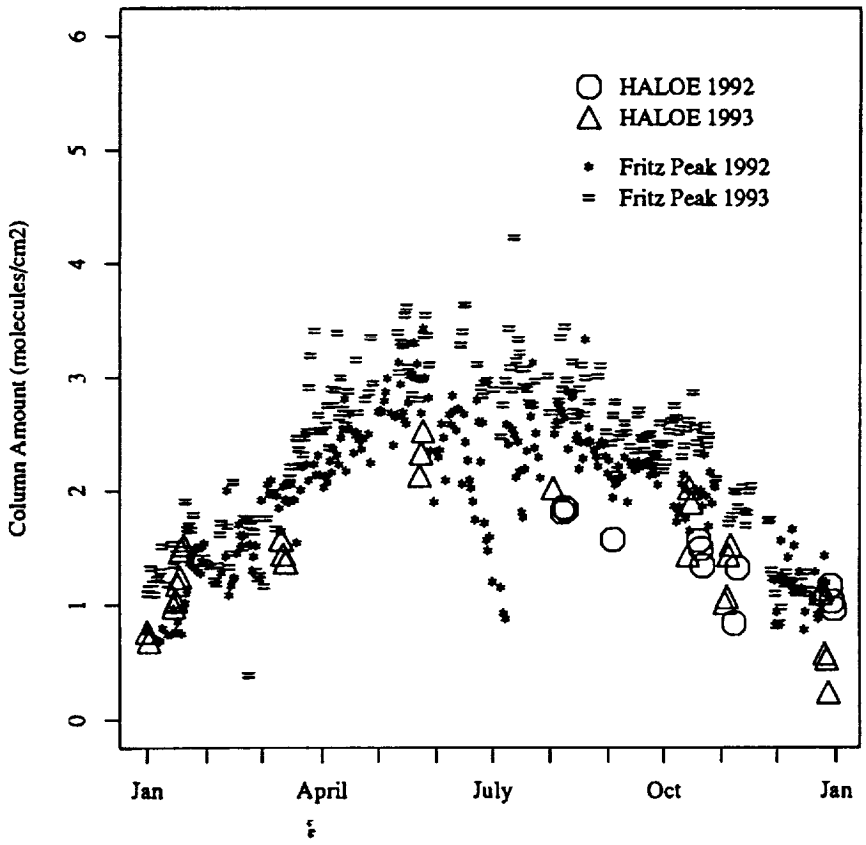

Figure 9. Same as preceding figure, but for sunset.

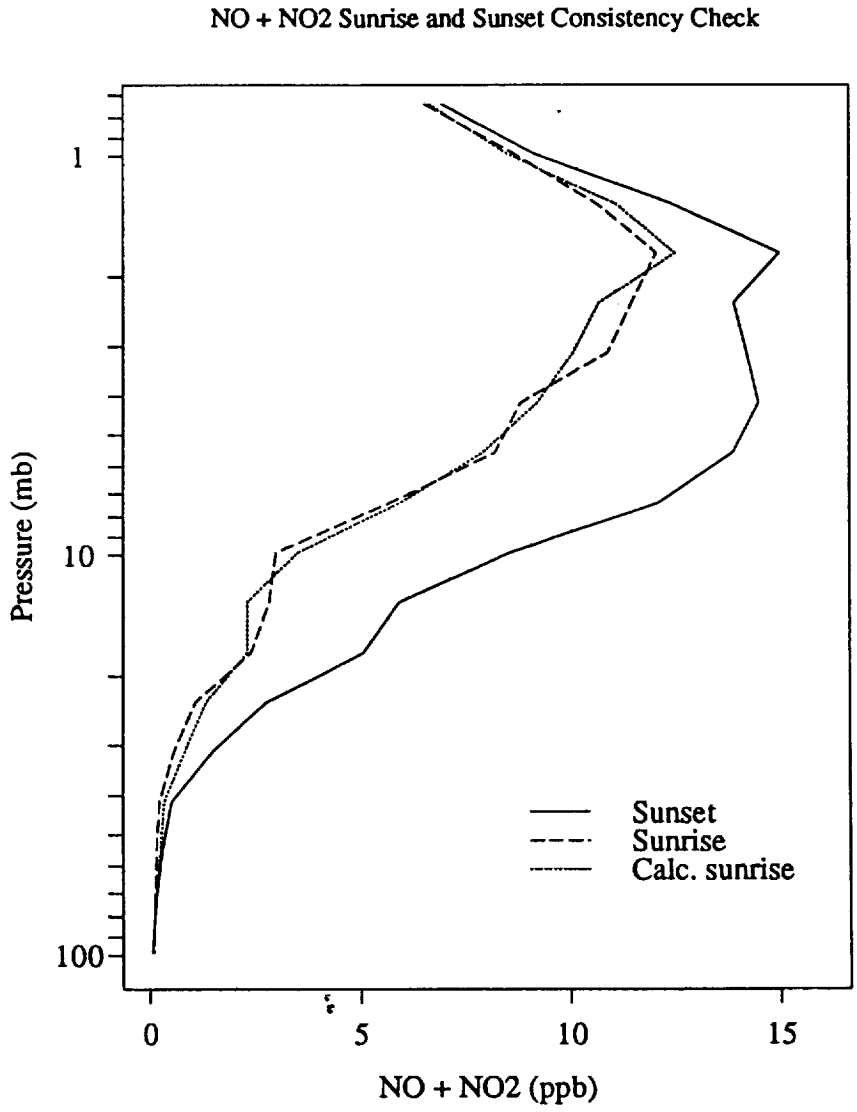

Figure 10. Comparison of model to HALOE sunrise $NO+NO_2$ profiles. The model was initialized with HALOE sunset observations of ozone, NO_2, and NO from the previous day. Data are from November 9, 1993, at about 17 N.

CHAPTER 3

MODELING STRATOSPHERIC CHEMISTRY

The basic goal of most chemical modeling efforts is to predict the evolution of chemical species over time. The key equation to be solved at each timestep is the mass continuity equation:

$$\frac{\delta c}{\delta t} = P - Lc - \frac{\delta F_x}{\delta x} - \frac{\delta F_y}{\delta y} - \frac{\delta F_z}{\delta z}, \tag{3.1}$$

where c is the concentration of a species, t is time, P is the production rate of c, L is the loss rate. and F_x, F_y, and F_z are the fluxes of c in the zonal, meridional, and vertical directions, respectively. One major difficulty in solving such an equation is that it represents just one in a coupled system of partial differential equations, with each equation describing the time rate of change of a different species. The entire system must be solved simultaneously at each time step. Modeling transport processes together with chemistry also presents difficulties. In addition, in order to evaluate the photolysis rates of reactive species, the flux of solar radiation through the atmosphere must be properly calculated.

For certain problems in the stratosphere, the mass continuity equation can be simplified somewhat and some or all of the flux terms dropped. For example, if our goal is to follow the chemistry occurring within an air parcel on the time scale of days, we may in some cases neglect mixing processes and utilize a simple box model describing the chemistry evolving at a discrete point. The point may be moved over time as the parcel is advected through space. Such an approach is taken for the

study described in Chapter 6 in which our concern is to track chemical change in a parcel of air within the Antarctic polar vortex in spring. The box-model approach is especially attractive when the goal of the study is to detect atmospheric change that is due solely to chemical processes, and not due to transport. For many studies that do require taking transport processes into account, a two-dimensional model of the atmosphere suffices. This is especially true in the stratosphere, where zonal mixing occurs rapidly, on timescales of days or weeks. The rapid zonal mixing ensures that the air along a latitude band is well-mixed and that the derivative of the flux with respect to x in Equation 3.1 may be dropped. We note that in regions such as the polar vortex where the horizontal gradients of species do not coincide with latitude circles, zonal averaging may lead to large error.

For this work, we have employed two models — a box model and a two-dimensional model. The models are discussed in the next two sections. We describe the box model in fuller detail since it is used more extensively for this research.

3.1. Box Model

The box model — previously described by Logan et al. (1978), Prather and Jaffe (1990), and Salawitch et al. (1994) — contains a set of 35 chemical species and about 220 chemical reactions. The model employs a Newton-Raphson iterative method to solve implicitly for the mixing ratios of the species with short and intermediate lifetimes. Most of the reaction rate constants and absorption cross-sections in the model are taken from DeMore et al. (1992). Input parameters include a temperature profile, aerosol surface area density, latitude, and solar declination angle.

The model has a variable timestep, ranging from tens of second at sunrise or sunset when many species are changing concentration rapidly to a couple hours during the night or at midday when chemical change is slow. The model may be initialized at either dawn or noon.

3.1.1. Newton-Rafson method

The Newton-Rafson method is useful for solving nonlinear systems of partial differential equations (Press et al., 1986). To understand this method, it is helpful to consider first just one equation in the system, i.e.,

$$0 = \frac{\delta c}{\delta t} + P - Lc, \tag{3.2}$$

$$= f(c), \tag{3.3}$$

which is simply Equation 3.1 rearranged and without the flux terms. The approach for solving this equation for c involves finding the slope of $f(c)$ at some initial guess c_i, extrapolating the line given by the slope to the abscissa, and taking the value of c at the zero-crossing as the next guess, c_{i+1}. The process is then repeated with the new c_{i+1}. The Newton-Rafson method is analogous to finding the Taylor series about some point c:

$$f(c+\delta) \overset{\xi}{\simeq} f(c) + \delta f'(c) + \delta^2 \frac{f''(x)}{2} + \ldots \tag{3.4}$$

where δ is the correction to the current guess, and $c + \delta$ is the next guess. For small values of δ, Equation 3.4 $\simeq 0$, and we may neglect the higher order terms in Equation 3.4 so that

$$\delta = -\frac{f(c)}{f'(c)}. \tag{3.5}$$

In this way, the correction δ for each guess may be readily calculated.

The advantage of the Newton-Rafson method is that the trial solutions converge rapidly onto the roots of the equations. It can be shown that having determined a correction δ_i, the next correction, δ_{i+1}, is

$$\delta_{i+1} = -\delta i^2 \frac{f''(c)}{f'(c)}. \tag{3.6}$$

For *delta* normalized to an initial guess, the squared dependence in this recurrence relation means that the guesses converge quadratically onto the solution.

Taking the derivative of $f(c)$ is straightforward. For example, consider a simplified continuity equation for NO:

$$f([\mathrm{NO}]) = \frac{\delta[\mathrm{NO}]}{\delta t} - J[\mathrm{NO_2}] + k[\mathrm{O_3}][\mathrm{NO}] \tag{3.7}$$

where the brackets denote concentration, J is the photolysis rate of NO_2, and k is the reaction rate constant of O_3 reacting with NO. The first term on the righthand side of the equation represents production of NO via NO_2 photolysis, and the second term, loss via $NO + O_3 \rightarrow NO_2 + O_2$. For this continuity equation, the derivative of f with respect to [NO] can be written

$$f'([\mathrm{NO}]) = \frac{1}{\Delta t} + k[\mathrm{O_3}][\mathrm{NO}] \tag{3.8}$$

What complicates the calculation of photochemistry is that some 30 species in the model are changing with time, and the Newton-Rafson technique must be used for all these species simultaneously. In other words, roots of the partial differential equations must be found such that the solutions work for all species in the model.

Each function f_i for each species c_i may in fact be a function of many variables, such that

$$f_i(c_1, c_2, ...c_n) = 0. \tag{3.9}$$

The Taylor series expansion of f_i in the neigborhood of the set of guessed concentrations is:

$$f_i(C + \delta C) = f_i(C) + \sum_{j=1}^{n} \frac{\delta f_i}{\delta c_j} \delta c_j + ... \tag{3.10}$$

where C is the vector of concentrations and δC is the vector of corrections. If the corrections are small, $f_i(C + \delta C) \simeq 0$, and we may rewrite Equation 3.10 as

$$\sum_{j=1}^{n} A_{ij} \delta c_j = -f_i \tag{3.11}$$

where

$$A_{ij} = \frac{\delta f_i}{\delta c_j} \tag{3.12}$$

Equation 3.11 may be readily solved for the vector of corrections, δC. These corrections are then added to the guessed vector C, and the process repeated with the new set of guesses. The iteration is halted when some degree of convergence is obtained.

The model may be run in one of two modes. In the first mode, the model cycles through each model day for a specified time period and calculates the day-to-day evolution of all species over the time period. This approach is useful for tracking short-term chemical change, on the order of days or weeks. In the second mode, the model day is repeated over and until *diel steady state* is achieved — that is, until the the production and loss rates for each species integrated over the day balance

and the output gives reproducible diurnal cycles for all species. This approach is useful for determining the steady-state chemical response of the atmosphere to some long-term perturbation such as the increase in the sulfate-aerosol burden in the stratosphere that may follow an especially forceful volcanic eruption.

3.1.2. Calculation of reaction rates

As noted above, nearly all of the reaction rate constants and absorption cross-sections in the model are those recommended by DeMore et al. (1992). The absorption cross-sections for HNO_3 are those of Burkholder et al. (1993), and a quantum yield of 0.5 is used for both the $ClO+NO_2$ and the $Cl+NO_3$ channels of $ClONO_2$ photolysis (Minton et al., 1992). The input temperature profile permits calculation of total air density, assuming hydrostatic equilibrium and estimating scale heights. The total air density profile may also be constructed from an input pressure profile together with temperature. Given the local temperature and density, all the reaction rates may be calculated.

To calculate photolysis rates, first the flux of ultraviolet light through the atmosphere must be determined. The model is divided up into plane-parallel layers, and the flux through each layer is computed by considering the direct and scattered beam separately. A correction is made to take into account the sphericity of the earth's atmosphere, and for twilight the flux of light scattered over the horizon is estimated for solar zenith angles up to 96 degrees (Prather, 1974). Two absorbers of ultraviolet radiation are considered: molecular oxygen and ozone. The profile of molecular oxygen is calculated from the total air density, and the profile of ozone

density is included as input. The temperature-dependent cross-sections of oxygen are those of Minschwaner et al. (1992 and 1993).

Heterogenous chemistry in the model is carried out with rate constants given by the following (Cadle et al., 1975):

$$k_{het} = \gamma \left(\frac{SA\, v}{4} \right) \tag{3.13}$$

where γ represents the reaction efficiency (also known as the sticking coefficient), SA is the surface area of the particles per cubic centimeter of air, and v is the mean speed of the gas-phase reactant. To calculate the reaction rates of chlorine species on cold sulfate particles, the method developed by Hanson et al. (1994) is implemented.

3.2. Two-Dimensional Model

The two-dimensional model was developed by Paul Cruzen and co-workers at the Max Planck Institute for Air Chemistry in Mainz, Germany (Crutzen and Gidel, 1983; Brühl and Crutzen, 1988; Prather and Remsberg, 1993). The model calculates the chemical composition of the stratosphere and troposphere along constant pressure surfaces spaced about 2 km apart. It ranges in altitude from the earth's surface to about 62 km and has a 10-degree latitude grid. The timestep of the model is usually set to be two hours long. The model includes about 120 gas-phase and heterogeneous chemical reactions and about 50 photodissociations. Changes in chemical concentrations due to transport or chemistry are determined at each timestep. In order to determine the photolysis rates, a set of 12 radiation fields in the ultraviolet and visible range is recalculated once every 15 model days, one

field for each two-hour timestep in a day. For information on the model calculation of ultraviolet flux, see Zdunkowski (1980).

Transport of chemical species in the model is split into two parts — transport by the net mean meridional and vertical winds and transport due to what is commonly called eddy diffusion. The net mean winds, which arise from temperature gradients and diabatic heating and cooling, are calculated off-line using temperature fields and heating rates. Eddy diffusion, here referring to turbulent processes that result from wave transience and dissipation, is parameterized in the model. To minimize computational time required to calculate transport, all the short-lived species are grouped into families of species that interconvert rapidly. Then transport of the family as a whole is calculated for the timestep.

The boundary conditions for the chemistry part of the model include the ground-level sources and sinks of many gases such as N_2O, CH_4, CO_2, and the chlorofluorocarbons. At each timestep, the chemistry calculations are carried out by making photochemical steady-state assumptions or by performing implicit or semi-implicit time integrations. Families are partitioned into member species.

For a more detailed description of the model, see Crutzen and Gidel (1983).

CHAPTER 4

USING TRACERS TO TRACK CHEMICAL CHANGE

Our goal for this research is to follow chemical change in the stratosphere on timescales of weeks to years. In particular, we are looking at the response of relatively short-lived species — those with chemical lifetimes on the order of seconds to weeks — to perturbations such as an influx of sulfate aerosol. The species examined include ozone as well as members of two long-lived chemical families — the total inorganic chlorine family (Cly) and the reactive nitrogen family (NOy). To distinguish between chemical change and change due to transport in these species, we use the chemical tracers CH_4 and HF. Tracer analysis proves especially reliable when the species of interest has a short chemical lifetime but belongs to a family that is long-lived. As will be discussed below, in the case of ozone, tracer analysis is somewhat less trustworthy as a means to detect chemical change.

Our work rests on the reasonable assumption that pairs of tracers show a linear correlation over a range of altitudes and latitudes (Kelly et al., 1989; Profitt et al., 1989; Profitt et al., 1990; and Plumb and Ko, 1992). Here tracers are defined as those species or families of species whose chemical lifetimes are very long relative to their lifetimes due to tranport. Lifetimes for transport processes or chemical loss are defined as the time it takes for a process to change the concentration of a species by a factor of *1/e*. For chemical production, the lifetime is the ratio of the

concentration of the species divided by the rate of production. Two tracers that show linear correlation are said to be in gradient equilibrium, and their isopleths correspond to surfaces of rapid exchange of air parcels. The shapes of these rapid exchange surfaces are defined entirely by transport processes, independent of chemical sources and sinks. Gradient equilibrium between two species breaks down in regions where one of the species experiences a rate of chemical loss or production that is comparable in magnitude to the rate of transport processes.

4.1. Background on the NOy and Cly Families and Ozone

The two nitrogen species observed by HALOE, NO and NO_2, belong to the NOy family. This family also includes HNO_3, N_2O_5, $ClONO_2$, HO_2NO_2, and a few other less abundant species. The source for nearly all NOy in the stratosphere is N_2O, a gas emitted by biological and anthropogenic processes in the troposphere and carried to the stratosphere through the tropical tropopause. In the stratosphere, the main sink of N_2O is photolysis, which forms molecular nitrogen and atomic oxygen. But about 10 per cent of N_2O reacts with $O(^1D)$ to produce two NO radicals. The NOy family as a whole is long-lived throughout the stratosphere except at high altitudes (above about 45 km), where the photolysis of NO becomes an important NOy sink. The long chemical lifetime of the family means that transport processes play an important role in determining the distribution of NOy, and the abundance of NOy at 40 S is not invariant year after year, but may change with, for example, changing phase of the quasibiennial oscillation (QBO). We note that though the lifetime of the family as a whole is long, the lifetime of the member species against

conversion to another member of the family ranges from seconds (NO and NO_2) to weeks (HNO_3). Thus our research will focus on the chemical repartioning of the family in response to perturbations.

The Cly family — which includes HCl, $ClONO_2$, ClO, ClOH, Cl_2O_2, and Cl — is derived mainly from CH_3Cl, a natural tropospheric gas, and from anthropogenic sources — the chlorofluorocarbons (CFCs) and methyl chloroform (CH_3CCl_3). As in the case of N_2O, these source gases are transported upward through the tropical tropopause into the stratosphere where they slowly photolyze to produce Cly. Transport back across the tropopause is the only sink of stratospheric Cly. Like NOy, Cly as a group has a long chemical lifetime in the stratosphere, on the order of years. Also like NOy, the member species have short lifetimes, ranging from seconds to weeks.

Ozone in the stratosphere is produced via photolysis of molecular oxygen and destroyed via several catalytic cycles involving radicals such as NO or ClO (Wennberg et al., 1994). Production of ozone is greatest over the tropics where the flux of ultraviolet radiation is greatest. Loss processes dominate the ozone budget at high latitudes.

4.2. The Tracers CH_4 and HF

Following the arguments of Plumb and Ko (1992), we may assume that parcels containing similar abundances of a tracer, such as CH_4, also have similar abundances of the two long-lived chemical families Cly and NOy. This assumption allows us to follow the evolution of short-lived species that belong to the NOy and

Cly families — here NO, NO_2, and HCl — and to draw conclusions regarding the partitioning of Cly and NOy into member species even though not all the member species have been measured.

HALOE measures the concentrations of two long-lived species — HF and CH_4. Both species appear to be good candidates for our choice as tracer for this study. HF is derived entirely from chlorfluorocarbons (CFCs), which like the NOy source gas N_2O are emitted in the troposphere and are slowly transported to the stratosphere. Production of HF is slow, with production lifetimes on the order of months to years, and transport back across the tropopause is the only sink. CH_4, on the other hand, is itself emitted in the troposphere by both anthropogenic and natural processes. In the stratosphere, CH_4 slowly oxidizes by reaction with the radical species OH, $O(^1D)$, and Cl. Both HF and CH_4 have chemical lifetimes on the order of years in the lower stratosphere and thus may be expected to correlate or anti-correlate linearly with other long-lived species or families.

Figure 11 shows a plot of calculated NOy vs HF at various altitudes through the year at 40 S. The values were generated by the Max Planck time-dependent, two-dimensional, photochemical model (Brühl and Crutzen, 1988; Prather and Remsberg, 1993). Each loop represents 24 output points taken every 2 weeks throughout the model year. The pressures represented range from 40 to 2 mb (about 20 to 40 km). It is clear from the plot that up to about 800 ppt (10 mb), HF correlates well with NOy. Our task, therefore, will be to compare abundances of NOx in parcels that have similar abundances of tracer material — either HF or CH_4. We may assume that such parcels contain similar abundances of NOy and that any change in NOx reflects changes in the partitioning of NOy and not changes in NOy itself due

to transport. Since NO and NO_2 have short chemical lifetimes against conversion to another NOy family member, we can assume that these species are sensitive to local conditions.

Because the correlation between NOy and tracers breaks down in photochemically older air, we will exclude from our analyses air that contains more than 800 ppt of HF. In other words, using HF as a measure of photochemical age, we can assume that signficant NO photolysis has taken place in air parcels of high HF content. In the mid-latitudes, air that has reached about 40 km and has spent about 2 or 3 years in the stratosphere (Rosenlof, 1995) shows signs of the breakdown of gradient equilibrium between NOy and other tracers.

A plot similar to Figure 11 may be constructed for NOy vs CH_4, Cly vs HF, and Cly vs CH_4. As noted above, Cly has no chemical sink in the stratosphere, and the correlation between Cly and tracers continues through high altitudes. Thus we can assume that parcels containing similar abundances of HF or CH_4 also contain similar abundances of Cly. Any changes in HCl in these parcels over time must then be due to repartitioning of the Cly family. Like the NOy family members, Cly species have short lifetimes and can be expected to respond readily to local conditions.

Tracking change in ozone poses special difficulties. In the regions focussed on in this study, ozone loss cycles dominate the ozone budget. These cycles proceed more rapidly in air that is photochemically older and therefore contains greater abundances of radicals. Thus ozone anti-correlates with HF and correlates with CH_4 in these regions. The long chemical lifetime of ozone, however, means that the response of ozone to perturbations is usually sluggish. While the NOy and Cly families

respond fairly rapidly to local conditions, ozone may take months. Nonetheless, as we will show below, tracer analysis can in some cases supply interesting information about changes in ozone concentrations due to chemical processes.

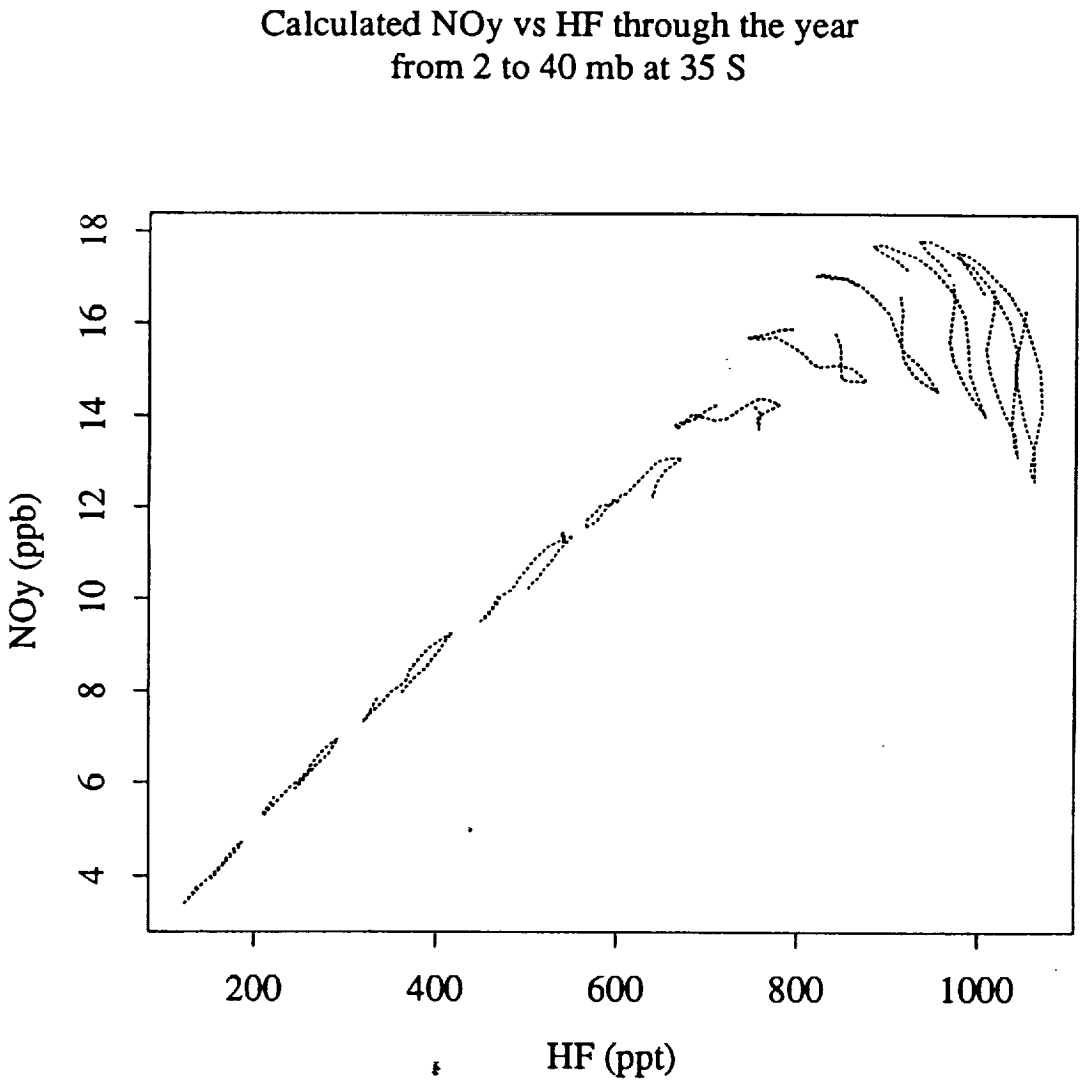

Figure 11. Annual cycles of NOy vs HF calculated by a two-dimensional, photochemical model for a range of altitudes (40 to 2 mb). Each loop represents a different altitude and connects the data points calculated every 15 days throughout the model year.

CHAPTER 5

RESPONSE OF SUMMERTIME ODD NITROGEN AND OZONE AT 17 MB TO MOUNT PINATUBO AEROSOL OVER THE SOUTHERN MID-LATITUDES

Abstract

Observations of stratsopheric NO, NO_2, and O_3 from the Halogen Occultation Experiment (HALOE) are examined over the southern mid-latitudes (35-45 S) in the summers following the eruption of Mount Pinatubo, from early 1992 through mid-1995. The tracers HF and CH_4, also observed by HALOE, are used to distinguish between the effects of transport on the distribution of total reactive nitrogen (NOy) and ozone and the chemical effects of aerosol on NOy partitioning and ozone loss processes. HF mixing ratios are adjusted to take into account the increasing burden of stratospheric HF due to emissions of chlorofluorcarbons at the earth's surface. Trends in aerosol surface area densities from the Stratospheric Aerosol and Gas Experiment II (SAGE II) are also studied for the same time period. Results show that at 17 mb (about 28 km), in parcels of similar photochemical age, the abundances of summertime odd nitrogen ($NO+NO_2$, or NOx) nearly doubled between 1992 and 1993 and then levelled off in subsequent years. The 1992-1993 increase, coincident in time with a rapid drop in aerosol surface area density as the Pinatubo aerosol cleared the atmosphere, matches trends previously observed at lower altitudes (16-20 km). The trend demonstrates the importance of heterogeneous chemistry in the partitioning of NOy even at these altitudes, where the higher photolysis rate of HNO_3 speeds up the cycling of nitrogen through the NOy family. Results also show that summertime ozone abundances, again in parcels of similar photochemical age, declined by nearly 10 per cent between 1992 and 1993 and then, like NOx, remained about constant for the next three summers. The trend in ozone is opposite in sign to that observed at lower altitudes in the aftermath of the Pinatubo eruption and shows the importance of the NOx catalytic cycles in the ozone loss budget above about 25 km.

5.1. Introduction.

The eruption of Mount Pinatubo in June 1991 injected about 20 million metric tons of SO_2 as high as 30 km into the stratosphere (Read et al., 1993; Bluth et al., 1992). On a timescale of weeks, the SO_2 was quickly converted to sulfuric acid, leading to surface area densities of sulfate aerosol 30 to 50 times that of background values (McCormick and Veiga, 1992; Deshler et al., 1993; Thomason et al., 1996). This large influx of aerosol perturbed the stratosphere in two important ways. First, the particles increased atmospheric heating by absorption of upwelling infrared radiation (Labitzke and McCormick, 1992), and in this way influenced stratospheric transport processes, including the timing of the phase change of the quasibiennial oscillation, or QBO (Kinne and Toon, 1992; Grant, 1995). Second, the particles provided surfaces upon which heterogeneous reactions took place, leading eventually to changes in the abundances of key radicals in the ozone loss cycles. At mid-latitudes, the most important of these heterogeneous reactions is:

$$N_2O_5(g) + H_2O(l) \rightarrow 2HNO_3(g), \tag{5.1}$$

where the symbol g indicates that the species is in gas phase and l, liquid phase. Other heterogeneous reactions, such as the hydrolysis of $ClONO_2$, achieve importance only at the cold temperatures present at high latitudes in winter (Hanson et al., 1994).

Reaction 5.1 shifts nitrogen from N_2O_5, a relatively reactive form, to HNO_3, a reservoir species with a lifetime on the order of weeks or months. Both N_2O_5 and HNO_3 belong to the NOy family of molecules, which also includes NO, NO_2, $ClONO_2$, NO_3, and HO_2NO_2. With the exception of HNO_3, all the NOy molecules

are short-lived, and exchange of nitrogen between these molecules takes place on timescales of seconds to hours. An increased rate of Reaction 5.1 thus repartitions the NOy family, leading to decreased abundances of $NO+NO_2$ (NOx), which in turn, leads to changes in the abundances of other radicals and, in some regions, ozone. With less NO_2 available to sequester chlorine in $ClONO_2$, chlorine radical abundances increase, and chlorine-catalyzed ozone loss cycles speed up. Smaller abundances of NO, on the other hand, slow the reaction

$$NO + HO_2 \rightarrow NO_2 + OH \tag{5.2}$$

and in this way shift the photochemical equilibrium between OH and HO_2 in favor of HO_2. Because HO_2 is involved in the rate-limiting step of the odd hydrogen ozone loss cycle, more HO_2 results in a faster rate of ozone loss via that cycle. In the lower stratosphere, where the halogen and odd hydrogen loss cycles dominate the ozone loss budget (Wennberg et al., 1994), increased abundances of sulfate aerosol may thus indirectly lead to significant ozone losses.

Above about 25 km, however, the NOx catalytic cycles which destroy ozone take on importance:

$$NO + O_3 \rightarrow NO_2 + O_2 \tag{5.3}$$

$$NO_2 + O \rightarrow NO + O_2 \tag{5.4}$$

$$net: O_3 + O \rightarrow 2\,O_2.$$

and

$$NO + O_3 \rightarrow NO_2 + O_2 \tag{5.5}$$

$$NO_2 + O_3 \rightarrow NO_3 + O_2 \quad (5.6)$$

$$NO_3 + h\nu \rightarrow NO + O_2 \quad (5.7)$$

$$net: 2O_3 \rightarrow 3\,O_2.$$

On a per-radical basis, these cycles are less efficient than the halogen or odd hydrogen cycles, but with increasing altitude both NOx and the atomic oxgyen necessary for Reaction 5.4 become quickly more abundant. NOx therefore is predicted to be a dominant player in ozone removal processes at higher altitudes (Wennberg et al., 1994).

In the years following the eruption of Mount Pinatubo, stratospheric NOx loss coincident in time and space with the presence of Pinatubo aerosol was reported in many studies. Most of these studies, however, involved ER-2 observations made at low altitudes (Fahey et al., 1993; Kawa et al., 1993; Mills et al., 1993) or observations of total column amounts (Johnston et al., 1992; Coffey and Mankin, 1993; Koike et al., 1994). Webster et al. (1994) measured low abundances of NO_2 in the 20-30 km range near latitude 31 N on one day in August 1992. In the same height range, Rinsland et al. (1994) compared data from the March 1992 Atmospheric Trace Molecule Spectroscopy experiment to March 1979 data from the Limb Infrared Monitor and found elevated levels of HNO_3 in 1994.

Ozone, on the other hand, showed losses in the lower stratosphere (12-22 km) in 1992 and 1993, consistent with theory (Weaver et al., 1993; Hofmann et al., 1994b). At altitudes above 24 km over North America during late 1992 and early 1993, Hofmann et al. (1994b) observed higher than usual ozone concentrations and speculated that aerosol leftover from Pinatubo had suppressed NOx abundances

there, leading to enhanced ozone. Lacking simultaneous measurements of NOx or a tracer, however, Hofmann et al. could not rule out transport as a cause of the increased ozone. Measurements of total ozone from ground-based instruments or from the Total Ozone Mapping Spectometer (TOMS) on Nimbus 7 show significant decreases in column amounts in 1991 over the tropics and in 1992-1993 over the northern mid-latitudes (Gleason et al., 1993; Bojkov et al., 1993; Kerr et al., 1993; Herman and Larko, 1994; Randel et al., 1995). No significant decreases in total column amount were observed over the southern mid-latitudes.

Data from HALOE provide for the first time a continuous record of NOx and ozone above 26 km in the aftermath of a major volcanic eruption. HALOE observations of two tracers, HF and CH_4, allow us to filter out the effects of transport on NOx abundances, including those transport effects brought on by the presence of Pinatubo aerosol itself. In the case of ozone, which has an intermediate chemical lifetime, transport effects are somewhat more difficult to filter out, as will be discussed below. We have focused this study on the southern mid-latitudes for two reasons. First, aerosol surface area densities in the Southern Hemisphere above 26 km reached 30-40 times background values, while those in the Northern Hemisphere in the same altitude range peaked at only 8-9 times background values (Thomason et al., 1996; World Meteorological Organization, 1992). Second, aerosol loading in both hemispheres over the mid-latitudes peaked during late 1991 and early 1992 — that is, during the summer months for the Southern Hemisphere and the winter months for the Northern Hemisphere. Given the shorter chemical lifetime of ozone during summer and the heavier aerosol burden of the Southern Hemisphere above

about 26 km, we expect to observe a more dramatic chemical response to Pinatubo aerosol in the summertime over the southern mid-latitudes.

Probing the sensitivity of ozone to changes in NOx at these altitudes may provide some insight into the response of ozone to increased NOy emissions from the proposed fleet of high-speed civilian transports (HSCTs). Although the HSCTs are slated to fly at low altitudes in the stratosphere (about 18 to 20 km), it is not known to what extent the NOy emitted by the proposed fleet will be transported vertically. If, as has been suggested by Wofsy et al. (1994), vertical transport is more efficient than predicted by many current models, injection of NOy at 20 km may indeed affect NOx abundances at 28 km. While this paper examines the question of how *decreases* of NOx affect ozone abundances at high altitudes, the study may also shed light on how *increases* in NOx may affect ozone in the event that a fleet of HSCTs is launched.

5.2. Method.

Our goal for this work is to follow the evolution of NOx and ozone over the southern mid-latitudes at 17 mb (27-28 km) in the years following the Mount Pinatubo eruption — from summer 1992 through summer 1995. Figure 12 shows the surface area density of sulfate aerosol at 27.4 km at 40 S as a function of time from January 1991 through most of 1995 (Thomason et al., 1996). The righthand axis gives the surface area as a multiple of background surface area (World Meteorological Organization, 1992). The huge surge in surface area density in fall 1991 marks the arrival of the Pinatubo aerosol in this region. The trend is consistent with other

observations which show the bulk of the volcanic material confined to the tropical stratospheric reservoir in the first months following the eruption and then slowly dispersing to other latitudes (Trepte et al., 1993). At 40 S, the aerosol surface area density declined rapidly during 1992, relaxing back to pre-Pinatubo levels by the last months of the year. Though HALOE began observations in October 1991, the presence of huge abundances of aerosol made the early data unreliable at 17 mb. Useful measurements at this altitude were not made until January 1992. We must therefore look for evidence of the response of chemical species not to the injection of the Pinatubo aerosol, but to the gradual decline of the aerosol as the particles settled out of the atmosphere.

It should be noted that lower in the stratosphere at this latitude, aerosol surface area densities remained at very high levels throughout 1992 and much of 1993 (Thomason et al., 1996). Thus the data from lower altitudes, especially the NO and NO_2 measurements, show larger uncertainty due to the significant contribution of aerosol to extinction in the infrared. Even in aerosol-free conditions, however, the estimated total error in the measurements increases rapidly below about 25 km due to the smaller NO and NO_2 mixing ratios in that region. For example, the total error for NO_2 increases from about 10 per cent at 30 km to about 40 per cent at 20 km (Gordley et al., 1996). Because of the uncertainty in the data below 25 km, especially under conditions of heavy aerosol, we do not analyze data from this region.

To accomplish our task at 17 mb, we examine a series of similar air parcels through the years. In the case of NOx, this means we need to select parcels with similar NOy content so that changes in NOx will reflect changes in the partitioning

of NOy and not simply changes in the abundance of the NOy family as a whole. As described in Chapter 4, the NOy family as a whole throughout much of the stratosphere is long-lived and can be viewed as a tracer. Thus we can expect that the NOy family should correlate with the HALOE tracers HF and CH_4. Changes in NOy partitioning can then be tracked by examining the NOx content of a series in air parcels that contain similar abundances of tracer material. Our calculations show that the timescale for conversion of NOx to HNO_3 is about one week, consistent with the observations of Kawa et al. (1993). We may infer then that NOy partitioning should indeed be sensitive to the local aerosol loading.

As noted in Chapter 4, ozone anti-correlates with HF in this region due to the greater abundance of radicals in photochemically older air. Unlike in the case of NOx, however, O_3 at this altitude has a chemical lifetime of about 70 days in summer, comparable to its lifetime due to transport (Brasseur and Solomon, 1986; Ko et al., 1989). Since the ozone at any given point in space will respond slowly to the local conditions while retaining a "memory" of conditions at another point, we expect therefore only weak anti-correlation or correlation of ozone with the tracer gases HF or CH_4. Nonetheless, as will be shown below, using tracers in our analysis will allow us to define with greater certainty the ozone response to the Pinatubo aerosol.

The next question to address in this study is which of the two tracers measured by HALOE best serves our purposes. Figure 13 shows a plot of observed CH_4 vs HF at 17 mb over the latitude range 35 to 45 S during the time interval from early 1992 through most of 1995. In this part of the atmosphere, the lifetimes of both HF and CH_4 are very long, on the order of years, so one would expect the

two species to exhibit a compact linear relationship (Plumb and Ko, 1992). Since the stratospheric burden of HF is increasing rapidly due to increasing emissions of CFCs at the earth's surface, we have adjusted the HF mixing ratios in Figure 13 as follows. The observed value of HF on any given day was multiplied by the factor $(1+0.066t/365)^{-1}$ where t is the time in days since the start of the observations and 6.6%/year is the annual growth rate of stratospheric HF (Russell et al., 1996). We have not adjusted the CH_4 mixing ratios since the annual increase for global CH_4 is less than one per cent (Dlugokencky et al., 1994). The correlation coefficient for CH_4 vs the adjusted HF is 0.91 for the 1280 data points, compared to only 0.81 for CH_4 vs unadjusted HF. The improved correlation coefficient for the adjusted data gives us confidence in our correction.

All of the scatter that remains in Figure 13 after the HF adjustment can be assigned to random instrument and retrieval algorithm error, estimated to be about 7 per cent for both CH_4 and HF at this altitude. We note that 7 per cent may, in fact, be an overestimate of the random error for these channels, given the extremely good correlation of the two species. In any case, since our work rests on the assumption that NOy as a family correlates well with long-lived tracers, we have chosen for this study to look at only those parcels whose HF-CH_4 relationships lie with two standard deviations of the least squares fit of the data in the Figure, about 55 per cent of the points. In this way, we use information from *both* tracers in our analysis.

We note here that for the purposes of this study, we have assumed that the eruption of Mount Pinatubo did not inject appreciable quantities of fluorine into the stratosphere. Although Symonds et al. (1988) predict that explosive volcanic

eruptions could transmit HCl and HF to the stratosphere, the model of Tabazedeh and Turco (1993) shows that HCl vapor in a volcanic plume is efficiently scavenged by the huge quanities of water droplets also present in the plume. The study of Tabazedeh and Turco did not include HF. HF is somewhat less soluble in water than is HCl, but we detect no perturbations in HF-CH_4 correlation during the time period of our study. Thus, we have assumed that, like HCl, whatever HF was emitted during the eruption was scavenged by water droplets, followed by rainout.

5.3. Observations

Figure 14 shows the relationship of measured summertime NOx to HF at 17 mb over the latitude region 35 S to 45 S for the four years following the eruption of Mount Pinatubo. For this and subsequent plots, the HF data have been adjusted to take into account the increasing emissions of CFCs, and all data points with CH_4-HF relationships outside two sigma of the least squares fit of Figure 13 have been filtered out. The red triangles represent data from 1992, the dark blue from 1993, the light blue from 1994, and the green from 1995. The 1993 data include some points from the last few days of December 1992. It is clear from Figure 14 that for similar values of HF, summertime NOx was markedly lower in 1992 than in subsequent years.

Note that plotting NOx vs HF allows us to distinguish easily between parcels with low NOx due to low NOy and parcels with low NOx due to unusual partitioning of NOy. Parcels with low HF values have spent less time in the stratosphere and have been exposed to less ultraviolet radiation than parcels with high

HF. Such parcels almost certainly have low NOy abundances, and consequently low NOx. Low NOx values in parcels with high HF, on the other hand, signify unusual partitioning of NOy towards more HNO_3. It is worth noting that in summer 1994, no parcel with an HF value less than about 480 ppt was observed, while during the other three summers, parcels with as little as 350 ppt were detected. This implies that in 1994 NOy mixing ratios were also higher than usual for reasons most likely having to do with transport.

In Figure 15a, we show the evolution of summertime NOx through the years for parcels characterized by an HF content of 500 to 550 ppt — that is, for parcels whose NOy content also falls within a similarly narrow range. Each data point is represented by a dot, while the average NOx and date for each summer is denoted by a triangle. The solid line connects the summer averages, and the dotted lines show the range of two standard deviations from the mean of the last three summers, 1993-1995. Not surprisingly, the plot shows extremely low NOx values for 1992, followed by a levelling off in subsequent years to almost double the 1992 values. The scatter in Figure 15a may be attributed to several sources. First, the HF increment of 50 ppt corresponds to an increment of about 0.3 ppb of NOx, so some scatter in the plot is to be expected. Second, the partitioning of NOy may vary somewhat with latitude due to differences in solar insolation, leading to a range of values of NOx for the same HF value. Lastly, instrument error almost certainly contributed to the scatter. Despite the scatter, however, the trend in NOx is clear, and all the points from 1992 lie outside the two-sigma range of the mean of the three subsequent years.

Figure 16 shows summertime O_3 vs HF for the same time interval and latitude range as Figure 14. The HF data have been adjusted as in Figure 14, and the colors of the triangles correspond to the same set of years. The correlation coefficient R for the 125 data points in the plot is -0.5, which indicates that the two species are only weakly anti-correlated, as expected. As noted above, the anti-correlation comes about since photochemically older air contains greater abundances of the radical species that destroy ozone. Much of the scatter in the plot probably arises from the long chemical lifetime of O_3, which means that the gas may retain evidence of chemical processes occurring in other regions. Nonetheless, we see that ozone abundances from the 1992 summer are among the highest for any given value of HF.

As in Figure 15a, we plot in Figure 15b the summertime O_3 values for those parcels whose HF content ranges between 500 to 550 ppt. As before, the dots represent all the data points, the triangles the season averages, and the two dotted lines signify the range of two standard deviations from the mean mixing ratios for the 1993-1995 summers. The mean O_3 mixing ratio for summer 1992, about 10 per cent greater than the mean of the following three summers, lies just outside the two-sigma range, indicating that ozone abundances were indeed unusual that year.

As a check on our methods, we have replotted Figures 15a and 15b, making use of all the summertime data available. In Figures 17a and 17b we have not imposed any limits on HF content of the points included; all data points for each summer at 17 mb are shown. Considerably more scatter is apparent in both plots. In Figure 17a, we see that NOx again increases between summer 1992 and summer 1993, but then continues to increase at nearly the same rate during the subsequent

year. Summertime NOx in 1995 shows a small drop. We believe that the high NOx data of 1994 merely reflect the high NOy values of that year, as predicted by the high HF values of Figure 14. In other words, the 1994 change in NOx is probably due to transport processes and not to chemistry. In Figure 17b, the dotted lines again show the two-sigma range for the 1993-1995 data, but this time summertime ozone for 1992 falls inside the range. The slight increase in ozone in 1995 may be linked to the decrease in NOx for that year. Since our goal is to determine changes in NOx and O_3 due solely to chemistry, Figures 17a and 17b are not useful to our study. As will be discussed in the next section, the trends in the unfiltered data are not consistent with the observed trends in surface area densities of sulfate aerosol.

A pair of plots similar to Figures 15a and 15b may be obtained for HALOE data from the latitude region 25 S to 35 S, again at 17 mb. In this region of photochemically younger air (compared to 35-45 S), the HF interval chosen was 450 to 500 ppt. In these plots (not shown) summertime NOx again nearly doubles from 1992 to 1993, and O_3 decreases by about 7 per cent. The smaller ozone change for the 25-35 S latitude range, compared to that for the 35-45 S latitude range, may reflect the lesser importance of ozone loss processes over lower latitudes.

5.4. Discussión and Model Calculations.

The dramatic rise in NOx abundances between summer 1992 and summer 1993 coincident in time with the rapid decline in aerosol surface area density demonstrates the importance of Reaction 5.1 in the partitioning of the NOy family at 17 mb in the mid-latitude stratosphere. The data suggest that by early 1992, when

HALOE observations began in this region, the presence of large abundances of sulfate aerosol leftover from the Mount Pinatubo eruption had led to a shift in reactive nitrogen from NOx to the reservoir molecule HNO_3, which even at these altitudes did not photolyze quickly enough to maintain NOx at its usual level. As the aerosol cleared the atmosphere, NOx concentrations apparently returned to pre-Pinatubo values.

We note that HNO_3 data from the Cryogenic Limb Array Etalon Spectrometer (CLAES), another instrument aboard UARS (Roche et al., 1993), agree well with this interpretation of the trends in HALOE odd nitrogen. CLAES ceased observations in April 1993, so only two summers of data are available for a comparison with HALOE. Zonally averaging CLAES HNO_3 at the 17 mb level between 42 and 44 S for the same days as the HALOE observations yields an average 6.6 ppb for summer 1992 and 4.1 ppb for summer 1993. This drop in mixing ratio of 2.5 ppb is larger than the corresponding increase in NOx by about 1.2 ppb. The missing 1993 NOy was probably tied up in N_2O_5, which during the night builds up to higher values when more NOx is available at sunset. Note that the HALOE observations are taken at sunrise, when N_2O_5 mixing ratios reach their peak.

The response of ozone to the increased burden of sulfate aerosol at this altitude was more complicated. As noted in the Introduction, NOx plays both a direct and an indirect role in the ozone budget. The direct role involves the two NOx catalytic cycles that destroy ozone, Reactions 5.3-5.7. The indirect role involves the sequestering of active chlorine by NO_2 in the molecule $ClONO_2$ as well as the

competition between the Reaction 5.2 and the rate-limiting step (Reaction 5.9) in the odd hydrogen catalytic cycle:

$$O_3 + OH \rightarrow O_2 + HO_2 \quad (5.8)$$

$$O_3 + HO_2 \rightarrow 2O_2 + OH \quad (5.9)$$

$$net: 2\,O_3 \rightarrow 3\,O_2.$$

NOx thus controls the abundance of chlorine radicals and the rate of Reaction 5.9. While the direct role of NOx in the ozone budget leads to the removal of ozone, the indirect role leads to slower rates of destruction of ozone by active chlorine and odd hydrogen radicals. At altitudes probed by the ER-2 (16-20 km), the halogen and odd hydrogen cycles dominate ozone removal processes, while the NOx catalytic cycles account for only about 20 per cent of ozone loss (Wennberg et al., 1994). The significant loss of NOx in the bottom few kilometers of the stratosphere that followed the eruption of Mount Pinatubo thus led to depressed ozone concentrations in that region (Weaver et al., 1993).

A few kilometers higher than the ER-2 observations, however, the response of ozone to perturbations in NOx abundances changes. Although the NOx catalytic cycles are less efficient than the other ozone loss cycles, NOx abundances increase rapidly with height because HNO_3 photolysis rates increase with the increased solar insolation available at higher altitudes. NO_3 photolysis rates also increase at higher altitudes, speeding up Reaction 5.7, and atomic oxygen becomes more abundant, resulting in a faster rate of Reaction 5.4. Both Reaction 5.4 and Reaction 5.7 are the rate-determining steps in their cycles. Although an important direct role for NOx in the O_3 budget has been predicted at the higher altitudes (e.g., Wennberg

et al., 1994), no unambiguous evidence of the sensitivity of O_3 to NOx above about 25 km has previously been observed. Figure 15b shows for the first time the sign of the change in ozone at 17 mb that accompanies a loss in NOx at that altitude. The plot suggests that although the suppressed levels of NOx in summer 1992 may have increased the rates of O_3 removal via the active chlorine and odd hydrogen cycles, they also decreased the rates of O_3 loss via the NOx catalytic cycle, leading to a net enhancement in O_3 mixing ratios for this altitude.

To test these ideas, we have performed calculations with a time-dependent, photochemical box model described in Chapter 3. We initialized the model with data from HALOE and ran a series of simulations at two altitudes (28 and 20 km), varying the aerosol surface area densities from background conditions to 50 times background conditions. For each run, initial mixing ratios were input at the sunrise timestep, and the model was run to diel steady-state, as described in Chapter 3. Data for NO, NO_2, O_3, HCl, H_2O, and CH_4 were taken from HALOE observations on February 11, 1992, when the mean latitude of HALOE observations was 43 S. For observations at 28 km (17 mb), we took the average of those data points whose HF content fell within the range of 500 to 550 ppt. For observations at 20 km (54 mb), we took the average of all the data points on that day, keeping in mind that the aerosol had a larger effect on NOx measurements in this region than at higher altitudes. We determined values for Cly and NOy at both altitudes by first calculating N_2O from HALOE CH_4, making use of a relationship between these two tracers derived from aircraft data (Woodbridge et al., 1995). The abundances of Cly and NOy were then derived from that of N_2O by the methods of Woodbridge et al. (1995) and Fahey et al. (1990), respectively. An initial value of $ClONO_2$ was determined by

simply subtracting HALOE HCl from Cly. We assumed N_2O_5 to be negligible at the high surface area densities of February 1992, and after $ClONO_2$ and NOx had been accounted for, we assigned the remaining NOy to HNO_3. In fact, since the model was run to diel steady-state conditions, the output was nearly insensitive to the input concentrations of the individual Cly and NOy member species (though not to the input values for the total families). For the bromine species, we used 5 ppt for BrO and 10 ppt for total inorganic bromine, or Bry (Avallone et al., 1995). Background aerosol densities were taken from the World Meteorlogical Organization (1992). To calculate the appropriate radiative flux and photolysis rates at the two altitudes studied, ozone column amounts were taken from HALOE data. A summary of key input values for the two altitudes is shown in Table 1.

As an aside, we note that we chose not to initialize the model with data from CLAES. Observations from CLAES and HALOE were not coincident in time and space. Zonally averaging CLAES N_2O data from February 11, 1992, for the latitude band 42-44 S yields a value of N_2O not consistent, according to the "rule" of Woodbridge et al. (1995), with the CH_4 mixing ratios observed by HALOE.

Figure 18 shows calculated NOx as a function of the multiple of background aerosol surface area density. The solid line represents data from 28 km, and the dotted line from 20 km. At each altitude, the concentrations have been normalized to the abundance of NOx calculated for background conditions of sulfate aerosol. As the surface area density of sulfate aerosol increases from 1 to 10 times background conditions, NOx abundances at both altitudes decline sharply, signifying a significant shift from NOx to HNO_3 in the presence of high aerosol concentrations. The slightly less rapid response of NOx at 28 km to increasing sulfate aerosol is caused

by the higher photolysis rate of HNO_3 at that altitude (about double the rate at 20 km). As expected, HNO_3 is a slightly less stable reservoir for NOy at the higher altitude.

At surface area densities greater than about 10 times background, NOx abundances begin to level off, a sign of the saturation of N_2O_5 hydrolysis (Reaction 5.1) on sulfate aerosol (Mills et al., 1993). Saturation is achieved when the photolysis rate of N_2O_5 becomes much slower than the rate of N_2O_5 hydrolysis, and the rate-limiting step in the heterogeneous conversion of NOx to HNO_3 becomes the three-body reaction of NO_2 and NO_3 to form N_2O_5, a process not dependent on surface area of aerosol. In other words, under conditions of high aerosol, the photolysis rate of N_2O_5 cannot compete with the rate of hydrolysis, and during the day little nitrogen is cycled back to NOx. This means that insufficient N_2O_5 is available to keep the heterogeneous reaction going as rapidly as might be expected. At night, when photolysis of N_2O_5 ceases, the concentration of that molecule builds. With increasing sulfate aerosol, however, less NOx becomes available at night to form N_2O_5, and the nighttime hydrolysis of N_2O_5 on aerosol proceeds more and more slowly. As shown in Figure 18, the saturation of N_2O_5 hydrolysis is achieved at a lower surface area density at 20 km than at 28 km because of the slower N_2O_5 photolysis rates at the lower altitude.

According to Figure 12, SAGE II measured surface area densities of sulfate aerosol at about 25 times the background value in this region of the atmosphere in February 1992. The calculated per cent change in NOx that accompanies a change in sulfate aerosol from background conditions to 25 times background conditions is about 60 per cent, consistent with the observations in Figure 15a.

In Figure 19, as in Figure 18, we plot O_3 as a function of multiple of aerosol surface area density. Again we show data from the two altitudes and normalize the data at both altitudes to the concentration of ozone under background conditions of sulfate aerosol. Calculated ozone abundances at 20 km decline with increasing aerosol surface area, consistent with earlier observations. At 28 km, calculated ozone concentrations increase with increasing aerosol surface area, reaching a value about 8 per cent greater than the value under background conditions. Above about 25 times background levels of aerosol, ozone concentrations begin to level off. The calculated ozone increase at 25 times background is consistent with the model results of Tie et al. (1994) in this region and is slightly less than the observed ozone increase of 10 per cent.

To gain understanding of the behavior of O_3 at 28 km, we plot in Figure 20 the rates of the major ozone loss cycles, grouped by family, again as a function of multiple of surface area density. The dotted line represents the total loss rate due to the halogens, the dashed line that due to odd hydrogen, and the solid line that due to NOx. The loss rates, in units of $molecules/cm^3/s$, have been normalized to the loss rate of NOx at background surface area densitites. For each family, the rates of the rate-limiting steps of each important cycle have been summed together. All rates are for February at 28 km at 40 S. At low multiples of background aerosol, NOx clearly dominates the ozone loss cycles, with rates about three times that of the halogen cycles. With increasing aerosol concentrations, NOx loss rates first decline and then level off, consistent with the levelling off of NOx abundances under saturation conditions. At higher aerosol surface areas, with less NOx available to sequester ClO in $ClONO_2$, the halogen cycles gain in importance in the ozone budget. The

faster loss rates of the halogen loss cycles, together with the levelling off of the NOx loss rates, limit to some extent the ozone increase that accompanies an increase in the sulfate aerosol burden at this altitude. Thus in Figure 19, as aerosol surface area density increases from 30 to 50 times background, the calculated ozone abundance at 28 km changes remarkably little.

The different responses of ozone to perturbations in NOx at the two altitudes studied give insight into the trends observed in total ozone in the years following the eruption of Mount Pinatubo. In the Southern Hemisphere, where aerosol loading at altitudes above about 25 km reached 30-40 times background (Thomason et al., 1996; World Meteorological Organization, 1992), significant ozone enhancement took place and may have offset the decreases in ozone at lower altitudes. This may explain why total column amounts of ozone in the Southern Hemisphere showed little or no change in the aftermath of the Pinatubo eruption. In the Northern Hemisphere, smaller aerosol abundances perturbed the region above 26 km, and the total column amounts of ozone reflect mainly the losses at lower altitudes.

5.5. Summary and Implications.

HALOE observations in the southern mid-latitudes of summertime NOx and ozone, together with SAGE II measurements of aerosol surface area densities, show the sensitivity at 17 mb of NOy partitioning and ozone loss processes to the presence of huge abundances of aerosol leftover from the 1991 eruption of Mount Pinatubo. As the aerosol cleared this region of the atmosphere, summertime NOx concentrations nearly doubled between 1992 and 1993, and then held steady through

summer 1995. The trend in NOx matches trends observed at lower altitudes and shows that even at 17 mb, where HNO_3 photolyzes twice as rapidly as in the lower stratosphere, NOy partitioning is extremely sensitive to the presence of aerosol. Ozone, on the other hand, decreased by about 10 per cent from summer 1992 to summer 1993, suggesting that the NOx catalytic cycles play a major role in the ozone budget at these altitudes. In the aftermath of the Pinatubo eruption, the loss of NOx, while leading to accelerated rates of the halogen and odd hydrogen loss cycles in the ozone budget, also resulted in slower rates of the NOx loss cycles. The net effect at this altitude, where the NOx cycles dominate the ozone budget, was a temporary increase in ozone. As NOx returned to pre-Pinatubo values, the rates of the NOx catalytic cycles sped up, and ozone abundances decreased and then levelled off.

These trends in NOx and O_3 were determined by using the tracers HF and CH_4, two other molecules observed by HALOE. Use of these tracers enabled us to compare parcels of similar photochemical age, containing similar abundances of NOy. For NOx, this meant that any changes we observed in $NO+NO_2$ abundances were due entirely to changes in the partitioning of NOy, and not due to transport effects on NOy itself. For O_3, this meant we could compare air parcels which under normal conditions would contain similiar abundances of radicals, leading to similiar rates of ozone loss. Ozone at this altitude anti-correlates with HF due to the increasing abundance of radicals in photochemically older air. Although this anti-correlation is somewhat weak due to the long chemical lifetime of ozone, tracer analysis allowed us to discern a trend in ozone which is in good agreement with the

trend predicted by our photochemical box model. Thus tracer analysis has proven to be a useful tool in tracking chemical change through several years.

In our work, we have focused on the response of O_3 at 17 mb to a significant loss of NOx, followed by a return of NOx to pre-Pinatubo values. These results have implications in the event that a fleet of HSCTs is launched, injecting large abundances of NOy and SO_2 into the stratosphere. Although the HSCT flight paths lie in the lower stratosphere, the fate of their emissions is under debate (Bekki and Pyle, 1993; Wofsy et al., 1994, Considine et al., 1995; Plumb et al., 1995; Weisenstein et al., 1996). If the vertical motions in the lower stratosphere are strong enough to transport NOy as high as 28 km, our work shows that we can expect a loss of ozone at these altitudes to accompany the enhanced NOx abundances. This loss could be mitigated somewhat if the aerosol surface area densities at this altitude increase as a result of the HSCT SO_2 emissions. In any event, the sensitivity of O_3 at these altitudes to perturbations in NOx abundances is clear.

Table 1. Initial conditions for photochemical box model

28 km: background aerosol 0.2 μ^2/cm^3			
NOy	13.5 ppb	O_3	7.25 ppm
Cly	2.8 ppb	CH_4	0.96 ppm
Bry	10.0 ppt	H_2O	4.40 ppm
20 km: background aerosol 0.8 μ^2/cm^3			
NOy	9.7 ppb	O_3	1.80 ppm
Cly	2.5 ppb	CH_4	1.16 ppm
Bry	10.0 ppt	H_2O	3.80 ppm

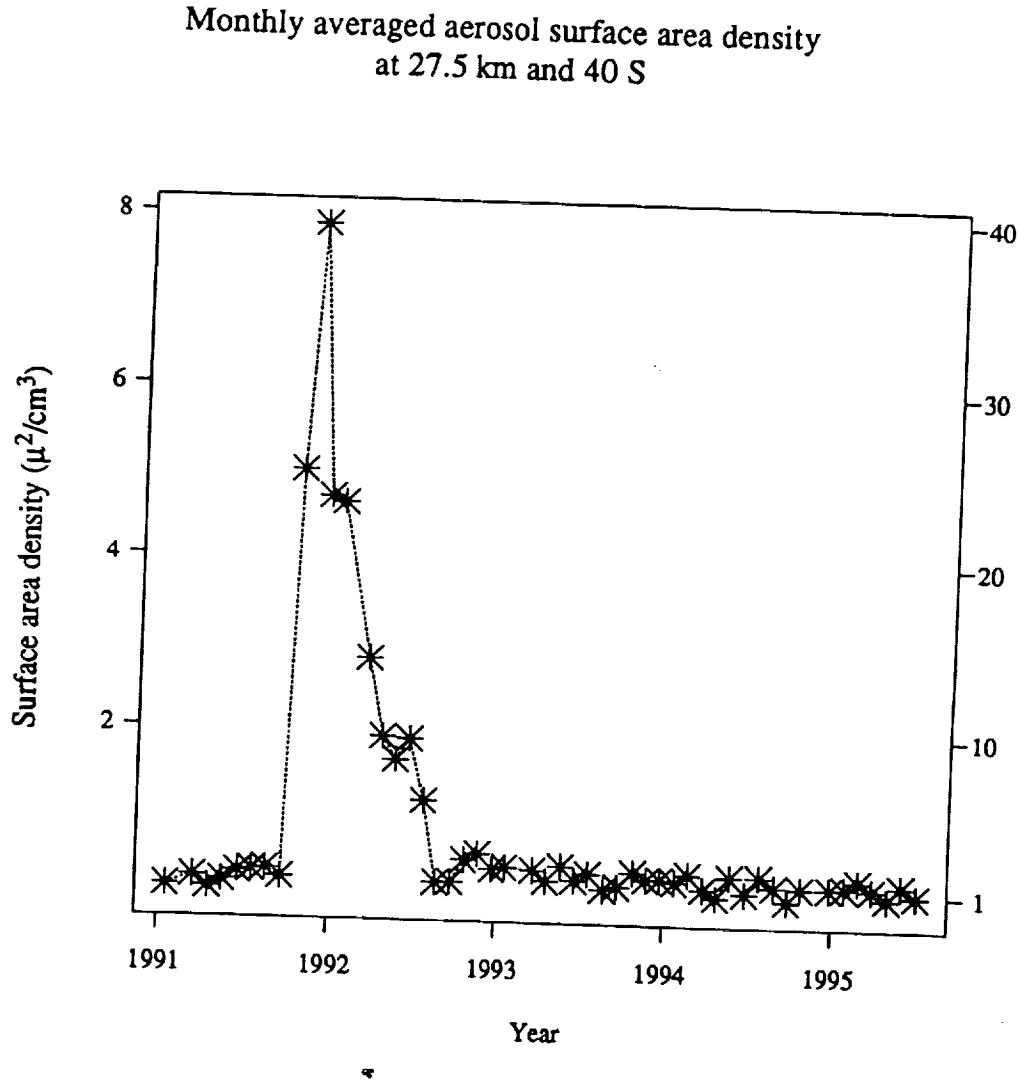

Figure 12. SAGE II aerosol surface area density at 27.5 km and 40 S. The stars represent the monthly averaged surface area density; the dotted line connects the stars for ease in reading the plot. The righthand axis shows multiples of background surface area, 0.2 μ^2/cm^3. The tickmarks denote the start of each year. The huge peak marks the arrival of Pinatubo aerosol to this region.

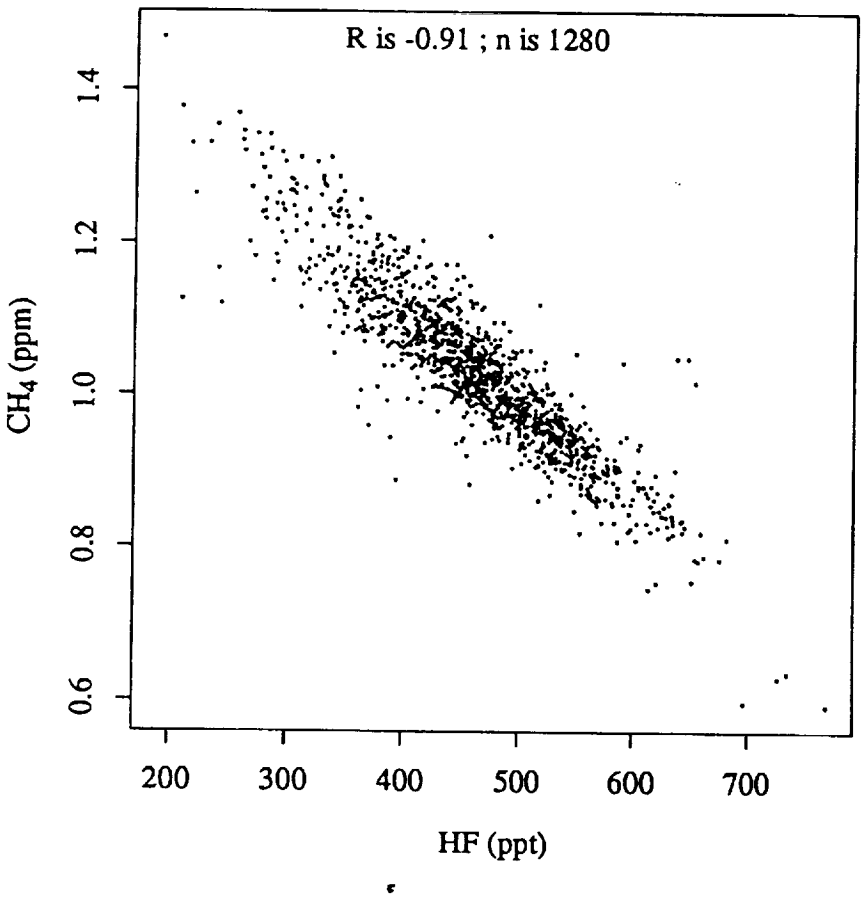

Figure 13. HALOE CH_4 vs HF from early 1992 through most of 1995 on the 17 mb surface over the southern mid-latitudes (35-45 S). HF has been adjusted to take into account the annual increase of stratospheric HF due to increasing emissions of CFCs at the earth's surface (see text).

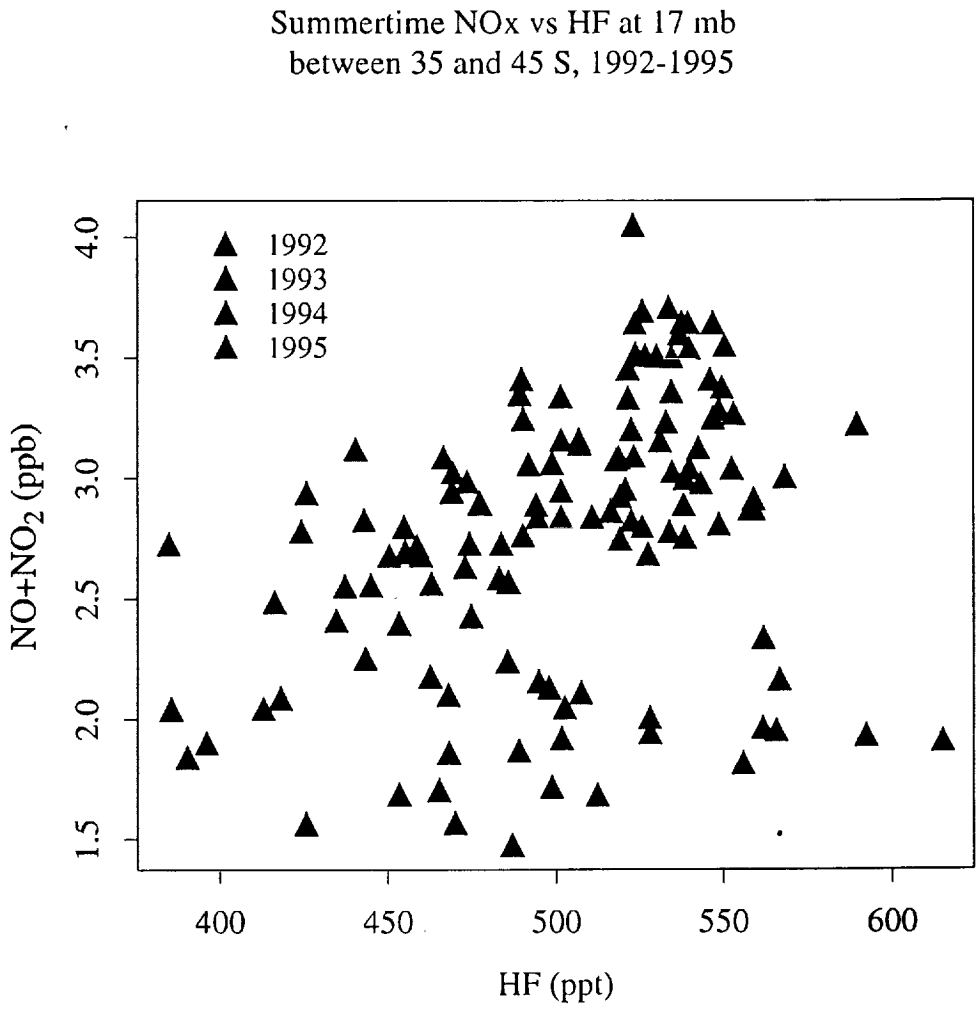

Figure 14. Summertime $NO+NO_2$ vs HF at 17 mb between 35 and 45 S during 1992-1995. The color for each year is indicated in the legend. HF has been adjusted, and the data filtered, as described in the text.

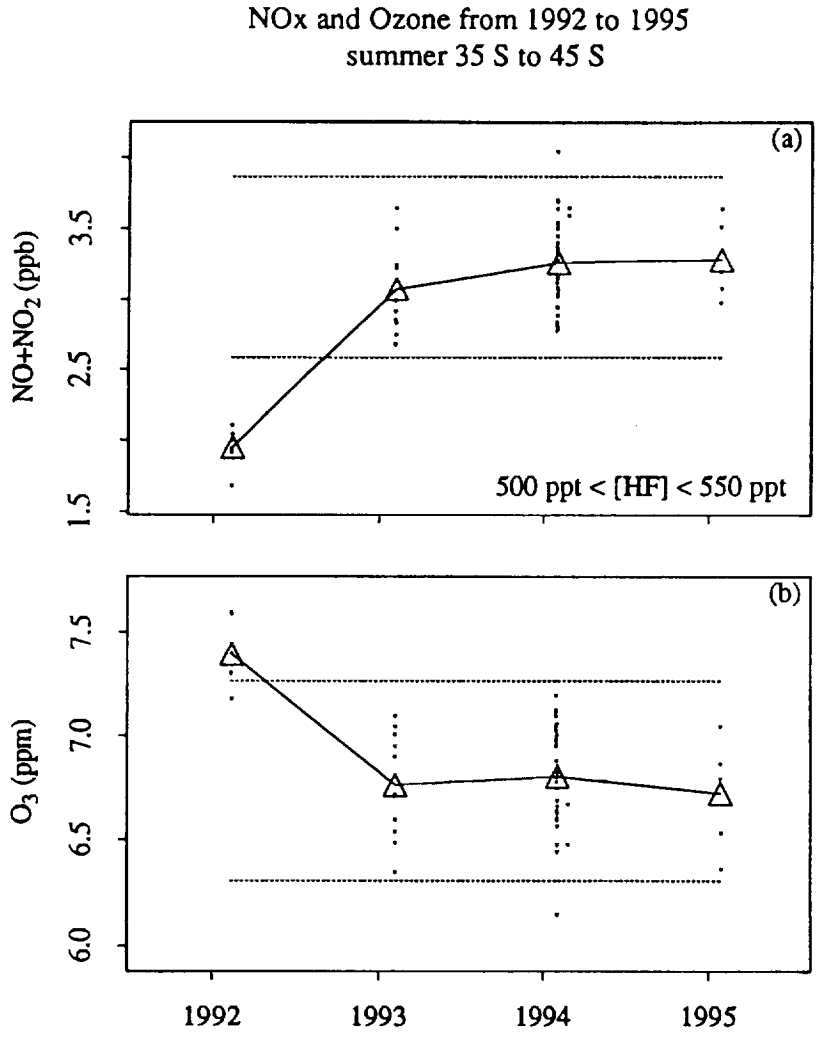

Figure 15. Summertime (a) $NO+NO_2$ and (b) O_3 at 17 mb over the southern mid-latitudes during the years 1992 through 1995. Only those points representing parcels with an HF content between 500 and 550 ppt are shown. Each dots denotes a separate observation, and the triangles show the seasonal mean for that year. The solid line connects the seasonal means, and the two dotted lines show the two-sigma range of the mean of the 1993-1995 summers.

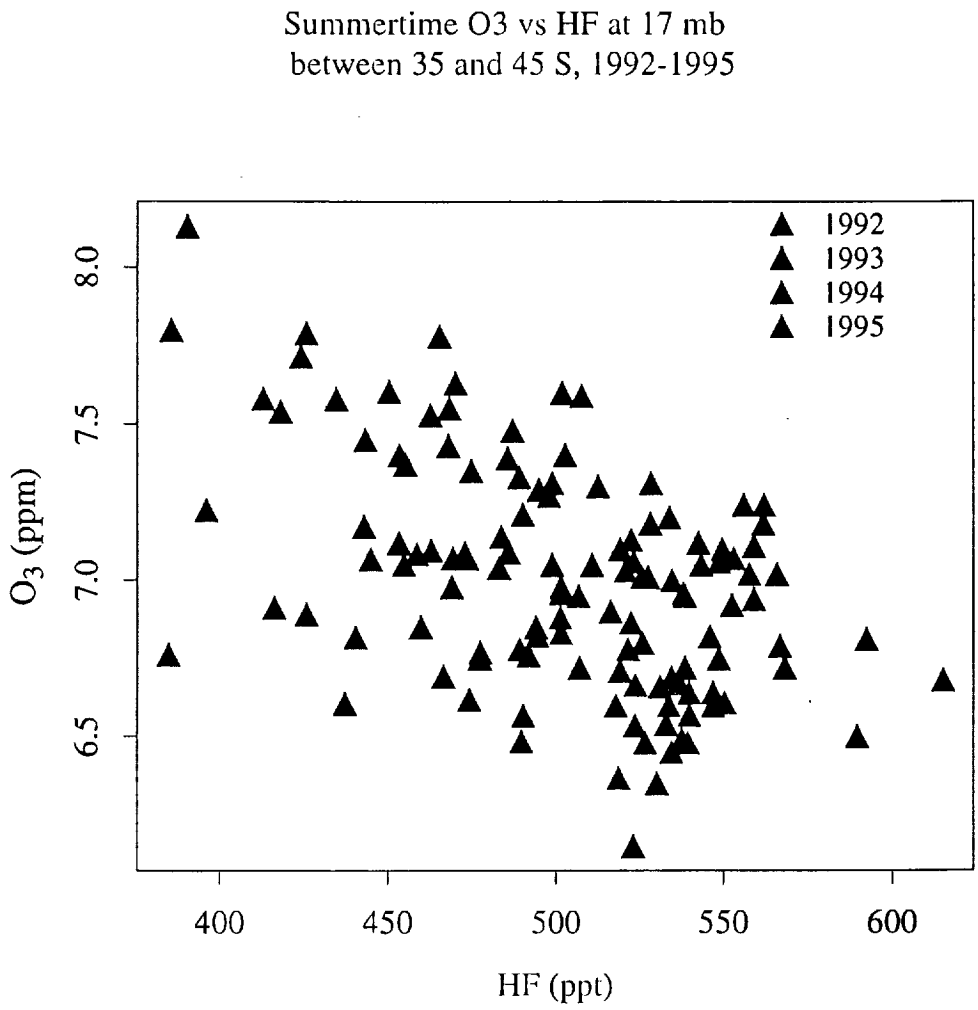

Figure 16. Summertime O_3 vs HF at 17 mb between 35 and 45 S during 1992-1995. As in Figure 14, the color for each year is indicated in the legend. HF has been adjusted, and the data filtered.

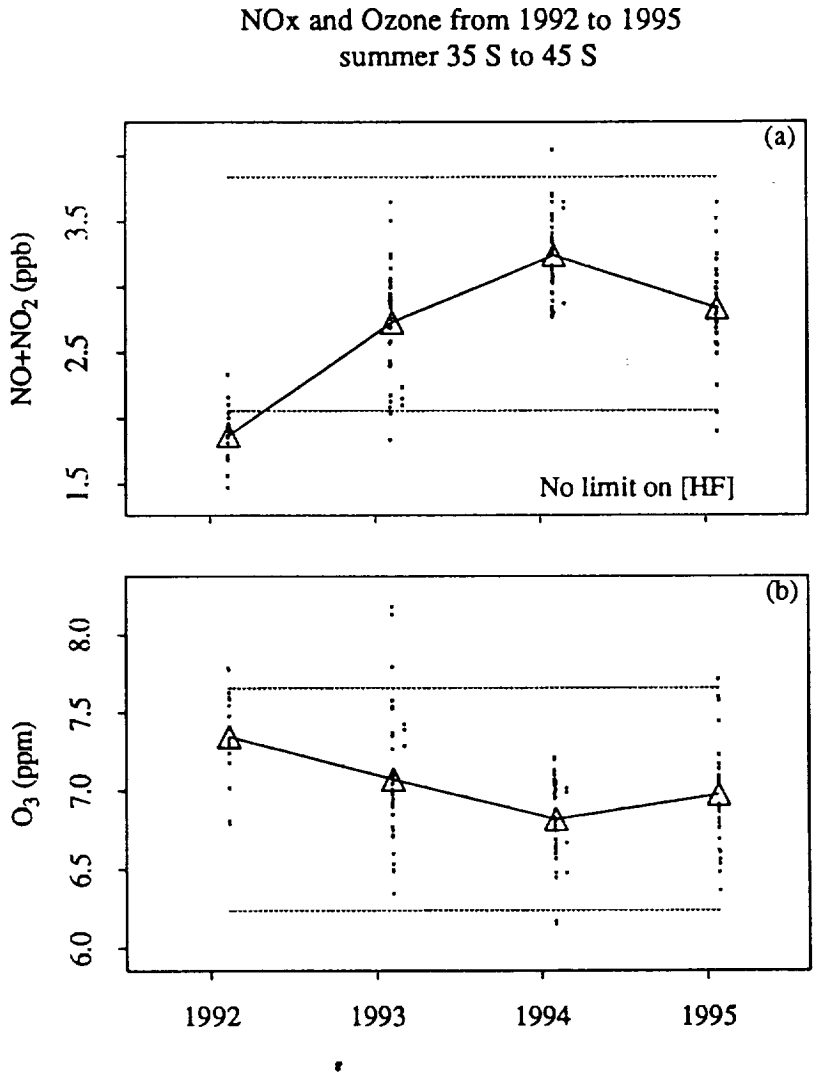

Figure 17. As in Figure 15. Here all data from parcels on the 17 mb surface, regardless of HF content, have been plotted.

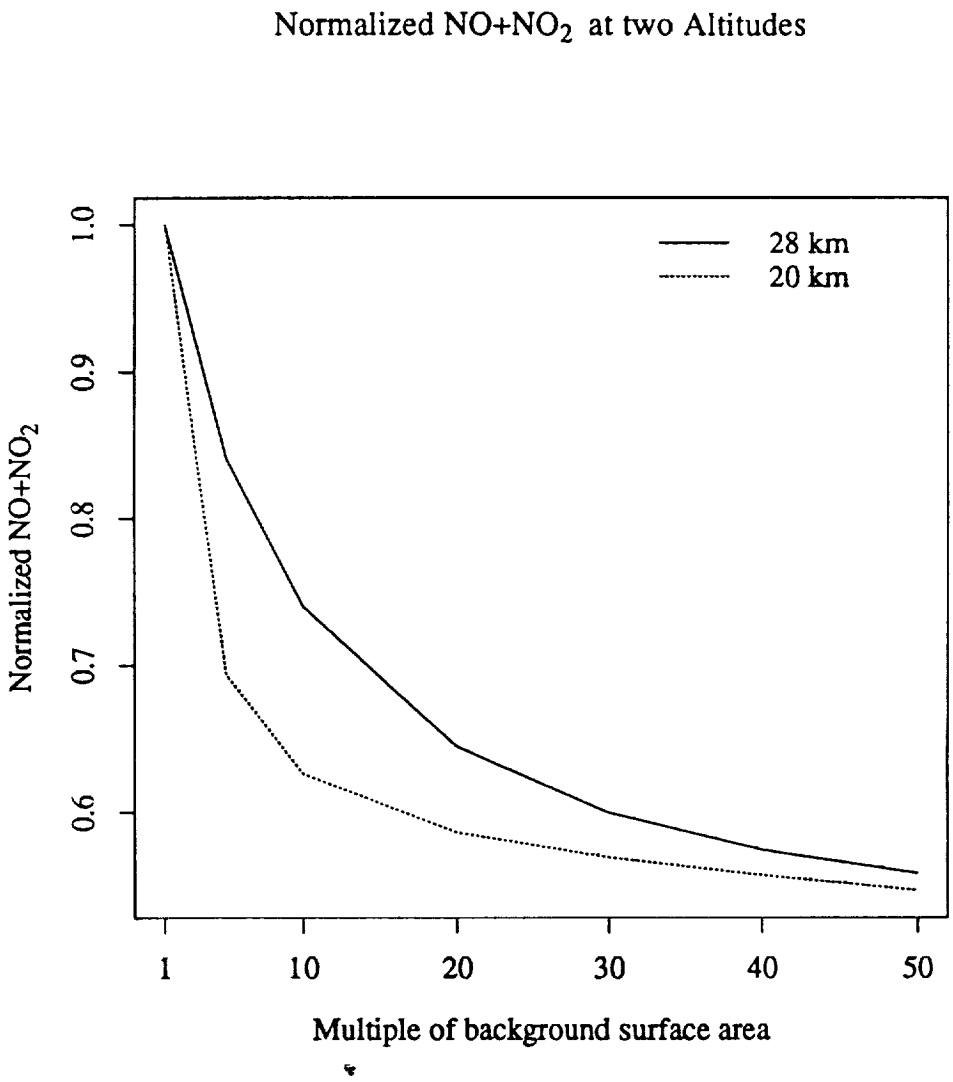

Figure 18. Calculated NOx vs multiple of surface area density. The solid line represents model output at 28 km; the dotted line at 20 km.

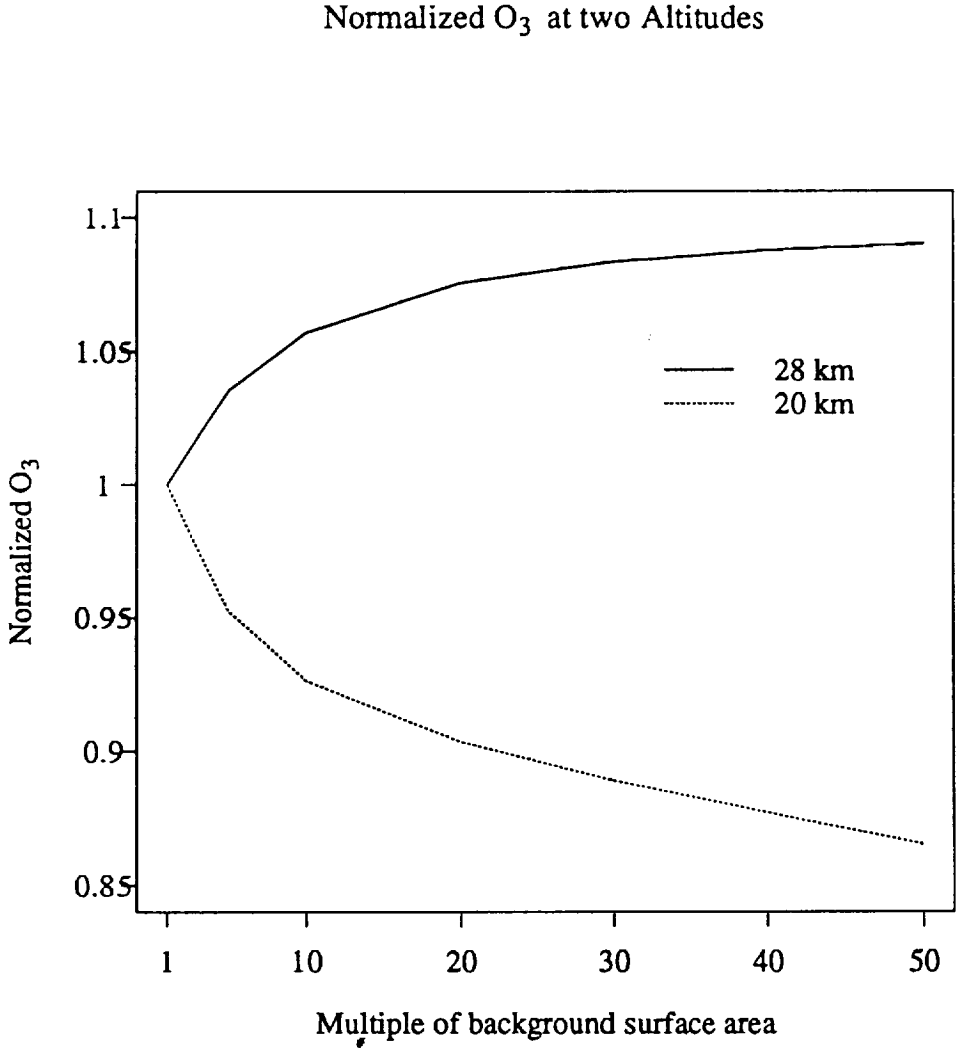

Figure 19. Same as Figure 18, but for O_3.

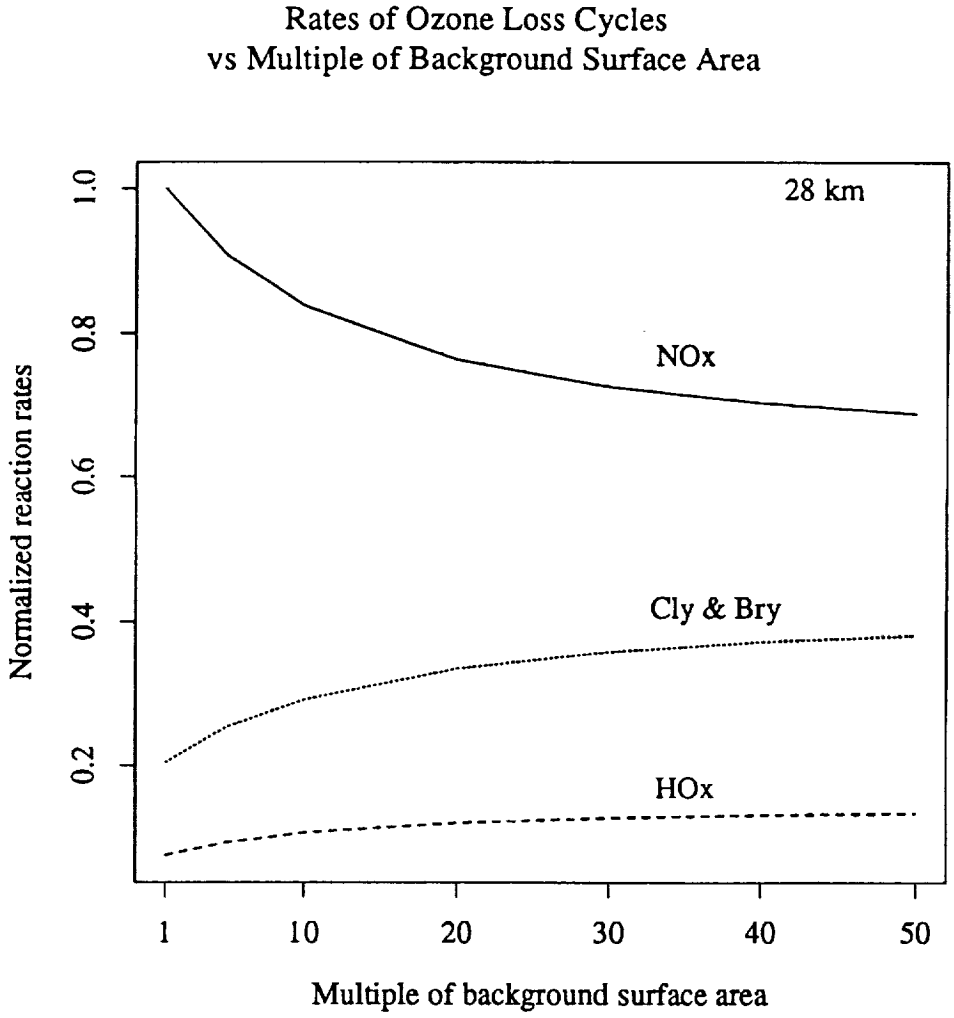

Figure 20. Calculated rates of the major ozone loss cycles, grouped according to family, vs multiple of background surface area density at 28 km. For each family, the rates of the rate-limiting steps for each cycle have been summed together. The solid line denotes the NOx cycles, the dotted line halogen cycles, and the dashed lines the odd hydrogen cycles. The loss rates, in units of $molecules/cm^3/s$, have been normalized to the loss rate of NOx at background surface area densitites.

CHAPTER 6

EVOLUTION OF CHLORINE AND NITROGEN SPECIES IN THE LOWER STRATOSPHERE DURING ANTARCTIC SPRING

Abstract

Observations of O_3, HCl, NO, and NO_2 from the Halogen Occultation Experiment (HALOE) provide a means to investigate chemical change in the lower stratosphere over Antarctica during 23 days in October of 1992. Two long-lived species also observed by HALOE, HF and CH_4, are used as tracers to identify a series of air parcels having similar Cly and NOy abundances and similar temperature histories. Most of the parcels chosen using tracer analysis show low O_3 mixing ratios, less than 1 ppm on the 480 K surface (about 20 km). Parcels with O_3 mixing ratios higher than 1 ppm were occasionally observed in regions of steep horizontal gradients of tracer concentrations where mixing with mid-latitude air may have occurred. HCl mixing ratios for those parcels with less than 1 ppm of ozone more than doubled from early to late October, and NO and NO_2 abundances rose sharply, by a factor of five for NO and a factor of three to four for NO_2. These trends in HCl, NO, and NO_2 agree with model calculations which show that the formation of HCl proceeds quickly when O_3 levels fall so low that (1) the rate of the reaction $Cl + O_3 \rightarrow ClO + O_2$ slows and (2) the rate of the reaction $NO + ClO \rightarrow NO_2 + Cl$ becomes faster than the rate of the competing reaction $NO + O_3 \rightarrow NO_2 + O_2$. Under these conditions, Cl increases at the expense of ClO, and HCl is formed via the reaction $Cl + CH_4 \rightarrow HCl + CH_3$. Stratospheric chlorine is thus shifted from reactive species to the long-lived, reservoir molecule HCl. The repartitioning of the active chlorine family in favor of HCl may limit the extent of ozone depletion. In addition, as the chlorine in $ClONO_2$ is shifted to HCl via ClO and Cl, more active nitrogen becomes available to form NO and NO_2.

6.1. Introduction

In recent years, in-situ and satellite measurements, together with laboratory experiments and model calculations, have increased our understanding of the chemical and transport processes leading to the rapid depletion of stratospheric ozone each spring over Antarctica. (See, for example, Solomon et al., 1986; Solomon et al., 1990; and the special issues of the *Journal of Geophysical Research*, *94*, nos. D9 and D14). The conditions for the annual springtime ozone losses are set the previous winter, when the steep temperature gradient between the pole and the equator leads to strong circumpolar winds, or the polar night jet. The winds act as a barrier to limit horizontal mixing between polar and mid-latitude air. As temperatures fall during winter, polar stratospheric clouds (PSCs) form, providing surfaces upon which heterogeneous chemical reactions may take place. These reactions shift reservoir forms of stratospheric chlorine — HCl and $ClONO_2$ — to photochemically active forms, such as Cl_2 or ClOH. The reactions also shift stratospheric nitrogen from active forms to the reservoir species HNO_3. In spring, when increased sunlight returns to the region, the active chlorine species readily photolyze, leading to large abundances of Cl, which then forms ClO via $Cl + O_3 \rightarrow ClO + O_2$. The radicals Cl and ClO both participate in several catalytic cycles that rapidly destroy ozone. Since active nitrogen abundances are low, there is little NO_2 available to react with ClO to form the less reactive species $ClONO_2$, and the chlorine catalytic cycles continue unimpeded.

While much recent work has studied the processes leading to ozone loss, less attention has been paid to the transport processes or chemical mechanisms that

shut off the fast catalytic cycles that destroy ozone. Mixing of perturbed with unperturbed air not only disperses the chlorine radicals, but also permits these radicals to react with the larger abundances of active nitrogen species present in unperturbed air. These reactions transfer chlorine to longer-lived, less reactive species. Schoeberl et al. (1992) have used aircraft data and model calculations to show that mixing is slow within the vortex, and that mixing at the vortex edge is essentially one-way, with filaments of vortex air being stripped away toward mid-latitudes. More recently, Schoeberl et al. (1995) have analyzed HALOE data and found evidence that the vortex itself remains isolated from mid-latitude air through October. There is, however, much evidence that suggests that rapid mixing between midlatitude and vortex air occurs in a band about 10 degrees latitude in width, centered near the polar night jet (e.g., Pierce et al., 1994a, and Tuck et al., 1995).

Regardless of the extent of mixing with midlatitude air, chemical processes within the vortex may put a brake on the chlorine catalytic cycles once ozone abundances drop to a certain threshold mixing ratio. The theoretical work of Prather and Jaffe (1990) predicted that in typical PSC-processed air — that is, air characterized by low abundances of ozone and high abundances of active chlorine — chlorine may suddenly shift from active forms to the long-lived species HCl through reactions involving NO and CH_4. This quick shift of chlorine to a reservoir species effectively shuts down the ozone loss cycles.

Using data from UARS, Douglass et al. (1995) have reported evidence of this shift in the Antarctic, where springtime ozone levels drop to very low levels, but not in the Arctic, where ozone is less depleted. Douglass et al. (1995) used modified potential vorticity (MPV) to bin parcels for their analysis. This approach

is based on the assumption that parcel trajectories tend to follow potential vorticity contours, and that parcels with the same potential vorticity have experienced similar conditions, such as time exposed to polar stratospheric clouds. Some recent studies, however, suggest that in the lower stratosphere inside the Antarctic and Arctic vortices, potential vorticity may not correlate as well with long-lived tracers such as N_2O as has been assumed (e.g., Tao and Tuck, 1994; Yang, 1995). Diabatic descent or mixing at the vortex edge may account for the deviations from the expected linear correlation between potential vorticity and long-lived tracers over time. As will be discussed below, these deviations pose difficulties in monitoring the repartitioning of long-lived chemical families into member species.

In our work, we have used the long-lived tracers CH_4 and HF to identify parcels within the Antarctic vortex that are of similar photochemical age, have experienced similar rates of denitrification, and thus have similar abundances of both total inorganic chlorine (Cly) and active nitrogen (NOy). In the series of air parcels chosen by tracer analysis, we detect a rapid rise in HCl during the spring of 1992, accompanined by similarly rapid rises in NO and NO_2. These trends are in qualitative agreement with those detected by Douglass et al. (1995). We have also used HALOE tracers CH_4 and HF, together with data from the Cryogenic Limb Array Etalon Spectrometer (CLAES), to determine the Cly and HNO_3 content of the parcels under investigation. Using this information and a photochemical box model, we have modeled the time evolution of HCl, NO, and NO_2.

6.2. Use of Tracers to Select Air Parcels

In 1992, HALOE sunrise observations swept toward and then away from the southern polar region in the last half of September. HALOE sunset observations then moved close to the polar region and then away during the month of October. We have used this sequence of measurements in our study of the chemical evolution of trace species during Antarctic spring.

In order to follow the evolution of short-lived chemical species in this vortex air using HALOE data, it is essential to identify a series of parcels of similar photochemical age and with similar histories — that is, parcels that contain like amounts of total inorganic chlorine and active nitrogen and that have experienced comparable temperatures. For this work, we have used long-lived chemical tracers to select a series of similar parcels during a period of 23 days beginning October 1, 1992.

Chapter 4 outlines the strategy for using tracers such as HF and CH_4 for our work. Briefly, we showed there that for a series of air parcels containing similar abundances of the tracers HF or CH_4, we could assume that the parcels also contained similar abundances of the families NOy and Cly. In this way, we could assign any changes observed in the member species of these families over time to chemical processes that repartition the family.

We note here that within the polar vortex, parcels of air may experience NOy loss through the process of denitrification, in which cloud particles containing HNO_3 grow to sufficient size to fall to lower altitudes. For our work, we assume that mixing takes place rapidly along isopleths, and thus parcels containing similar

quantities of a tracer such as CH_4 have also experienced similar temperature histories and similar growth rates of polar stratospheric clouds. These conditions would lead to similar rates of denitrification for all the parcels under consideration, and similar abundances of NOy leftover after denitrification.

Much recent work has documented the descent of photochemically older air within the Antarctic vortex during the winter months (e.g., Russell III et al., 1993b). Such air is characterized by low abundances of CH_4 and high abundances of HF. Figure 21 shows the distribution of sunrise HF on the 480-K surface during September and early October of 1992. High values of HF mixing ratio (greater than 500 ppt) are apparent in the region poleward of 60 S in the region between about 90 W and 90 E. The mid-latitudes northward of about 45 S are characterized by mixing ratios of 200 ppt or less. In between these two extremes, a steep horizontal gradient in mixing ratios is observed.

Figure 22 shows the correlation of HF with CH_4 at high latitudes in the lower stratosphere during the period October 1-23, 1992. A large degree of scatter is apparent in this plot. There are three possible sources for the scatter in Figure 22. First, the annual increase in stratospheric fluorine due to increasing emissions at the earth's surface may affect the correlation between HF and another tracer when air characterized by a range of ages is plotted. Russell et al. (1996) estimate the rate of increase of stratospheric fluorine to be 6.6 per cent per year.

The second possible reason for the scatter in Figure 22 may be traced to the shorter chemical lifetime of CH_4 in older air containing smaller amounts of CH_4 (less than 1 ppm). Figure 23 shows the chemical lifetimes of CH_4 and HF in tropical air calculated by the Max Planck model. The height interval in the plot (30

to 55 km) was chosen since it is here that the mixing ratios of HF and CH_4 most closely match those observed at lower altitudes close to the poles. It is thus probable that the vortex air we focus on in our study was once carried aloft to this region of rapid chemistry before being tranported poleward in the typical Brewer-Dobson circulation. The Figure shows the chemical lifetime of CH_4 declining rapidly with height above about 35 km. At these high altitudes over the tropics, meridional mixing may compete with chemical processes, and the CH_4 content of a parcel may become more sensitive to the path the parcel takes in the atmosphere. This increased sensitivity may lead to parcels of similar age close to the pole containing variable amounts of CH_4.

The third possible reason for the scatter in Figure 22 may have to do with the small-scale mixing processes within the polar night jet as described by Pierce et al. (1994b). Luo et al. (1995) have noted that the slopes of scatterplots of CH_4 versus HF within the vortex differ from those of similar plots of these tracers outside the vortex. Small-scale mixing could bring together mid-latitude and vortex air and blur the tight linear correlation between these two tracers observed at other latitudes.

Because of the scatter in Figure 22, we have chosen to sort parcels by *both* CH_4 and HF content in order to accomplish our goal of identifying a series of parcels with similar age and temperature history. In other words, we have set limits on both the CH_4 and the HF content for those parcels we wish to examine most closely. For CH_4 we have chosen the interval of 0.75 to 0.9 ppm; for HF, 560 to 650 ppt. In this way, the parcels represented by the outliers in Figure 22 are excluded from the analysis. The box in Figure 22 encloses those parcels we have chosen for

our study. These parcels contain mixing ratios of HF and CH_4 that are typical of air just poleward of the vortex edge (Pierce et al., 1994; Luo et al., 1995). The chosen range of HF mixing ratios, well below the 900 ppt limit, excludes air that has experienced the rapid rates of NO photolysis mentioned above. We must emphasize that parcels characterized by CH_4 and HF mixing ratios outside the chosen ranges have also shown evidence of PSC-processing and ozone loss (e.g., Tuck et al., 1995). These parcels were omitted from our study simply because during the time period under investigation HALOE did not observe a sufficient number of such parcels to unambiguously define trends in the evolution of short-lived trace gases.

It is important to check whether parcels selected by this method show any trend in tracer mixing ratio over time, even within the small intervals chosen. Such a trend could bias the results discussed in the next section. Figure 24 shows a plot of HF versus day of year for October 1-23, 1992, on the 480 K surface for those parcels specified by our constraints on HF and CH_4 mixing ratios. The dotted line shows the average latitude of the parcels selected on each day. The correlation coefficient R of mixing ratios with day is only 0.02. Figure 25 shows a similar plot for CH_4 using the same constraints. Again no trend over time is observed (R = -0.04).

6.3. Observations of Chemical Change

To study the chemistry of air parcels close to the pole during Antarctic spring, HALOE observations during October of 1992 were interpolated to surfaces of constant potential temperature. Following the reasoning of the preceding section, we selected those parcels on the 480-K surface whose CH_4 mixing ratios fell between 0.75

and 0.9 ppm and whose HF mixing ratios fell between 560 and 650 ppt. Figure 26 shows the ozone data for those parcels during the same time period as Figures 24 and 25. Most of the points cluster below about 1 ppm although there are outliers.

A closer look at the parcels with higher ozone shows that many of them are located in regions of steep horizontal gradients in HF or CH_4 mixing ratios. Figure 27 shows the distribution of HF on the 480-K surface during October 14-23, 1992. During this time period, HALOE sunset observations gradually circled away from the vortex region. The triangles represent the parcels whose HF and CH_4 mixing ratios are within the specified ranges. The empty triangles denote those parcels with O_3 less than 1 ppm; the solid triangles, those parcels with O_3 more than 1 ppm. Nine out of 10 parcels with high O_3 are located at about 77 S between 90 E and 170 W, a region where the HF distribution changes rapidly with latitude. Bithell et al. (1994) have noted that the HALOE observations in this region in October 1992 were made close to the strongest winds (i.e., within the jet core), where mixing between mid-latitude and vortex air was most likely to occur. Thus the high O_3 mixing ratios are likely to be evidence of such mixing. Despite this mixing, the median of all the O_3 points in Figure 26 is only 0.6 ppm.

Figure 28 shows HCl during the same time period. For this and subsequent data plots, we show the daily average of observations for those parcels that meet our criteria for CH_4 and HF and also contain ozone mixing ratios of less than 1 ppm. The plot shows a steep rise in HCl, from about 0.8 ppb to 2.2 ppb, during the first ten days of the period, followed by a leveling off to about 2.3 ppb. This trend is consistent with the increase in HCl column amounts observed by Liu et al. (1992) in late October at McMurdo Station.

Some care must be taken in presenting the NO data since the sequence of measurements begin with sunrise observations and end with sunset. Because of nighttime odd nitrogen chemistry, sunset measurements of NO are not expected to match sunrise measurements the following morning, and comparing sunrise measurements from early October to the sunset measurements from the rest of the month may be misleading. Immediately after sunset, when NO_2 photolysis ceases, all NO is converted rapidly to NO_2. During the night NO_2 converts more slowly to N_2O_5. In regions of high ClO, the nighttime chemistry must also include the three-body reaction of ClO + NO_2 to make $ClONO_2$. At dawn, NO_2 photolysis begins renewed production of NO, but the sunrise sum of NO+NO_2, or NOx, will be less than the sunset sum because of the nighttime conversion NO_2 to N_2O_5 and, possibly, to $ClONO_2$.

To correct the sunset values of NO to sunrise values, we first assume that ClO abundances are small by the time HALOE begins making sunset measurements, on October 9. As is discussed below, it is doubtful that much ClO remains by this point. We then follow the procedure outlined in Section 2.4.2 to calculate sunrise NO+NO_2 from the NO+NO_2 of the previous sunset. In Figure 29, the daily average NO for sunrise (October 1 through 7) and corrected sunrise (October 10 through 23) is plotted for the same set of parcels as was selected for Figure 28. Low levels of NO are observed for the first few days, followed by a rapid rise in mixing ratio. Correcting the sunset NO to sunrise value decreases the mixing ratio by an average of 15 per cent. Even with the correction, the NO mixing ratios increase by about a factor five for the time period.

Figure 30 shows the daily average of HALOE measurements of NO_2 for the same set of parcels. As for NO, the NO_2 data in the second part of the period were corrected to show sunrise mixing ratio on the following morning. Again, making the correction decreases the NO_2 values by about 15 per cent. The trend in NO_2 resembles that of NO with, however, much more scatter, perhaps due to the greater difficulty in measuring NO_2 at low altitudes (Gordley et al., 1996). Nonetheless a general increase in mixing ratio is apparent from values of about 0.15 ppb to values of more than 0.4 ppb.

6.4. Model Results

To interpret our observations of trace species during Antarctic spring, calculations were performed with the photochemical box model descibed in Chapter 3. The model was initialized at dawn in the following manner. First, since little work has been done to infer inorganic chlorine from either CH_4 or HF abundances, we used the method of Woodbridge et al. (1995), which infers Cly from N_2O. In this method, total chlorine — the sum of both inorganic and organic chlorine — is first calculated using N_2O observations, the 1992 tropospheric mixing ratio of total chlorine (3670 ppt), and a growth rate of tropospheric chlorine of 2.8 per cent (WMO 1992). An empirical relationship between organic chlorine and N_2O is then implemented to determine the inorganic fraction of total chlorine. In our analysis, we used N_2O observations made by the Cryogenic Limb Array Etalon Spectrometer (CLAES), another instrument on UARS, 13 days prior to the arrival of HALOE in the region (Roche et al., 1993). In the same regions that HALOE later measured

HF and CH_4 values between the limits specified above, N_2O observations averaged about 130 ppb and inferred Cly mixing ratio, about 2.7 ppb. We chose 2.7 ppb as our input value for Cly. As an aside, the value of N_2O mixing ratio obtained from CLAES data for the specified range of CH_4 agrees well with observed correlations of CH_4 and N_2O from ER-2 data (e.g., Kelly et al., 1989).

We partitioned Cly into three species: HCl, $ClONO_2$, and ClO. Based on HALOE data, a value of 1.0 ppb was assigned to HCl. Although $ClONO_2$ was also measured by CLAES, the lifetime of $ClONO_2$ at this time of year is on the order of days, and chlorine partitioning may well have changed in the days before HALOE arrived in the region. To determine an input value for $ClONO_2$, we first note that the sum of HALOE $NO+NO_2$ increased about 1.0 ppb during the period. Our calculations show that little HNO_3 can photolyze to make $NO+NO_2$ during the 23 days under study. We have therefore chosen to assign the missing nitrogen, 1.0 ppb, to $ClONO_2$ and to make 1.0 ppb the input value of that gas. (Our calculations show that nearly all the $ClONO_2$ photolyzes during the time period, so it is doubtful that the initial mixing ratio exceeded 1.0 ppb.) That choice leaves 0.7 ppb of remaining Cly, which we have assigned entirely to ClO. Given these initial values for ClO and $ClONO_2$, the model calculates the mixing ratios of Cl and Cl_2O_2 at each timestep.

For the NOy species, we again relied on HALOE data for the input values of NO and NO_2 (0.1 ppb each). For HNO_3, we looked at CLAES data from the previous month in the same region that HF and CH_4 mixing ratios met our specifications, and found that HNO_3 mixing ratios there averaged about 3.2 ppb. Total active nitrogen ($ClONO_2$ + HNO_3 + NO + NO_2) was thus input as 4.4 ppb, a value consistent with previous observations of denitrification in the region a few degrees poleward of

the vortex edge (Fahey et al., 1990). Input mixing ratios of O_3 and CH_4 were both taken from HALOE measurements — 0.6 ppm in the case of O_3 and 0.8 for CH_4. Aerosol surface areas were input as 3.6 μ^2/cm^3, or half the value of that calculated from HALOE aerosol extinction data (M. Hervig, personal communication). Only half the calculated value was used since comparisons with balloon data show some discrepancies, with HALOE overestimating aerosol surfaces areas (Hervig et al., 1996).

The model was run for 23 days at 20 km and 72 S, with increasing sunlight on each day. Temperature was held fixed at 206 K, which was the average temperature for the time interval for those parcels with less than 1 ppm of ozone (i.e., those parcels that had experienced the least mixing with mid-latitude air). The O_3 column amount, which influences photolysis rates, was also held fixed at 3.8×10^{18} molecules/cm^2, the average HALOE value for the period. Model results show that O_3 declined slightly (about 0.5 ppm) during the first ten days, but then held constant at about 0.55 ppm for the remaining days. Figure 31 shows the evolution of $ClONO_2$, ClO, and HCl during the 23 days of the model run. While $ClONO_2$ values are high in the first part of the period, they fall rapidly as the HCl abundance quickly builds. By the 15th day, HCl has reached a value of 2.6 ppb, somewhat higher than the 2.3 ppb observed by HALOE. This represents a model overestimate of about 13 per cent.

Figure 32 presents model results for four active nitrogen species — HNO_3, NO_2, NO, and $ClONO_2$. The trace gas $ClONO_2$ is shown a second time for comparison with other nitrogen-containing species, and NO and NO_2 are shown here as the sum $NO+NO_2$. Calculated HNO_3 shows an initial decline during the period

due to increased photolysis as the days lengthen. By about the 15th day, however, when much of the chlorine in $ClONO_2$ has shifted to HCl, the nitrogen contained in $ClONO_2$ has shifted mainly to $NO+NO_2$. Some of the nitrogen ends up in HNO_3, which returns to its initial value. The abundance of $NO+NO_2$ rises steadily over the course the period, reaching a level of about 1.0 ppb, a value about the same as the observations.

6.5. Discussion

Using HF and CH_4 as tracers to identify parcels of similar air, we have detected a rapid rise of HCl during October in air that has experienced springtime vortex conditions in the lower stratosphere over Antarctica. The rise in HCl is accompanied by similar rises in NO and NO_2. Ozone mixing ratios show no trend during the time interval. Following the reasoning laid out in Section 3, we can assume that Cly and NOy levels remain roughly constant for all the parcels considered in this study. Thus, the observed changes in the short-lived species are probably not due to mixing processes bringing in air of higher Cly or NOy content to the region, but to rapid chemistry occurring in the aftermath of extensive ozone loss. The model results support our conclusion that these changes are indeed due to chemistry.

Douglass et al. (1995), using MPV as a tracer on the 460 K surface, saw similar rises in the three trace gases under investigation here — HCl, NO, and NO_2. While the trends detected by both methods show some scatter, those using tracer analysis show less, especially for HCl and NO. In addition, our model results better matched observations than the predictions of Douglass et al. (1995), probably

because our input values for Cly and NOy were signficantly lower. In the Douglass et al. study, model results overpredicted these gases in the latter part of October by about 25 per cent for HCl and more than 50 per cent for the sum of $NO+NO_2$.

To understand the dramatic chemical changes occurring in the partitioning of the Cly family, one must look closely at the set of reactions that govern the partitioning of Cly. HCl is formed by the following reaction

$$Cl + CH_4 \rightarrow HCl + CH_3 \tag{6.1}$$

and destroyed by

$$HCl + OH \rightarrow Cl + H_2O \tag{6.2}$$

Both reactions occur slowly in the lower stratosphere, and the lifetime of HCl in this region is on the order of weeks. Even with abundant CH_4 and low levels of O_3, Reaction 6.1 takes place several orders of magnitude more slowly than the corresponding reaction of atomic chlorine with O_3:

$$Cl + O_3 \rightarrow ClO + O_2 \tag{6.3}$$

In order for HCl abundances to rise rapidly in springtime Antarctica, the Cl fraction of available chlorine must increase at the expense of other reactive chlorine species. As O_3 levels fall, the rate of Reaction 6.3 declines slightly, thus increasing Cl abundances and the rate of Reaction 6.1. An even more effective mechanism to increase the Cl fraction of Cly involves two competing reactions of the NO radical:

$$NO + ClO \rightarrow Cl + NO_2 \tag{6.4}$$

$$NO + O_3 \rightarrow O_2 + NO_2 \tag{6.5}$$

Under normal stratospheric conditions of abundant ozone and little ClO, Reaction 6.4 occurs many times slower than Reaction 6.5. Under the perturbed conditions that are typical of springtime over Antarctica, with low O_3 and high ClO, the rate of Reaction 6.4 may become similar to, or faster than, the rate of Reaction 6.5.

Figure 33 presents the rates of three reactions important to springtime chemistry in the stratosphere over Antarctica. The plot shows the daily average rate of Reactions 6.1, 6.4, and 6.5 for each day of the period of the HALOE observations. As in the preceding model plots, the altitude of the calculations is 20 km and the latitude is 72 S. The model has been initialized in the same manner as described above. For clarity, the rate of Reaction 6.1 has been multiplied by a factor of .01, while the other two reaction rates have been multiplied by 10^{-5}. In the early days shown in the plot, the rates of all the reactions considered are increasing with time. After about the 9th day, however, as the rate of the Reaction 6.5 begins to overtake the rate of the competing Reaction 6.4, the rate of HCl production peaks and then declines.

The plot suggests that it is the relative magnitudes of the rates of two NO reactions, Reactions 6.4 and 6.5, that determine the pace of HCl recovery during Antarctic spring. In the early days of the simulation, when large abundances of ClO are present, Reaction 6.4 proceeds more rapidly than Reactions 6.5, and chlorine as a consequence is shifted from ClO to HCl via atomic chlorine. With less ClO in abundance, $ClONO_2$ concentrations also fall, due to a decreased rate of the following reaction:

$$ClO + NO_2 + M \rightarrow ClONO_2 + M. \qquad (6.6)$$

Less $ClONO_2$, in turn, means that more odd nitrogen is available in the form of NO and NO_2, and Reaction 6.4 may proceed even more quickly in a positive feedback loop. At some point, however, so much chlorine has been shifted to HCl that Reaction 6.4 slows down. The rate of Reaction 6.5, on the other hand, continues to increase steadily as NO abundances increase, and will eventually overtake the rate of Reaction 6.4.

To test these ideas, we can run the box model with varying amounts of initial ozone abundance. Figure 34 shows the evolution of chlorine species for an initial O_3 of only 0.3 ppm, or half the initial O_3 of the calculations described above. Figure 35 shows the same set of reactions as Figure 33, but with the smaller ozone input value. With less initial ozone, HCl production peaks earlier, on about day 5, but the magnitude of the peak is about double that with 0.6 ppm of ozone. Again, the rate of HCl production declines once the rate of Reaction 6.5 overtakes that of Reaction 6.4. The earlier peak of HCl production is reflected in Figure 34, with a surge of HCl produced at the expense of $ClONO_2$ early in the time period.

In Figure 36, we show the model calculation of Cly with an initial input of 2.4 ppm of ozone, or 4 times as much ozone as in the first model run. Figure 37 shows the same set of relevant reactions as above. With 2.4 ppm of ozone, HCl mixing ratios climb much more slowly, gaining only about 0.1 ppb during the entire period. As the greater ozone abundance shifts Cl to ClO and NO to NO_2, $ClONO_2$ mixing ratios climb to a daytime value of about 1.5 ppb. ClO levels decline somewhat but still reach noontime values greater than 0.1 ppb throughout the period. In Figure 37, the rates of all three key reactions rise steadily during the 23 days. However, the rates of Reactions 6.1 and 6.4 are much slower than the corresponding rates in

the previous model runs, and even by the end of the period have not yet reached the same values as the peak values obtained before. Reaction 6.5 rises most rapidly of the three reactions, and by day 15 has overtaken Reaction 6.4.

As Douglass et al. (1995) and others have shown, one may express the balance of Cl to ClO mathematically by assuming that all of the relevant radicals are in steady state, and that the reactions of greatest importance under these conditions are Reactions 6.3, 6.4, 6.5, and the photolysis of NO_2:

$$NO_2 + h\nu \rightarrow NO + O. \tag{6.7}$$

With these assumptions, the ratios of NO/NO_2 and Cl/ClO may be written:

$$\frac{[NO]}{[NO_2]} = \frac{J_{6.7}}{k_{6.5}[O_3] + k_{6.4}[ClO]} \tag{6.8}$$

$$\frac{[Cl]}{[ClO]} = \frac{k_{6.4}[NO]}{k_{6.3}[O_3]}. \tag{6.9}$$

Solving for NO in Equation 6.8 and rewriting Equation 6.9, we have:

$$\frac{[Cl]}{[ClO]} = \frac{k_{6.4}J_{6.7}[NO_2]}{k_{6.5}k_{6.3}[O_3]^2 + k_{6.4}k_{6.3}[ClO][O_3]} \tag{6.10}$$

Thus, the steady-state ratio of Cl to ClO depends on the inverse of the square of the O_3 abundance. In regions of low ozone, chlorine is shifted rapidly from ClO to Cl, and then on to HCl. According to the model, nearly all the available chlorine (2.6 out of 2.7 ppb) has been shifted to HCl by the end of the 23-day period, while observations show that only about 2.3 ppb of HCl has been formed by the 23rd day. Reasons for this minor discrepancy are not clear. In any case, since HCl is so long-lived, the repartitioning of the Cly family quickly shuts off further O_3 loss due

to chlorine catalysis. As a final test of the effect of the reaction of CH_4 with atomic chlorine, we have calculated the evolution of O_3 during this time period in a run that excludes Reaction 6.1 from the reaction scheme. The plot also shows model ozone for the standard run. As noted above, ozone in the standard run drops only slightly in the first few model days and then levels off. Model ozone in the run that neglects Reaction 6.1 shows a precipitous drop to about two-thirds its initial value.

6.6. Summary

HALOE observations of trace species within the Antarctic vortex in late September and through October of 1992 suggest a rapid repartitioning of stratospheric chlorine from reactive species to the reservoir species HCl. This dramatic chemical change may be detected by using HF and CH_4 together as tracers to select a series of air parcels of similar photochemical age, having similar abundances of Cly and NOy and similar temperature histories. The rapid repartitioning of chlorine comes about when ozone abundances are very low and abundances of reactive chlorine are very high. Under these conditions, (1) the rate of the reaction $Cl + O_3 \rightarrow ClO + O_2$ slows, and (2) the rate of the reaction $NO + ClO \rightarrow NO_2 + Cl$ becomes faster than the rate of the competing reaction $NO + O_3 \rightarrow NO_2 + O_2$. Both consequences lead to increases in Cl at the expense of ClO. Increased abundances of Cl allow chlorine to be shifted much more rapidly to HCl through the reaction $Cl + CH_4 \rightarrow HCl + CH_3$. Since HCl has a long lifetime, on the order of weeks, the sudden rise in HCl effectively shuts down the chlorine catalytic processes

that deplete ozone. The shift in chlorine may have importance as filaments of vortex air peel off the vortex edge in spring and are transported toward mid-latitudes.

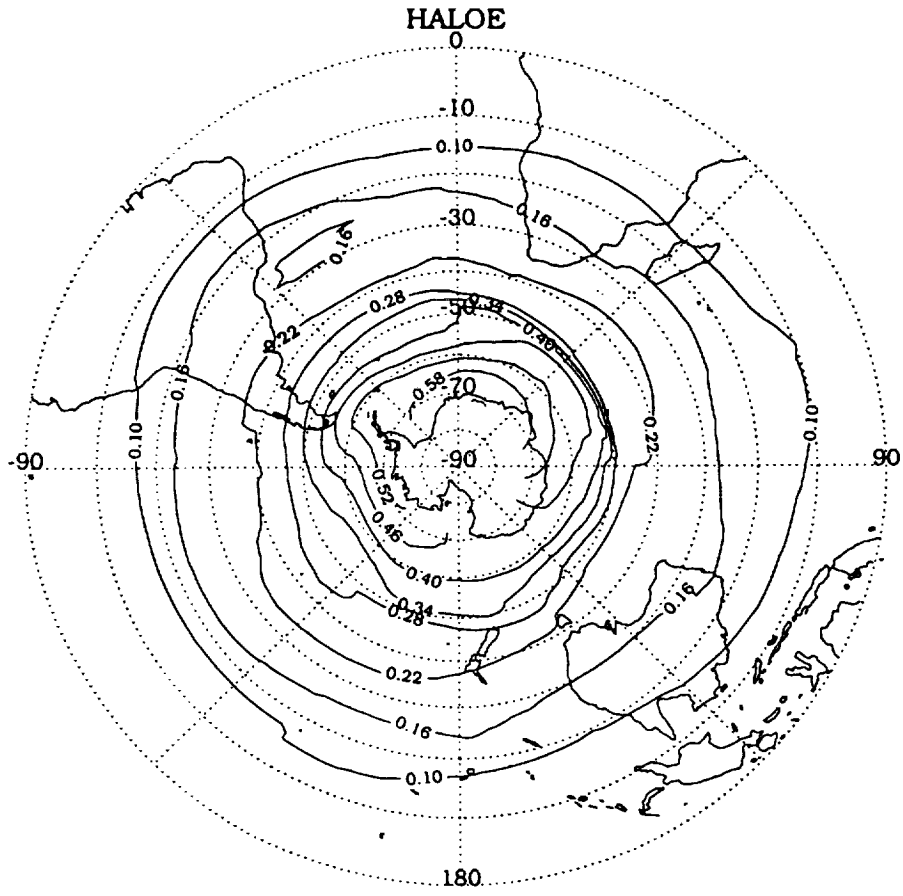

Figure 21. Polar stereographic contour plot of HALOE sunrise HF on the 480-K surface from September 7 to October 5, 1992. Contours are in parts per billion.

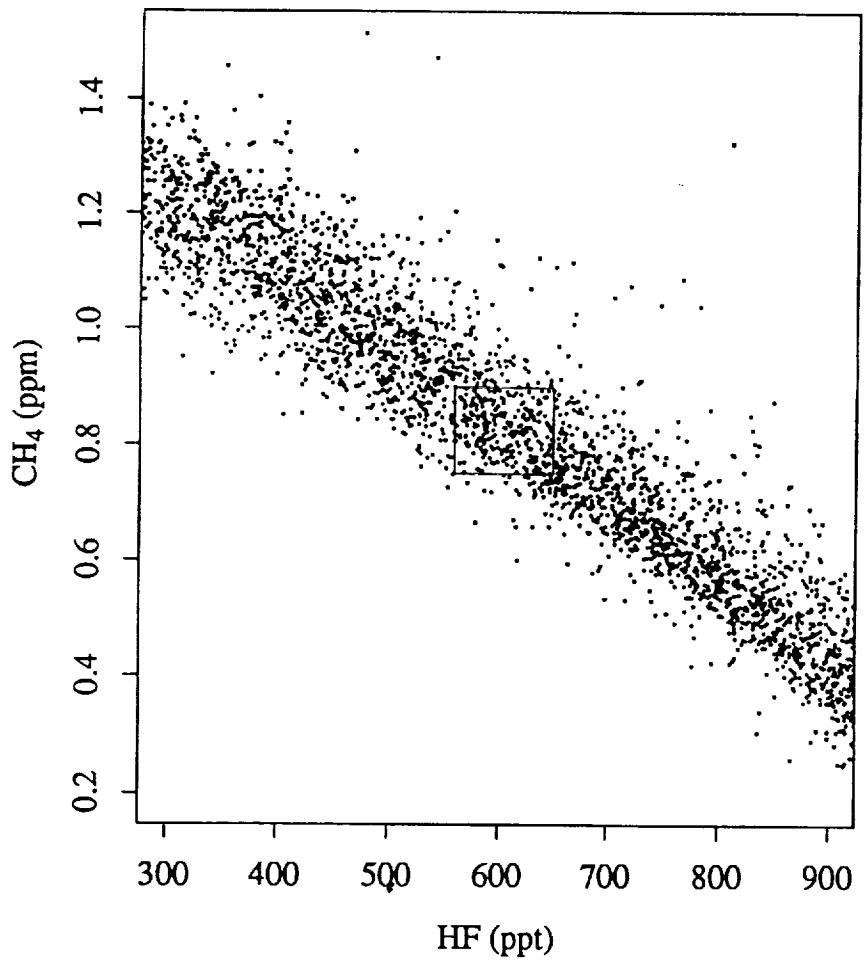

Figure 22. Correlation of HALOE CH_4 vs HF mixing ratios between 15 and 25 km and 62 and 78 S during the time period October 1-23, 1992.

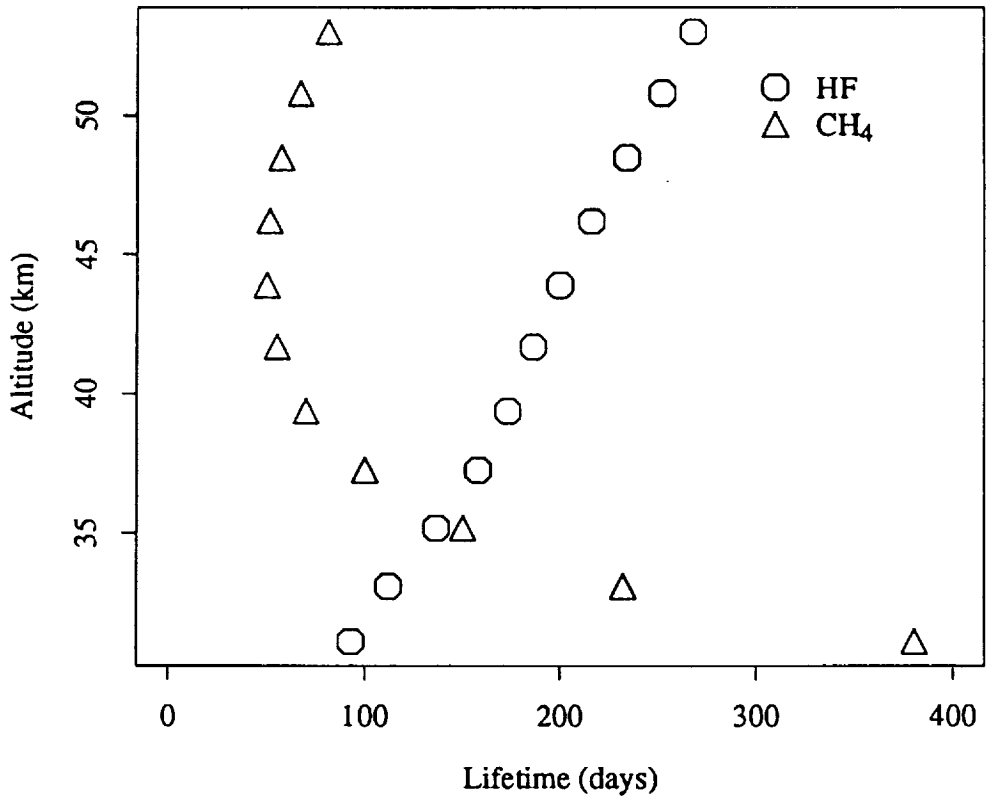

Figure 23. Chemical lifetimes of HF and CH_4, calculated by a two-dimensional, photochemical model. The circles denote HF production lifetime due to CFC photolysis; the triangles show net CH_4 loss by reaction with $O(^1D)$, Cl, and OH.

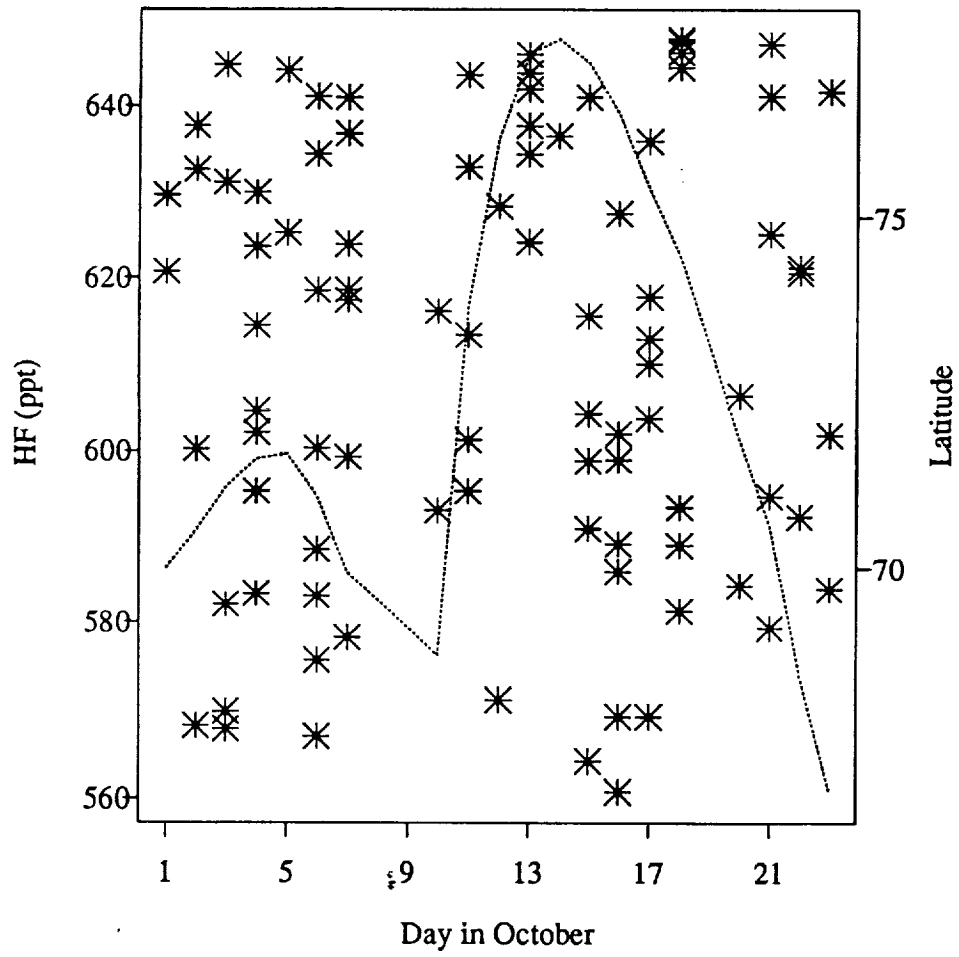

Figure 24. HALOE sunrise and sunset HF observations (stars) on the 480 K surface for October 1-23, 1992. Only those parcels containing 560 to 650 ppt of HF and 0.75 to 0.9 ppm of CH_4 are shown. The dotted line shows the average daily latitudes observed for the parcels within the specified limits of HF and CH_4.

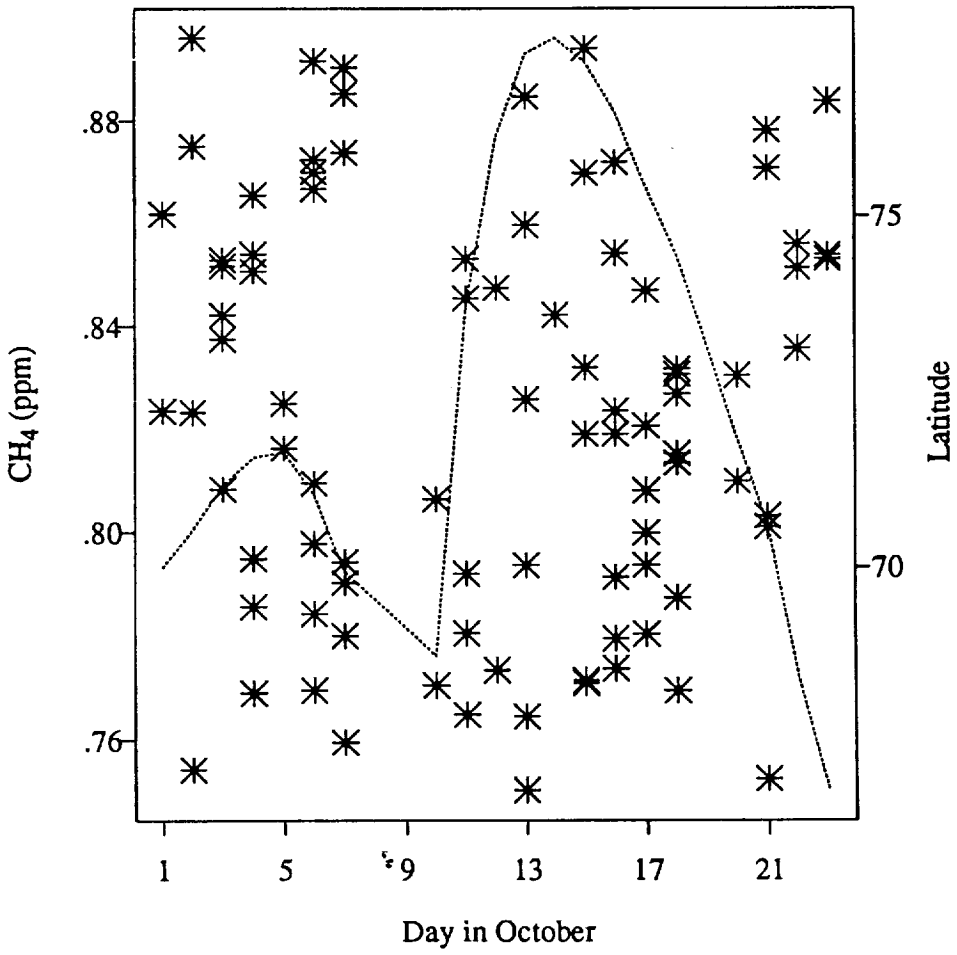

Figure 25. HALOE sunrise and sunset CH_4 observations, as in Figure 24.

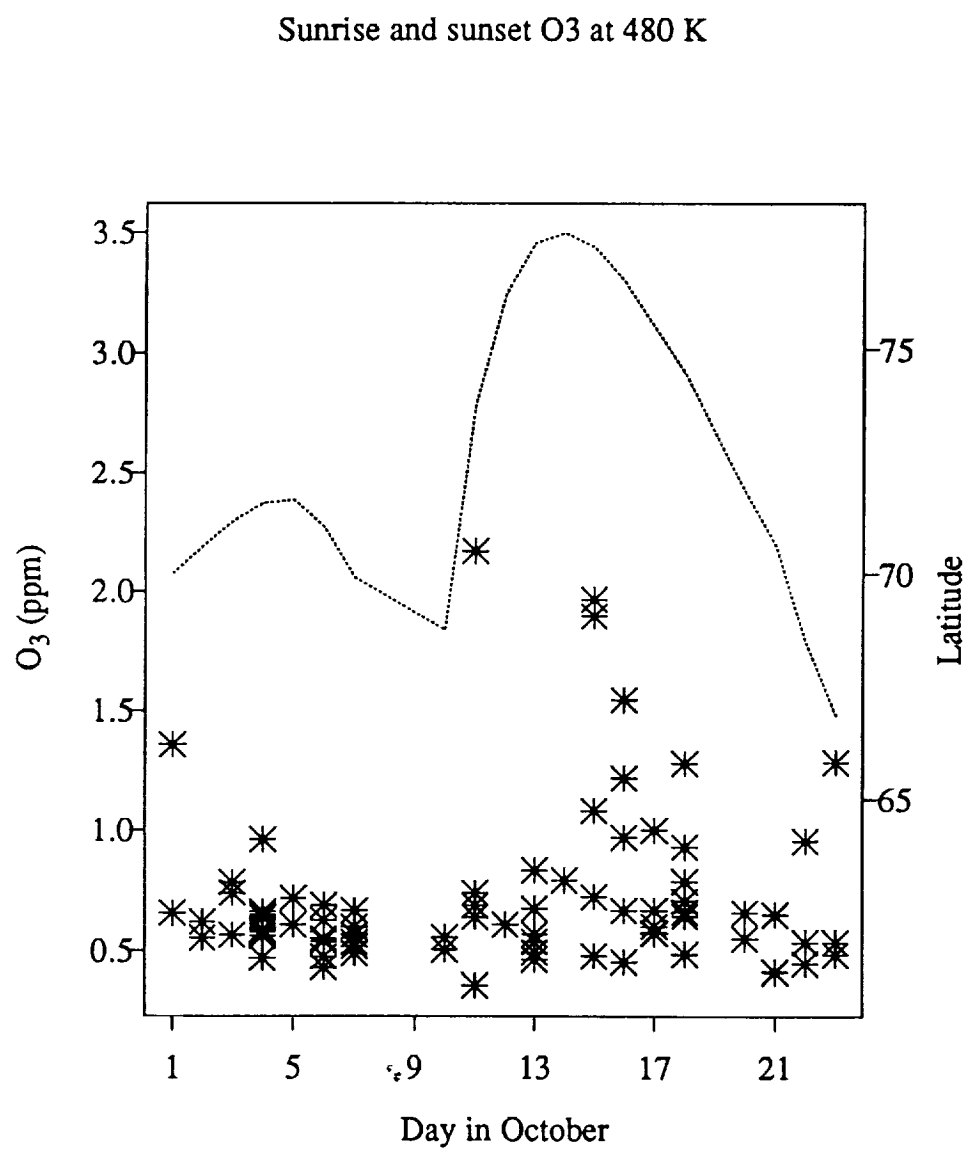

Figure 26. HALOE sunrise and sunset O_3 observations on the 480-K surface. Only those parcels containing 560 to 650 ppt of HF and 0.75 to 0.9 ppm of CH_4 ppt are shown.

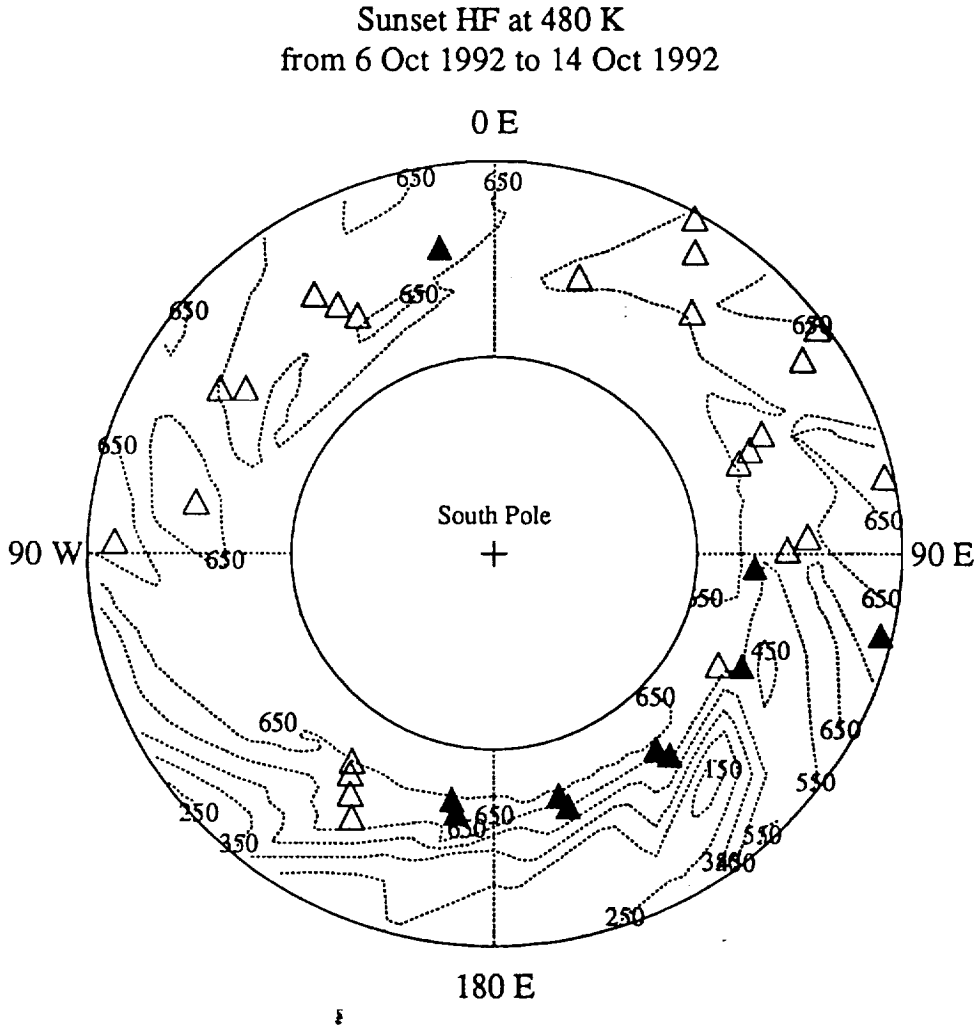

Figure 27. Polar stereographic contour plot of HALOE sunset observations of HF on the 480 K surface from October 14 to October 31, 1992. The outer latitude ring is 70 S. The triangles represent the parcels with a HF and CH_4 content within the specified limits (see text). The solid triangles denote those parcels containing more than 1 ppm of ozone; the unfilled triangles, those parcels containing less than 1 ppm.

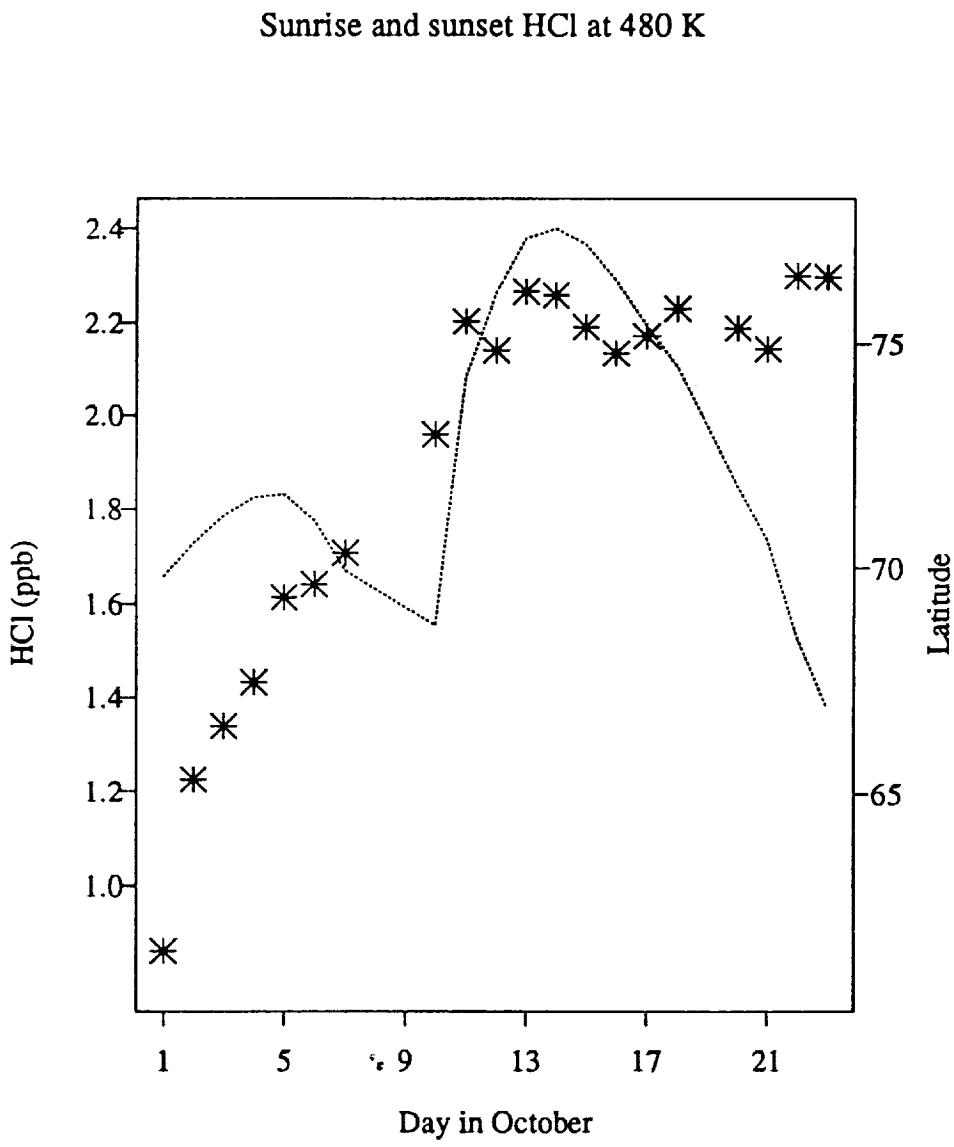

Figure 28. Daily average HALOE sunrise and sunset HCl at 480 K for the same time period and HF and CH_4 constraints as Figure 26.

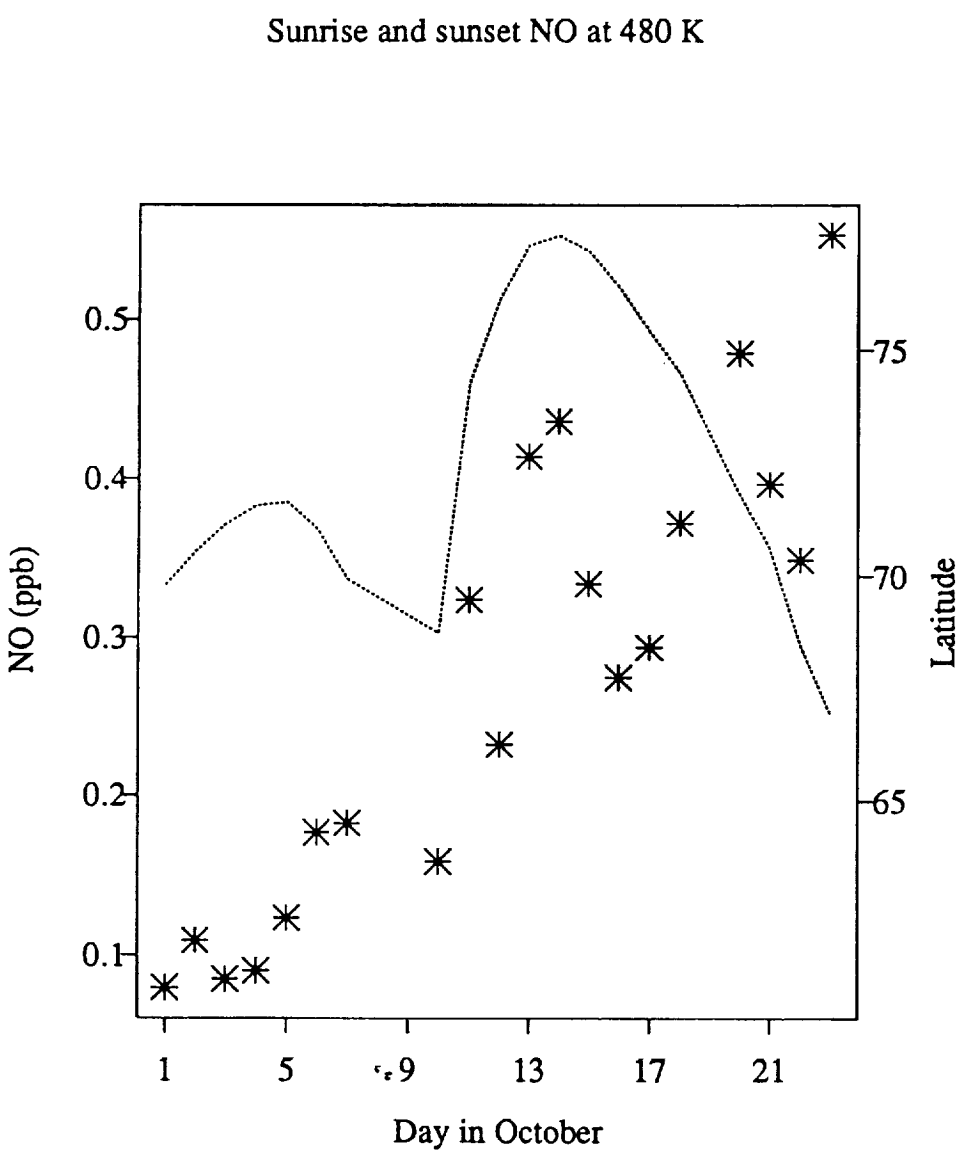

Figure 29. Daily average HALOE NO at 480 K for the same time period and HF and CH_4 constraints as in Figure 26. The data points before October 10 represent sunrise observations; after that date the data have been corrected to sunrise.

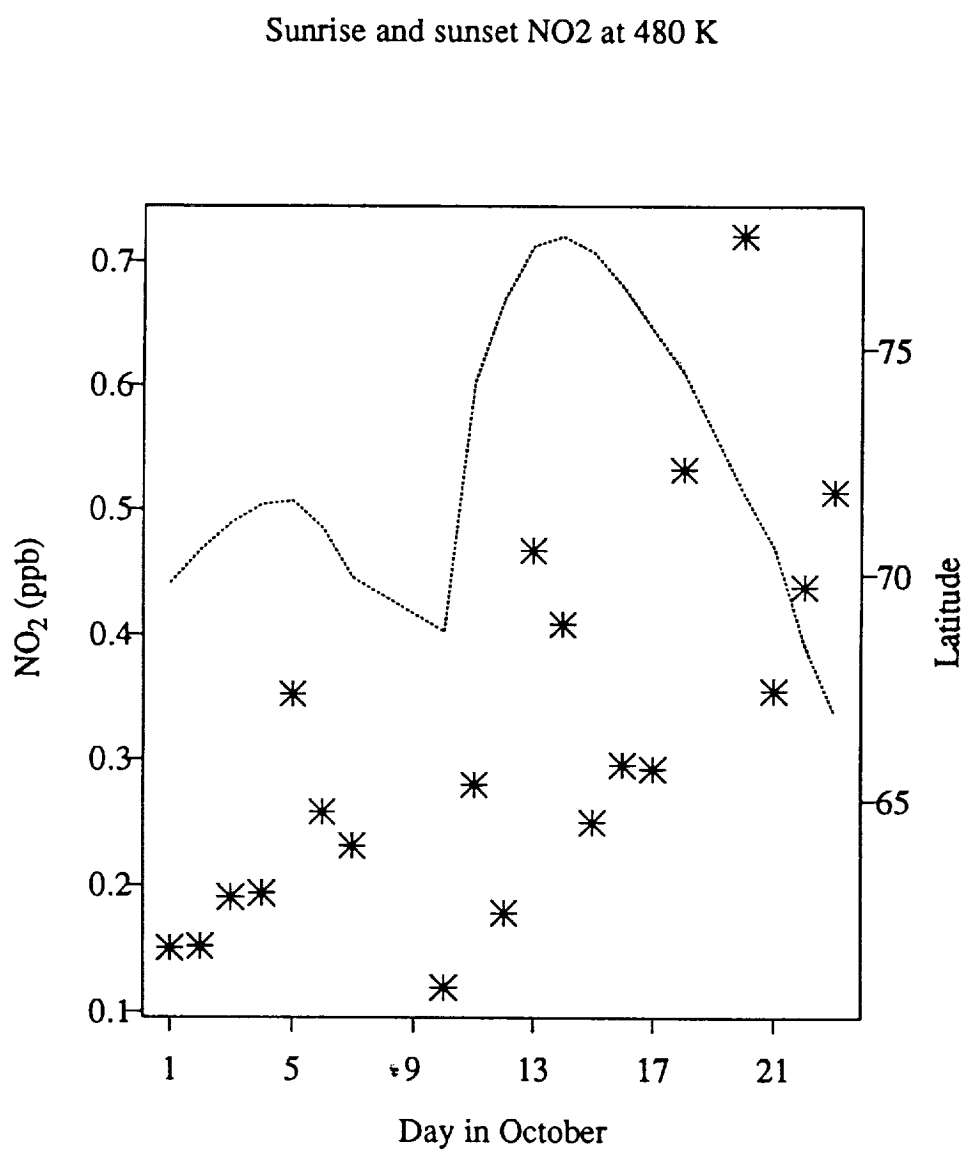

Figure 30. Daily average HALOE NO_2 at 480 K for the same time period and HF and CH_4 constraints as in Figure 26. The data points before October 10 represent sunrise observations; after that date the data have been corrected to sunrise.

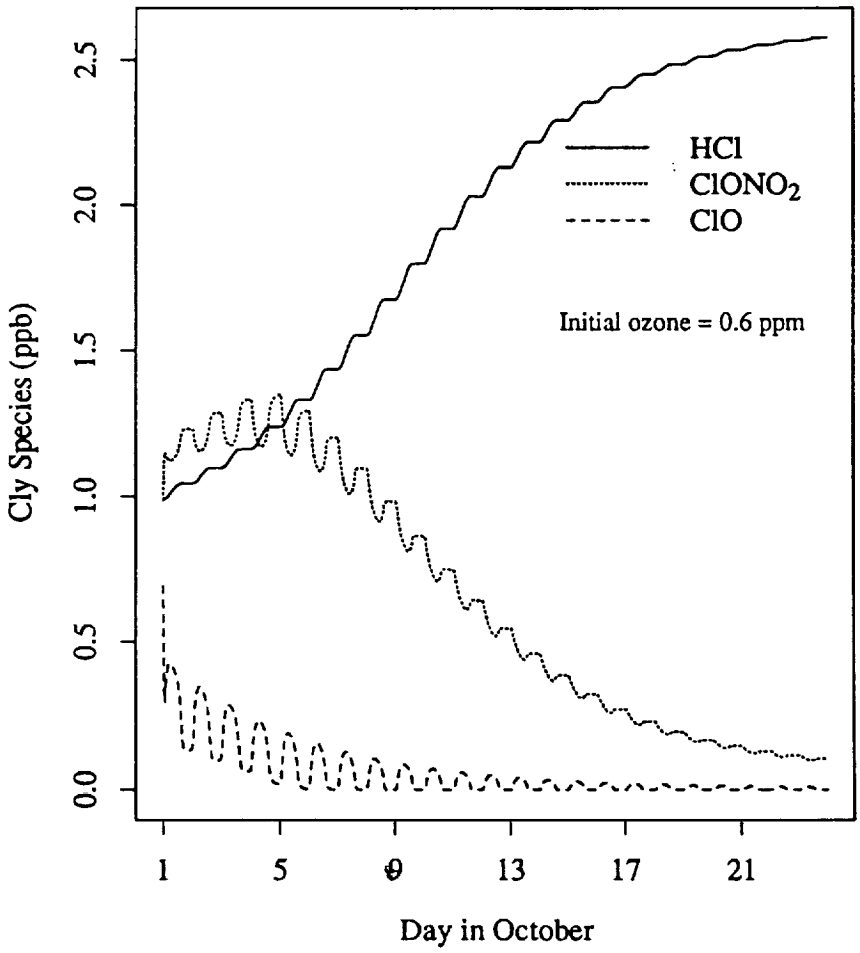

Figure 31. Calculated HCl, $ClONO_2$, and ClO at 20 km during the same time period as the HALOE observations.

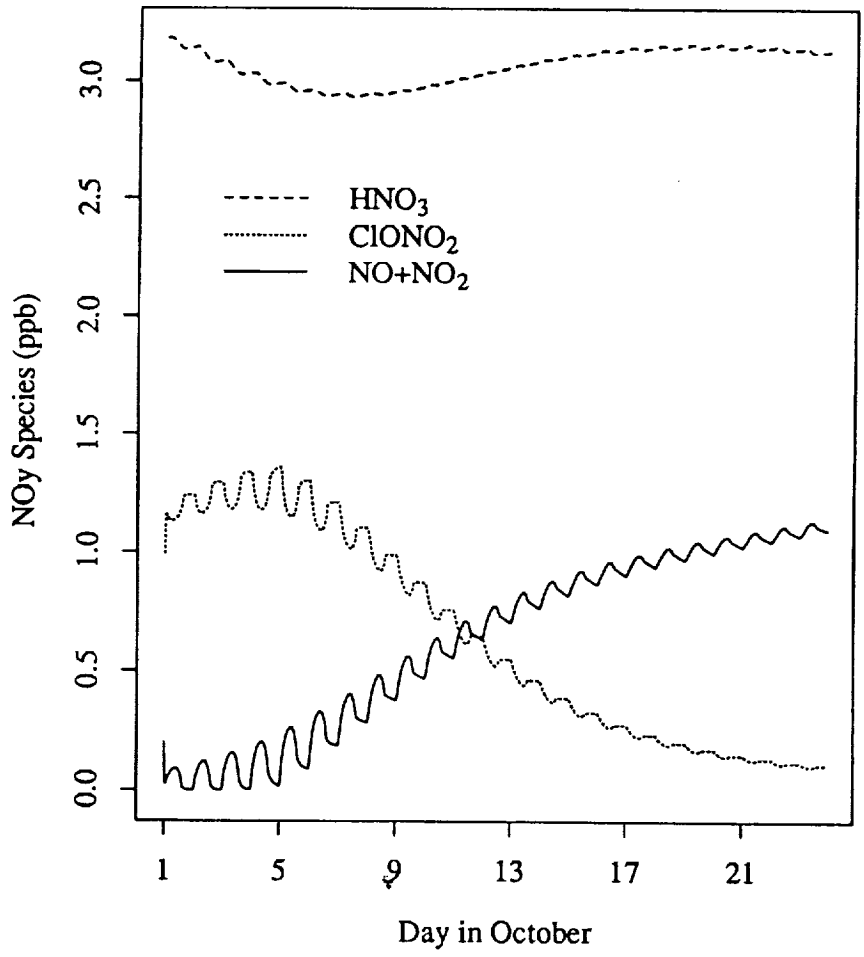

Figure 32. Calculated HNO_3, $ClONO_2$, and $NO+NO_2$ at 20 km during the same time period as the HALOE observations.

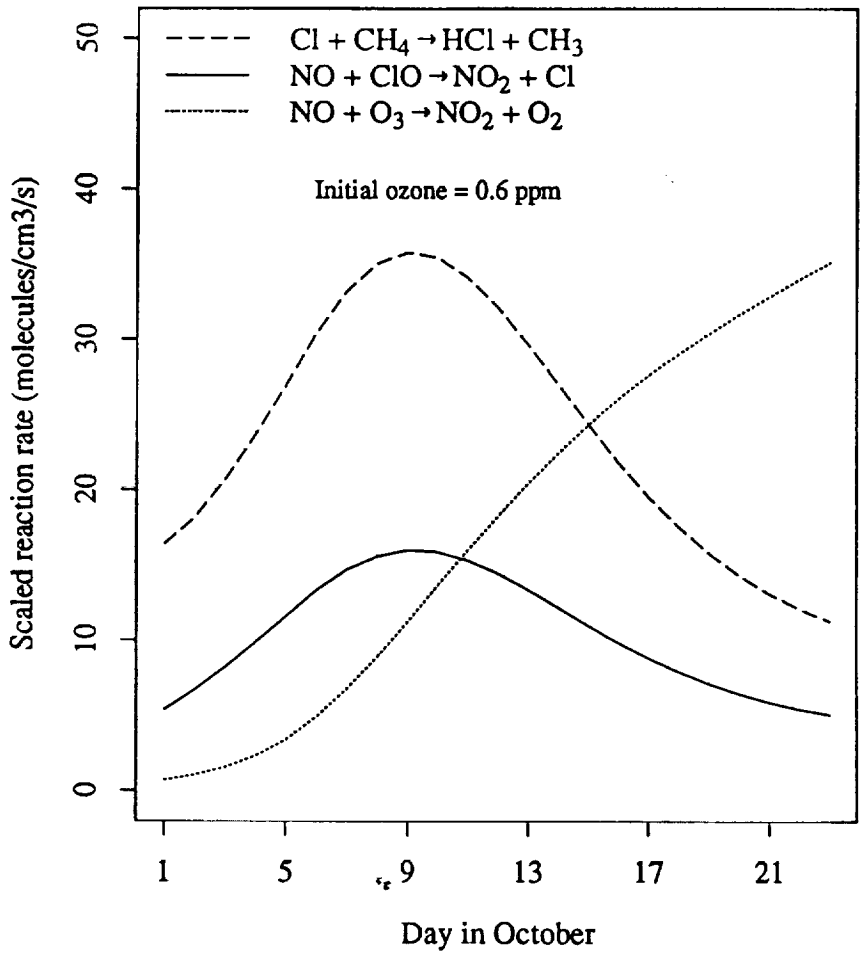

Figure 33. Rates of three key reactions in springtime chemistry over Antarctica calculated with the same model conditions as above. The rate of the Reaction Cl + CH_4 has been multiplied by a a factor of .01, while the other two reaction rates have been multiplied by 10^{-5}.

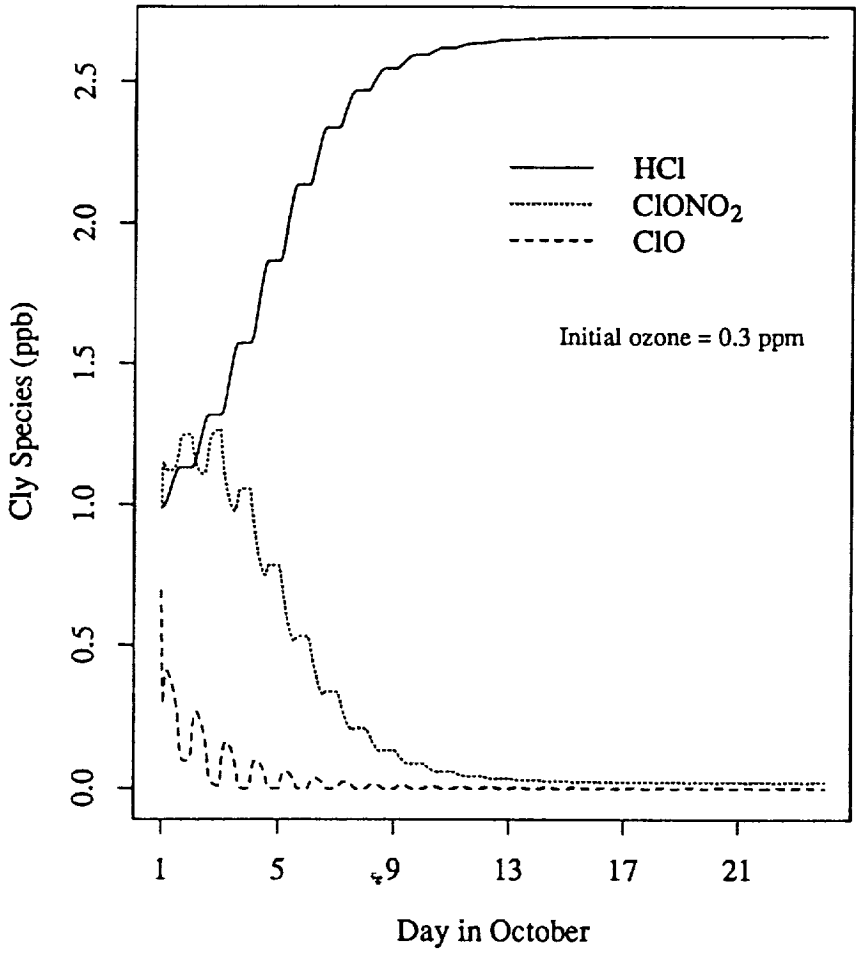

Figure 34. Calculated HCl, $ClONO_2$, and ClO at 20 km as Figure 31, but with only 0.3 ppm initial ozone.

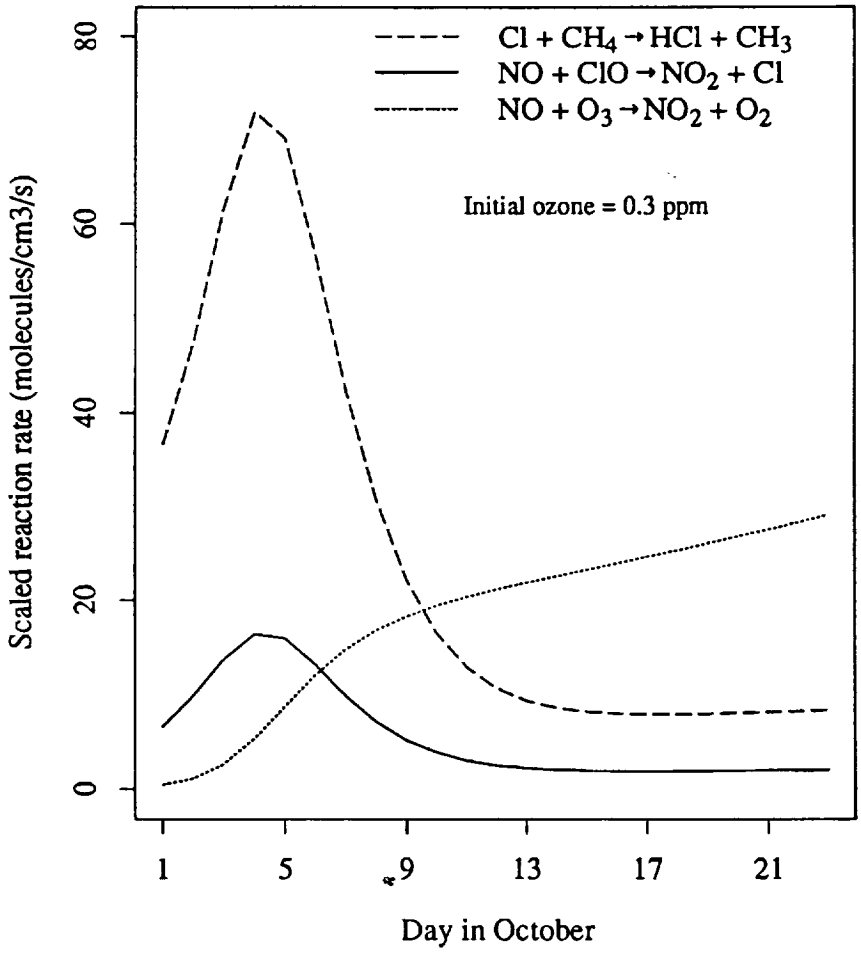

Figure 35. Rates of key reactions in springtime chemistry as in Figure 33, but with only 0.3 ppm initial ozone.

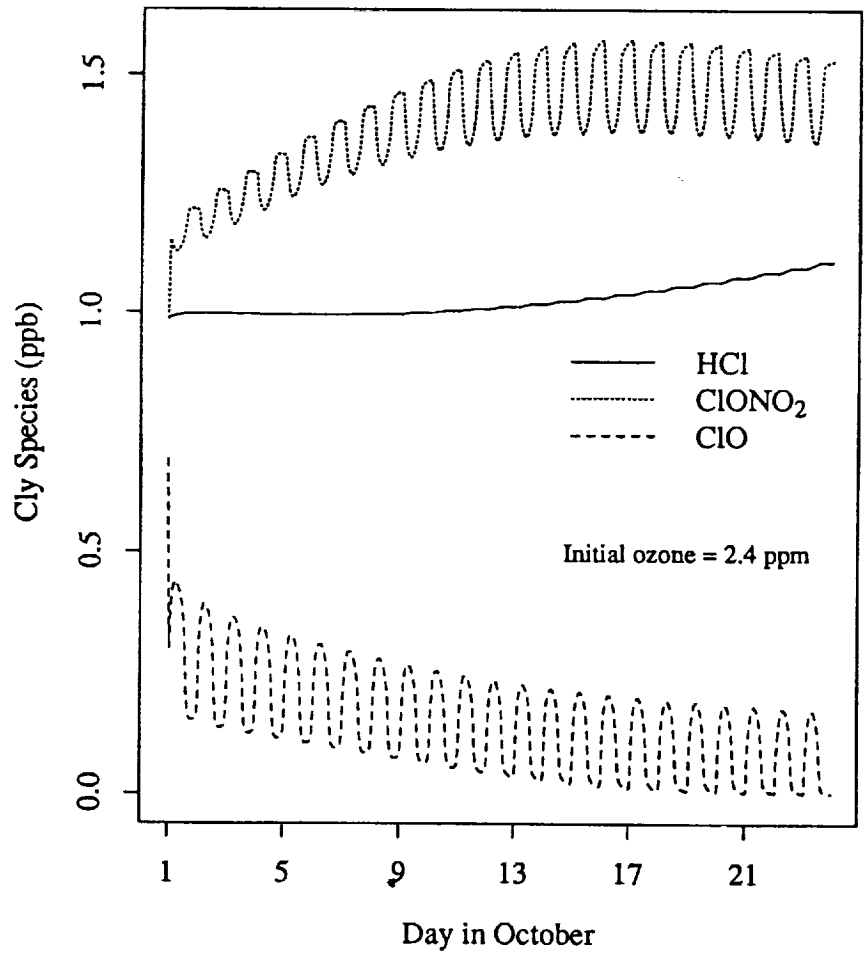

Figure 36. Calculated HCl, $ClONO_2$, and ClO at 20 km as in Figure 31, but with 2.4 ppm initial ozone.

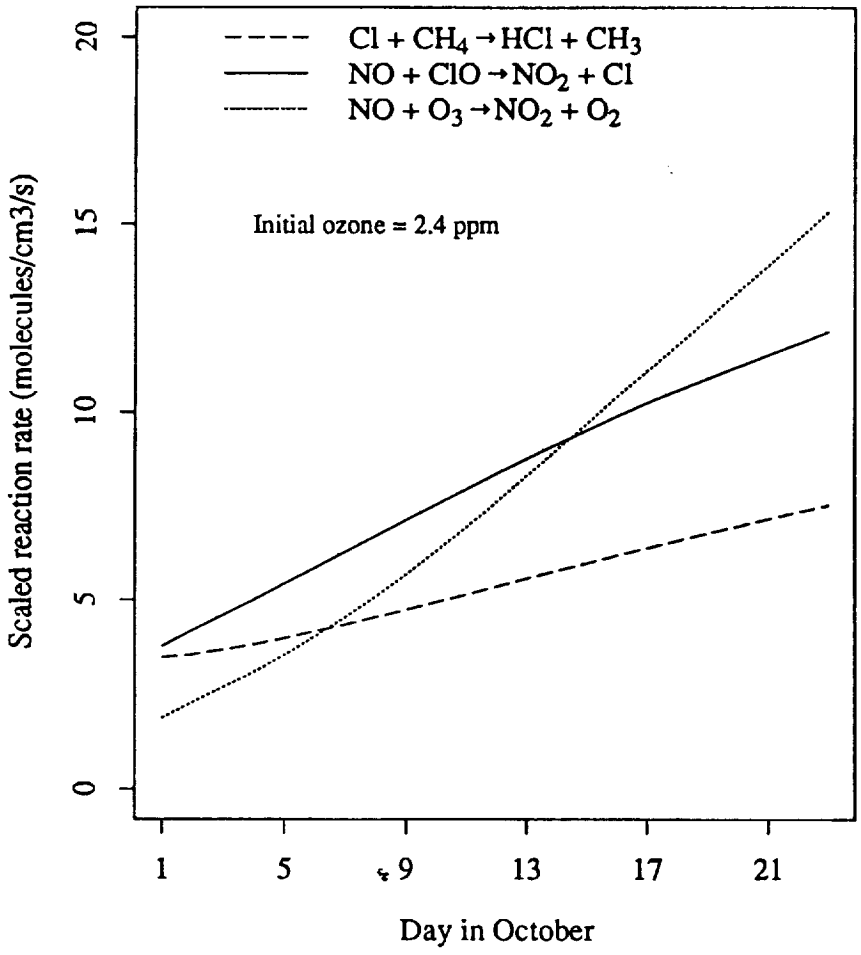

Figure 37. Rates of key reactions in springtime chemistry as in Figure 33, but with 2.4 ppm initial ozone.

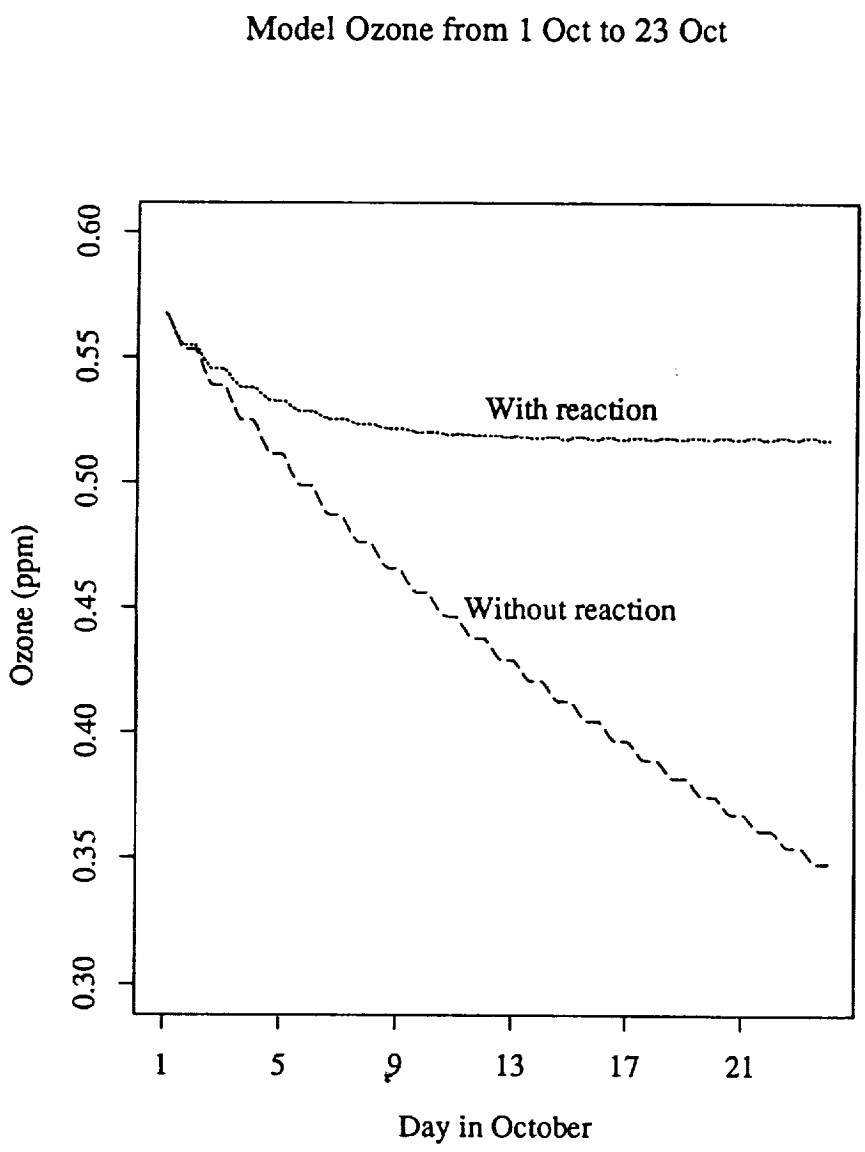

Figure 38. Ozone calculated with and without the reaction $Cl + CH_4 \rightarrow HCl + CH_3$ for the same days as the HALOE observations.

CHAPTER 7

CONCLUSIONS.

This work shows the utility of tracer analysis as a means to distinguish between change due to transport processes in the stratosphere and change due to chemistry. Tracer material serves as a kind of clock that assigns a photochemical age to the air parcels observed. We may assume that parcels with similar abundances of tracer material have been exposed to similar quantities of solar radiation and thus contain similar abundances of the chemical families that derive from source gases, such as N_2O or the CFCs. Thus for any series of air parcels, observations of just one or two member species of a family provide sufficient information to draw conclusions about the partitioning of that family over timescales of weeks or even years.

In two studies, we used tracer analysis to follow chemical processes of importance to the stratospheric ozone budget. In the first study, we examined the response of NOx and ozone at 17 mb to the presence of aerosol leftover from the 1991 eruption of Mount Pinatubo. One important conclusion of this study was that NOx in this region of the stratosphere plays a dominant role in ozone loss chemistry. This result could have implications in the event that a fleet of high-speed civilian transport aircraft is launched, and aircraft emissions of reactive nitrogen reach this high in the stratosphere. In the second study, we tracked the abundances of chlorine and nitrogen species in the wake of significant ozone depletion over Antartica in spring. Here we found that under these conditions, a dramatic shift in chlorine from

radical species to the reservoir species HCl takes place, shutting down further ozone loss via catalytic chlorine cycles.

BIBLIOGRAPHY

Abbatt, J. P. D., and M. J. Molina. The heterogeneous reaction ClOH + HCl $\rightarrow$ Cl_2 + H_2O on ice and nitric acid trihydrate: reaction probabilities and stratospheric implications. *Geophysical Research Letters 19*, 461–464, 1992.

Avallone, L. M., and M. J. Prather. Photochemical evolution of ozone in the lower tropical stratosphere. *Journal of Geophysical Research 101*, 1457–1461, 1996.

Avallone, L. M., D. W. Toohey, W. M. Schauffler, W. H. Pollock, L. E. Heidt, E. L. Atlas, and K. R. Chan. In situ measurements of BrO during AASE II. *Geophysical Research Letters 22*, 831–834, 1995.

Bekki, S., and J. A. Pyle. Potential impact of combined NOx and SOx emissions from future high speed civil transport aircraft on stratospheric aerosols and ozone. *Geophysical Research Letters 20*, 723–726, 1993.

Bithell, M., L. J. Gray, J. E. Harries, J. M. Russell III, and A. F. Tuck. Synoptic interpretation of measurements from HALOE. *Journal of the Atmospheric Sciences 51*, 2942–2956, 1994.

Bluth, G. J. S., S. D. Doiron, C. C. Schnetzler, A. J. Krueger, and L. S. Walter. Global tracking of the SO_2 clouds from the June, 1991, Mount Pinatubo eruptions. *Geophysical Research Letters 19*, 151–154, 1992.

Bojkov, R. D., C. S. Zerefos, D. S. Balis, I. C. Ziomas, and A. F. Bais. Record low total ozone during Northern winters of 1992 and 1993. *Geophysical Research Letters 20*, 1351–1354, 1993.

Boughner, R., J. C. Larsen, and M. Natarajan. The influence of NO and ClO variations at twilight on the interpretation of solar occultation measurements. *Geophysical Research Letters 7*, 231–234, 1980.

Brasseur, G., and C. Granier. Mount Pinatubo aerosols, chlorofluorocarbons, and ozone depletion. *Science 257*, 1239–1242, 1992.

Brasseur, G., and S. Solomon. *Aeronomy of the Middle Atmosphere.* Dordrecht: D. Reidel, 1986.

Browell, E. V., C. F. Butler, S. Ismail, M. A. Fenn, S. A. Kooi, A. F. Carter, A. F. Tuck, O. B. Toon, M. H. Proffitt, M. Loewenstein, M. R. Schoeberl, I. Isaksen, and G. Braathen. Airborne lidar observations in the wintertime Arctic stratosphere: ozone. *Geophysical Research Letters 17*, 325–328, 1990.

Brühl, C., and P. J. Crutzen. Scenarios of possible changes in atmospheric temperatures and ozone concentrations due to man's activities, estimated with a one-dimensional coupled photochemical climate model. *Climate Dynamics 2*, 173–203, 1988.

Burkholder, J. B., R. K. Talukdar, A. R. Ravishankara, and S. Solomon. Temperature dependence of the HNO_3 UV absorption cross sections. *Journal of Geophysical Research 98*, 22937–22948, 1993.

Cadle, R. D., P. Crutzen, and D. Ehhalt. Heterogeneous chemical reactions in the stratosphere. *Journal of Geophysical Research 80*, 3381–3385, 1975.

Chandra, S., C. H. Jackman, and E. L. Fleming, 1995. Recent trends in ozone in the upper stratosphere: Implications for chlorine chemistry. In *AGU 1995 Fall Meeting Abstract Supplement*, Washington, D.C. American Geophysical Union.

Chapman, S. On ozone and atomic oxygen in the upper atmosphere. *Philosophical Magazine 10*, 369–383, 1930.

Coffey, M. T., and W. G. Mankin. Observations of the loss of stratospheric NO_2 following volcanic eruptions. *Geophysical Research Letters 20*, 2873–2876, 1993.

Considine, D. B., A. R. Douglass, and .C. H. Jackman. Sensitivity of two-dimensional model predictions of ozone response to stratospheric models: An update. *Journal of Geophysical Research 100*, 3075–3090, 1995.

Crutzen, P. J. The influence of nitrogen oxides on the atmospheric ozone content. *Quarterly Journal of the Royal Meteorological Society 96*, 320–328, 1970.

Crutzen, P. J. Ozone production rates in oxygen-hydrogen-nitrogen oxide atmosphere. *Journal of Geophysical Research 76*, 7311–7327, 1971.

Crutzen, P. J., and F. Arnold. Nitric acid formation in the cold Antarctic stratosphere: a major cause for the springtime "ozone hole". *Nature 324*, 651–655, 1986.

Crutzen, P. J., and L. T. Gidel. A two-dimensional model of the atmosphere. 2. The tropospheric budgets of anthropogenic chlorocarbons, co, CH_4, CH_3Cl and the effect of various NOx sources on tropospheric ozone. *Journal of Geophysical Research 88*, 6641–6661, 1983.

Crutzen, P. J., J. U. Groose, C. Brühl, R. Müller, and J. M. Russell III. A reevaluation of the ozone budget with HALOE UARS data: No evidence for the ozone deficit. *Science 268*, 705–708, 1995.

DeMore, W. B., S. P. Sander, D. M. Golden, R. F. Hampson, M. J. Kurylo, C. J. Howard, A. R. Ravishankara, C. E. Kolb, and M. J. Molina. *Chemical Kinetics and Photochemical Data for Use in Stratospheric Modeling.* JPL Publication 92-20. Pasadena: National Aeronautics and Space Administration, 1992.

Deshler, T., B. J. Johnson, and W. R. Rozier. Balloonborne measurements of Pinatubo aerosol during 1991 and 1992 at 41 N: vertical profiles, size distribution, and volatility. *Geophysical Research Letters 20*, 1435–1438, 1993.

Dessler, A. E., S. R. Kawa, D. B. Considine, J. W. Waters, L. Froidevaux, and J. B. Kumer. UARS measurements of ClO and NO_2 at 40 and 46 km and implications for the model "ozone deficit". *Geophysical Research Letters 23*, 339–342, 1996.

Dlugokencky, E. J., L. P. Steele, P. M. Lang, and K. A. Masarie. The growth rate and distribution of atmospheric methane. *Journal of Geophysical Research 99*, 17021–17043, 1994.

Douglass, A. R., M. R. Schoeberl, R. S. Stolarski, J. W. Waters, and J. M. Russell III. Interhemispheric differences in springtime production of HCl and $ClONO_2$ in the polar vortices. *Journal of Geophysical Research 100*, 13967–13978, 1995.

Fahey, D. W., S. R. Kawa, E. L. Woodbridge, P. Tin, J. C. Wilson, H. H. Jonsson, J. E. Dye, D. Baumgardner, S. Borrmann, D. W. Toohey, L. M. Avallone, M. H. Proffitt, J. Margitan, M. Loewenstein, J. R. Podolske, R. J. Salawitch, S. C. Wofsy, M. K. W. Ko, D. E. Anderson, M. R. Schoeberl, and K. R. Chan. *In situ* measurements constraining the role of sulphate aerosols in mid-latitude ozone depletion. *Nature 363*, 509–514, 1993.

Fahey, D. W., K. K. Kelly, S. R. Kawa, A. F. Tuck, M. Loewenstein, K. R. Chan, and L. E. Heidt. Observations of denitrification and dehydration in the winter polar stratospheres. *Nature 344*, 321–324, 1990.

Farman, J. C., B. G. Gardiner, and J. D. Shanklin. Large losses of total ozone in Antarctica reveal seasonal ClO_x/NOx interaction. *Nature 315*, 207–210, 1985.

Frederick, J. E., and A. D. Alberts. Prolonged enhancement in surface ultraviolet radiation during the Antarctic spring of 1990. *Geophysical Research Letters 18*, 1869–1871, 1991.

Frederick, J. E., and C. Erlick. Trends and interannual variations in erythemal sunlight, 1978-1993. *Photochemistry and Photobiology 9*, 476–484, 1995.

Frederick, J. E., E. C. Weatherhead, and E. K. Haywood. Long-term variations in ultraviolet sunlight reaching the biosphere: calculations for the past three decades. *Photochemistry and Photobiology 54*, 781–788, 1992.

Garcia, R. R., and S. Solomon. A new numerical model of the middle atmosphere 2. Ozone and related species. *Journal of Geophysical Research 99*, 12937–12951, 1994.

Gleason, J. F., P. K. Bhartia, J. R. Herman, R. McPeters, P. Newman, R. S. Stolarski, L. Flynn, G. Labow, D. Larko, C. Seftor, C. Wellemeyer, W. D. Komhyr, A. J. Miller, and W. Planet. Record low global ozone in 1992. *Science 260*, 523–526, 1993.

Gordley, L. L., J. M. Russell III, L. J. Mickley, J. E. Frederick, J. H. Park, K. A. Stone, G. M. Beaver, J. M. McInerney, L. E. Deaver, G. C. Toon, F. J. Murcray, R. D. Murcray, M. R. Gunson, J. P. D. Abbatt, R. L. Mauldin III, G. H. Mount, and J. F. Blavier. Validation of nitric oxide and nitrogen dioxide measurements made by HALOE for the UARS platform. Accepted for publication in *Journal of Geophysical Research*, 1996.

Grant, W. B., 1995. Tropical stratospheric ozone changes following the eruption of Mount Pinatubo. In *The effects of the Mt. Pinatubo eruption on the atmosphere and climate*, NATO Advanced Research Workshop. Springer-Verlag.

Hanson, D. R., A. R. Ravishankara, and S. Solomon. Heterogeneous reactions in sulfuric acid aerosols: A framework for model calculations. *Journal of Geophysical Research 99*, 3615–3629, 1994.

Hauglustaine, D. A., C. Granier, G. P. Brasseur, and G. Mégie. The importance of atmospheric chemistry in the calculation of radiative forcing on the climate system. *Journal of Geophysical Research 99*, 1173–1186, 1994.

Herman, J. R., and D. Larko. Low ozone amounts during 1992-1993 from Nimbus 7 and Meteor 3 total ozone mapping spectrometers. *Journal of Geophysical Research 99*, 3483–3496, 1994.

Hervig, M. C., J. M. Russell III, T. Deshler, L. L. Gordley, and L. Thomason. Aerosol size distributions and compositions obtained from HALOE multiwavelength aerosol extinction measurements. Manuscript in preparation, 1996.

Hofmann, D. J., J. W. Harder, J. M. Rosen, J. V. Hereford, and J. R. Carpenter. Ozone profile measurements at McMurdo Station, Antarctica, during the spring of 1987. *Journal of Geophysical Research 94*, 16527–16536, 1989a.

Hofmann, D. J., S. J. Oltmans, W. D. Komhyr, J. M. Harris, J. A. Lathrop, A. O. Langford, T. Deshler, B. J. Johnson, A. Torres, and W. A. Matthews. Ozone loss in the lower stratosphere over the United States in 1992-1993: Evidence for heterogeneous chemistry on Pinatubo aerosol. *Geophysical Research Letters 21*, 65–68, 1994b.

Hofmann, D. J., S. J. Oltmans, J. A. Lathrop, J. M. Harris, and H. Vömel. Record low ozone at the South Pole in the spring of 1993. *Geophysical Research Letters 21*, 421–424, 1994c.

Hofmann, D. J., and S. Solomon. Ozone destruction through heterogeneous chemistry following the eruption of El Chicon. *Journal of Geophysical Research 94*, 5029–5041, 1989b.

Jackman, C. H., R. S. Stolarski, and J. A. Kaye. Two-dimensional monthly average ozone balance from Limb Infrared Monitor of the Stratosphere and Strato-

spheric and Mesospheric Sounder data. *Journal of Geophysical Research 91*, 1103–1116, 1986.

Johnston, H. Reduction of stratospheric ozone by nitrogen oxide catalysts from supersonic transport exhaust. *Science 173*, 517–522, 1971.

Johnston, P. V., R. L. McKenzie, J. G. Keys, and W. A. Matthews. Observations of depleted stratospheric NO_2 following the Pinatubo volcanic eruption. *Geophysical Research Letters 19*, 211–213, 1992.

Kawa, S. R., D. W. Fahey, J. C. Wilson, M. R. Schoeberl, A. R. Douglass, R. S. Stolarski, E. L. Woodbridge, H. Jonsson, L. R. Lait, P. A. Newman, M. H. Proffitt, D. E. Anderson, M. Loewenstein, K. R. Chan, C. R. Webster, R. D. May, and K. K. Kelly. Interpretation of NOx/NOy observations from AASE-II using a model of chemistry along trajectories. *Geophysical Research Letters 20*, 2507–2510, 1993.

Kelly, K. K., A. F. Tuck, D. M. Murphy, M. H. Proffitt, D. W. Fahey, R. L. Jones, D. S. McKenna, M. Loewenstein, J. R. Podolske, S. E. Strahan, G. V. Ferry, K. R. Chan, J. F. Vedder, G. L. Gregory, W. D. Hypes, M. P. McCormick, E. V. Browell, and L. E. Heidt. Dehydration in the lower Antarctic stratopshere during late winter and early spring, 1987. *Journal of Geophysical Research 94*, 11317–11357, 1989.

Kerr, J. B., D. I. Wardle, and D. W. Tarasick. Record low ozone values over Canada in early 1993. *Geophysical Research Letters 20*, 1979–1982, 1993.

Kinne, S., and O. B. Toon. Buffering of stratospheric circulation by changing amounts of tropical ozone: a Pinatubo case study. *Geophysical Research Letters 19*, 1927–1930, 1992.

Ko, M. K. W., N. D. Sze, and D. K. Weisenstein. The roles of dynamical and chemical processes in determining the stratospheric concentration of ozone in one-dimensional and two-dimensional models. *Journal of Geophysical Research 94*, 9889–9896, 1989.

Koike, N., N. B. Jones, W. A. Matthews, P. V. Johnston, R. L. McKenzie, D. Kinnison, and J. Rodriguez. Impact of Pinatubo aerosols on the partitioning between NO_2 and HNO_3. *Geophysical Research Letters 21*, 597–600, 1994.

Labitzke, K., and M. P. McCormick. Stratospheric temperature increases due to Pinatubo aerosols. *Geophysical Research Letters 19*, 207–210, 1992.

Liu, X., R. D. Blatherwick, F. J. Murcray, J. G. Keys, and S. Solomon. Measurements and model calculations of HCl column amounts and related parameters over McMurdo during the austral spring in 1989. *Journal of Geophysical Research 97*, 20795–20804, 1992.

Logan, J. A. Trends in the vertical distribution of ozone: an analysis of ozonesonde data. *Journal of Geophysical Research 99*, 25553–25585, 1994.

Logan, J. A., M. J. Prather, S. C. Wofsy, and M. B. McElroy. Atmospheric chemistry: response to human influence. *Philosophical transactions of the Royal Society of London, BA 290*, 187–234, 1978.

Lubin, D., and E. H. Jensen. Effects of clouds and stratospheric ozone depletion on ultraviolet radiation trends. *Nature 377*, 710–712, 1995.

Luo, M., R. J. Cicerone, and J. M. Russell III. Analysis of Halogen Occultation Experiment HF versus CH_4 correlation plots: Chemistry and transport implications. *Journal of Geophysical Research 100*, 13927–13937, 1995.

Manney, G. L., L. Froidevaux, J. W. Waters, L. S. Elson, E. F. Fishbein, R. W. Zurek, R. S. Harwood, and W. A. Lahoz. The evolution of ozone observed by UARS MLS in the 1992 late winter Southern polar vortex. *Geophysical Research Letters 20*, 1279–1282, 1993.

Manney, G. L., L. Froidevaux, J. W. Waters, R. W. Zurek, W. G. Read, L. S. Elson, J. B. Kumer, J. L. Mergenthaler, A. E. Roche, A. O'Neill, R. S. Harwood, I. MacKenzie, and R. Swinbank. Chemical depletion of ozone in the Arctic lower stratosphere during winter 1992-93. *Nature 370*, 429–434, 1994a.

Manney, G. L., R. W. Zurek, A. O'Neill, and R. Swinbank. On the motion of air through the stratospheric polar vortex. *Journal of the Atmospheric Sciences 51*, 2973–2994, 1994b.

McCormick, M. P., and R. E. Veiga. SAGE II measurements of early Pinatubo aerosols. *Geophysical Research Letters 19*, 155–158, 1992.

McCormick, M. P., R. E. Veiga, and W. P. Chu. Stratospheric ozone profile and total ozone trends derived from the SAGE I and SAGE II data. *Geophysical Research Letters 19*, 269–272, 1992.

McElroy, M. B., R. J. Salawitch, S. C. Wofsy, and J. A. Logan. Reductions of Antarctic ozone due to synergistic interactions of chlorine and bromine. *Nature 321*, 759–762, 1986.

Middlebrook, A. M., L. T. Iraci, L. S. McNeill, B. G. Koehler, M. A. Wilson, O. W. Saastad, M. A. Tolbert, and D. R. Hanson. Fourier transform-infrared studies of thin H_2SO_4/H_2O films: Formation, water uptake, and solid-liquid phase changes. *Journal of Geophysical Research 98*, 20473–20481, 1993.

Mills, M. J., A. O. Langford, T. J. O'Leary, K. Arpag, H. L. Miller, M. H. Profitt, R. W. Sanders, and S. Solomon. On the relationship between stratospheric aerosols and nitrogen dioxide. *Geophysical Research Letters 20*, 1187–1190, 1993.

Minschwaner, K., G. P. Anderson, L. A. Hall, and K. Yoshino. Polynomial coefficients for calculating O_2 Schumann-Runge cross sections at 0.5 cm^{-1} resolution. *Journal of Geophysical Research 97*, 10103–10108, 1992.

Minschwaner, K., R. J. Salawitch, and M. B. McElroy. Absorption of solar radiation by O_2: implications for O_3 and lifetimes of N_2O, $CFCl_3$, and CF_2Cl_2. *Journal of Geophysical Research 98*, 10543–10561, 1993.

Minton, T. K., C. M. Nelson, T. A. Moore, and M. Okumura. Direct observation of ClO from chlorine nitrate photolysis. *Science 258*, 1342–1345, 1992.

Molina, M. J., and F. S. Rowland. Stratospheric sink for chlorofluoromethanes: chlorine atom-catalyzed destruction of ozone. *Nature 249*, 810–812, 1974.

Molina, M. J., J. R. Zhang, P. J. Wooldridge, J. R. McMahon, J. E. Kim, H. Y. Chang, and K. D. Beyer. Physical chemistry of the $H_2SO_4/HNO_3/H_2O$ system: Implications for the formation of polar stratospheric clouds and heterogeneous chemistry. *Science 261*, 1418–1423, 1993.

Natarajan, M., and L. B. Callis. Examination of stratospheric ozone photochemistry in light of recent data. *Geophysical Research Letters 16*, 473–476, 1989.

Pierce, R. B., , W. L. Grose, J. M. Russell III, A. F. Tuck, R. Swinbank, and A. O'Neill. Spring dehydration in the Antarctic stratospheric vortex observed by HALOE. *Journal of the Atmospheric Sciences 51*, 2931–2941, 1994a.

Pierce, R. B., T. D. Fairlie, W. L. Grose, R. Swinbank, and A. O'Neill. Mixing processes within the polar night jet. *Journal of the Atmospheric Sciences 51*, 2957–2972, 1994b.

Pitari, G., and L. Ricciardulli. Stratospheric denitrification due to polar aerosol formation: Implications for a future atmosphere with increased CO_2. *Geophysical Research Letters 21*, 1791–1794, 1994.

Plumb, R. A., and M. K. W. Ko. Interrelationships between mixing ratios of long-lived stratospheric constituents. *Journal of Geophysical Research 97*, 10145–10156, 1992.

Plumb, R. A., M. K. W. Ko, and R. Shia. Representation of localized aircraft NOy emissions in a two-dimensional model of stratospheric ozone. *Journal of Geophysical Research 100*, 20901–20911, 1995.

Plumb, R. A., D. W. Waugh, R. J. Atkinson, P. A. Newman, L. R. Lait, M. R. Schoeberl, E. V. Browell, A. J. Simmons, and M. Loewenstein. Intrusions in the the lower stratospheric Arctic vortex during the winter of 1991-1992. *Journal of Geophysical Research 99*, 1089–1105, 1994.

Prather, M. Solution of the inhomogeneous Rayleigh scattering atmosphere. *The Astrophysical Journal 192*, 787–792, 1974.

Prather, M., and A. H. Jaffe. Global impact of the Antarctic ozone hole: chemical propagation. *Journal of Geophysical Research 95*, 3473–3492, 1990.

Prather, M. J., and E. E. Remsberg (Eds.). *The atmospheric effects of stratospheric aircraft: Report of the 1992 Models and Measurements Workshop.* Washington, DC: National Aeronautics and Space Administration, 1993.

Press, W. H., B. P. Flannery, W. A. Teukolsky, and W. T. Vetterling. *Numerical recipes: the art of scientific computing.* Cambridge, UK: Cambridge University Press, 1986.

Profitt, M. H., K. Aikin, J. J. Margitan, M. Loewenstein, J. R. Podolske, A. Weaver, K. R. Chan, H. Fast, and J. W. Elkins. Ozone loss inside the northern polar vortex during the 1991-1992 winter. *Science 261*, 1150–1154, 1993.

Profitt, M. H., D. W. Fahey, K. K. Kelly, and A. F. Tuck. High-latitude ozone loss outside the Antarctic ozone hole. *Nature 342*, 233–237, 1989.

Profitt, M. H., J. J. Margitan, K. K. Kelly, M. Loewenstein, J. R. Podolske, and K. R. Chan. Ozone loss in the Arctic polar vortex inferred from high-altitude aircraft measurements. *Nature 347*, 31–36, 1990.

Ramaswamy, V., M. D. Schwarzkopf, and K. P. Shine. Radiative forcing of climate from halocarbon-induced global stratospheric ozone loss. *Nature 355*, 810–812, 1992.

Randel, W. J., F. Wu, J. M. Russell III, J. W. Waters, and L. Froidevaux. Ozone and temperature changes in the stratosphere following the eruption of Mt. Pinatubo. *Journal of Geophysical Research 100*, 16753–16764, 1995.

Read, W. G., L. Froidevaux, and J. W. Waters. Microwave Limb Sounder measurement of stratospheric SO_2 from the Mt. Pinatubo volcano. *Geophysical Research Letters 20*, 1299–1302, 1993.

Reinsel, G. C., G. C. Tiao, J. J. DeLuisi, C. L. Mateer, A. J. Miller, and J. E. Frederick. Analysis of upper stratospheric Umkehr ozone profile data for trends and the effects of stratospheric aerosols. *Journal of Geophysical Research 89*, 4833–4840, 1984.

Reinsel, G. C., G. C. Tiao, D. J. Wuebbles, J. B. Kerr, A. J. Miller, R. M. Nagatani, L. Bishop, and L. H. Ying. Seasonal trend analysis of published ground-based and TOMS total ozone data through 1991. *Journal of Geophysical Research 99*, 5449–5464, 1994.

Rinsland, C. P., M. R. Gunson, M. C. Abrams, L. L. Lowes, R. Zander, E. Mahieu, A. Goldman, M. K. W. Ko, J. M. Rodriguez, and N. D. Sze. Heterogeneous

conversion of N_2O_5 and HNO_3 in the post-Mount Pinatubo eruption stratosphere. *Geophysical Research Letters 99*, 8213–8219, 1994.

Roche, A. E., J. B. Kumer, J. L. Mergenthaler, G. A. Ely, W. G. Uplinger, J. F. Potter, T. C. James, and L. W. Sterritt. The Cryogenic Limb Array Etalon Spectrometer (CLAES) on UARS: experiment description and performance. *Journal of Geophysical Research 98*, 10763–10776, 1993.

Rosenlof, K. H. Seasonal cycle of the residual mean meridional circulation in the stratosphere. *Journal of Geophysical Research 100*, 5173–5191, 1995.

Russell III, J. M., L. L. Gordley, J. H. Park, S. R. Drayson, W. D. Hesketh, R. J. Cicerone, A. F. Tuck, J. E. Frederick, J. E. Harries, and P. J. Crutzen. The Halogen Occultation Experiment. *Journal of Geophysical Research 98*, 10777–10797, 1993a.

Russell III, J. M., M. Luo, R. J. Cicerone, and L. E. Deaver. Satellite confirmation of the dominance of chlorofluorocarbons in the global stratospheric chlorine budget. *Nature 379*, 526–529, 1996.

Russell III, J. M., A. F. Tuck, L. L. Gordley, J. H. Park, S. R. Drayson, J. E. Harries, R. J. Cicerone, and P. J. Crutzen. HALOE Antarctic measurements in the spring of 1991. *Geophysical Research Letters 20*, 719–722, 1993b.

Salawitch, R. J., et al. The diurnal variation of hydrogen, nitrogen, and chlorine radicals: implications for the heterogeneous production of HNO_3. *Geophysical Research Letters 21*, 2551–2554, 1994.

Schoeberl, M. R., L. R. Lait, P. A. Newman, and J. E. Rosenfield. The structure of the polar vortex. *Journal of Geophysical Research 97*, 7859–7882, 1992.

Schoeberl, M. R., M. Luo, and J. E. Rosenfield. An analysis of the Antarctic Halogen Occulation Experiment trace gas observations. *Journal of Geophysical Research 100*, 5159–5172, 1995.

Solomon, S. Progress towards a quantitative understanding of Antarctic ozone depletion. *Nature 347*, 347–354, 1990.

Solomon, S., R. R. Garcia, and A. R. Ravishankara. On the role of iodine in ozone depletion. *Journal of Geophysical Research 99*, 20491–20499, 1994.

Solomon, S., R. R. Garcia, F. S. Rowland, and D. J. Wuebbles. On the depletion of Antarctic ozone. *Nature 321*, 755–758, 1986.

Stolarski, R., R. Bojkov, L. Bishop, C. Zerefos, J. Staehelin, and J. Zawodny. Measured trends in stratospheric ozone. *Science 256*, 342–349, 1992.

Stolarski, R. S., and R. J. Cicerone. Stratospheric chlorine: a possible sink for ozone. *Canadian Journal of Chemistry 52*, 1610–1615, 1974.

Symonds, R. B., W. I. Rose, and M. H. Reed. Contribution of Cl- and F-bearing gases to the atmosphere by volcanoes. *Nature 334*, 415–418, 1988.

Tabazadeh, A., and R. P. Turco. Stratospheric chlorine injection by volcanic eruptions: HCl scavenging and implications for ozone. *Science 260*, 1082–1086, 1993.

Tao, X., and A. Tuck. On the distibution of cold air near the vortex edge in the lower stratosphere. *Journal of Geophysical Research 99*, 3431–3450, 1994.

Thomason, L. W., L. R. Poole, and T. Deshler. A global climatology of stratospheric aerosol surface area density as deduced from SAGE II: 1984-1994. Submitted to *Journal of Geophysical Research*, 1996.

Tie, X., G. P. Brasseur, B. Briegleb, and C. Granier. Two-dimensional simulation of Pinatubo aerosol and its effect on stratospheric ozone. *Journal of Geophysical Research 99*, 20545–20562, 1994.

Tolbert, M. A., M. J. Rossi, R. Malhotra, and D. M. Golden. Reaction of chlorine nitrate with hydrogen chloride and water at Antarctic stratospheric tmperatures. *Science 238*, 1258–1259, 1987.

Toon, G. C. The JPL MIKV interferometer. *Optics and Photonics News 2*, 19–21, 1991.

Toon, G. C., P. Hamill, R. P. Turco, and J. Pinto. Condensation of HNO_3 and HCl in the winter polar stratospeheres. *Geophysical Research Letters 13*, 1284–1287, 1986.

Trepte, C. R., R. E. Viega, and M. P. McCormick. The poleward dispersal of Mount Pinatubo volcanic aerosol. *Journal of Geophysical Research 98*, 18563–18573, 1993.

Tuck, A. F., et al. Polar stratospheric cloud processed air and potential vorticity in the Northern Hemisphere lower stratosphere at mid-latitudes during winter. *Journal of Geophysical Research 97*, 7883–7904, 1992.

Tuck, A. F., C. R. Webster, R. D. May, D. C. Scott, S. J. Hovde, J. W. Elkins, and K. R. Chan. Time and temperature dependences of fractional HCl abun-

dances from airborne data in the Southern Hemisphere during 1994. *Faraday Discussions*. in press, 1995.

Waters, J. W., L. Froidevaux, G. L. Manney, L. S. Elson, D. A. Flower, R. F. Jarnot, and R. S. Harwood. Stratospheric ClO and ozone from the Microwave Limb Sounder on the Upper Atmosphere Research Satellite. *Nature 362*, 597–602, 1993.

Weaver, A., M. Loewenstein, J. R. Podolske, S. E. Strahan, M. H. Proffitt, K. Aikin, J. J. Margitan, H. H. Jonsson, C. A. Brock, J. C. Wilson, and O. B. Toon. Effects of Pinatubo aerosol on stratospheric ozone at mid-latitudes. *Geophysical Research Letters 20*, 2515–2518, 1993.

Webster, C. R., R. D. May, M. Allen, L. Jaeglé, and M. P. McCormick. Balloon profiles of stratospheric NO_2 and HNO_3 for testing the heterogeneous hydrolysis of N_2O_5 on sulfate aerosols. *Geophysical Research Letters 21*, 53–56, 1994.

Webster, C. R., R. D. May, D. W. Toohey, L. M. Avallone, J. G. Anderson, P. Newman, L. Lait, M. R. Schoeberl, J. W. Elkins, and K. R. Chan. Chlorine chemistry on polar stratospheric cloud particles in the Arctic winter. *Science 261*, 1130–1134, 1993.

Weisenstein, D. K., M. K. W. Ko, N. D. Sze, and J. M. Rodriguez. Potential impact of SO_2 emissions from stratospheric aircraft on ozone. *Geophysical Research Letters 23*, 161–164, 1996.

Wennberg, P. O., J. W. Brault, T. F. Hanisco, R. J. Salawitch, and G. H. Mount. The atmospheric column abundance of IO: Implications for strato-

spheric ozone. *Journal of Geophysical Research*. Submitted to *Journal of Geophysical Research*, 1996.

Wennberg, P. O., R. C. Cohen, R. M. Stimpfle, J. P. Koplow, J. G. Anderson, R. J. Salawitch, D. W. Fahey, E. L. Woodbridge, E. R. Keim, R. S. Gao, C. R. Webster, R. D. May, D. W. Toohey, L. M. Avallone, M. H. Proffitt, M. Loewenstein, J. R. Podolske, K. R. Chan, and S. C. Wofsy. Removal of stratospheric O_3 by radicals: in situ measurements of OH, HO_2, NO, NO_2, ClO, and BrO. *Science 266*, 398–404, 1994.

Wofsy, S. C., K. A. Boering, B. C. Daube, Jr., and M. B. McElroy. Vertical transport rates in the stratosphere in 1993 from observations of CO_2, N_2O, and CH_4. *Geophysical Research Letters 21*, 2571–2574, 1994.

Woodbridge, E. L., J. W. Elkins, D. W. Fahey, L. E. Heidt, S. Solomon, T. J. Baring, T. M. Gilpin, W. H. Pollock, S. M. Schauffler, E. L. Atlas, M. Loewenstein, J. R. Podolske, C. R. Webster, R. D. May, J. M. Gilligan, S. A. Montzka, K. A. Boering, and R. J. Salawitch. Estimates of total organic and inorganic chlorine in the lower stratosphere from in situ and flask measurements during AASE II. *Journal of Geophysical Research 100*, 3057–3064, 1995.

World Meteorological Organization. *Scientific Assessment of Ozone Depletion: 1991*. Global Ozone Research and Monitoring Project, report 25. Geneva, Switzerland: World Meteorological Organization, 1992.

World Meteorological Organization. *Scientific Assessment of Ozone Depletion: 1994*. Global Ozone Research and Monitoring Project, report 37. Geneva, Switzerland: World Meteorological Organization, 1995.

Yang, H. Three-dimensional transport of the Ertel potential vorticity and N_2O in the GFDL SKYHI model. *Journal of the Atmospheric Sciences 52*(9), 1513–1528, 1995.

Zdunkowski, W. G., R. M. Welch, and G. Korb. An investigation of the structure of typical two-stream-methods for the calculation of solar fluxes and heating rates in clouds. *Contributions to Atmospheric Physics 53*, 147–166, 1980.

Standard Bibliographic Page

1. Report No.	2. Government Accession No.	3. Recipient's Catalog No.

4. Title and Subtitle

Scientific Studies in Association with the Halogen Occultation Experiment

5. Report Date

May 1996

6. Performing Organization Code

7. Author(s)

Loretta J. Mickley and John E. Frederick

8. Performing Organization Report No.

9. Performing Organization Name and Address

Department of the Geophysical Sciences
The University of Chicago
Chicago, IL 60637

10. Work Unit No.

11. Contract or Grant No.

NAS1-18239

12. Sponsoring Agency Name and Address

National Aeronautics and Space Administration
Washington, D.C. 20546

13. Type of Report and Period Covered

Contractor Report

14. Sponsoring Agency Code

15. Supplementary Notes

Langley Technical Monitor: John Wells
Final Report

16. Abstract

This work examines measurements of ozone, NO, NO_2, and HCl made by the Halogen Occultation Experiment (HALOE) to track chemical change in the stratosphere. In addition, HALOE observations of two long-lived species, HF and CH4, are used as tracers to distinguish between change due to transport processes and change due to chemistry. The first study investigates the response of NO_x (NO and NO_2) and ozone to the presence of large amounts of sulfate aerosol in the stratosphere following the 1991 eruption of Mount Pinatubo. As the Pinatubo aerosol cleared the atmosphere at 17 mb (about 27-28 km), the partitioning of total reactive nitrogen shifted more toward NO_x, and ozone amounts declined. This trend is opposite that observed at lower altitudes. The second study examines the chemical aftermath of severe ozone depletion over Antarctica in spring. When ozone levels drop to a threshold amount (about 1 ppm near 20 km), the partitioning of the total chlorine family shifts rapidly from reactive species to the reservoir molecule HCl. This sudden repartitioning shuts down further ozone loss and may be significant as filaments of air peel off the polar vortex and mix with mid-latitude air.

17. Key Words (Suggested by Authors(s))	18. Distribution Statement
HALOE, UARS, ozone, photochemistry	Unclassified - Unlimited

19. Security Classif.(of this report)	20. Security Classif.(of this page)	21. No. of Pages	22. Price
unclassified	unclassified	158	

For sale by the National Technical Information Service, Springfield, Virginia 22161

NASA Langley Form 63 (June 1985)